学位論文

Mg-calcite dissolution in coral reefs estimated by laboratory experiment and field observation

(室内実験及び現場観測によるサンゴ礁砂地のマグネシウム方解石溶解反応の評価)

平成 25 年 5 月博士（理学）申請

東京大学大学院理学系研究科

地球惑星科学専攻

山本　将史

論文内容の要旨

論文題目　Mg-calcite dissolution in coral reefs estimated by laboratory experiment and field observation
（室内実験及び現場観測によるサンゴ礁砂地の
マグネシウム方解石溶解反応の評価）

氏名　　山本 将史

海洋は炭素の大きなリザーバーであり、人間活動によって放出された二酸化炭素の 30%以上を吸収している(Sabine et al., 2004)。この吸収により、表層海水の pH 及び鉱物の飽和度は低下する(Kleypas et al., 2006)。今世紀中に海水の pH が 0.3 から 0.5 低下する、海洋酸性化が問題となっている(Caldeira and Wickett, 2003)。これまでの海洋酸性化に関する研究では、上昇する二酸化濃度に対して、生物（主に炭酸塩鉱物を殻に持つ石灰化生物）の生産量や石灰化速度がどのように影響を受けるかということに着目してきた。一方、炭酸塩の溶解については、その影響がより強く出る極域や深海では重要と考えられてきたが、サンゴなどの石灰化生物が棲息する熱帯域の浅海は、アラレ石の飽和度（Ω_a）が 1 以下になることはないため、炭酸塩鉱物の溶解は考慮されていなかった。しかし近年の観測で、表層海水のΩ_aが 1 より大きい過飽和の状態にもかかわらず、夜間に炭酸塩の溶解がサンゴ礁域で起きていることが報告された(Yates and Halley, 2006; Cyronak et al. 2013)。これは、有孔虫や紅藻がつくるアラレ石よりも溶けやすいマグネシウム方解石が溶解している影響だと考えられる。しかし、生物起源のマグネシウム方解石の溶解閾値については正確には定まっていない。さらに、実際のフィールドにおいて、潮位や流れ、光量などを考慮したサンゴ礁砂地の溶解メカニズムは依然として分かっていない。またそもそも、これまでの研究では、現場で起きている溶解反応は、水柱の海水と堆積物の表面における単純な反応として捉えられていた。しかし、実際に溶解反応で表れる水柱の海水のアルカリ度の増加は、堆積物中の間隙水のアルカリ度プロファイルと、流れや水温といった物理要素によって決まる拡

散係数の積によって決まるはずである。すなわち、堆積物中のアルカリ度及び酸素などのプロファイルがどのような条件によって決まるかを明らかにし、自然界における流動環境での拡散係数を求めることが、水柱のアルカリ度の増加のメカニズムを解明するうえで重要となる。
こうしたことを踏まえ本研究では、
（１）CO_2 添加によって作り出された海水を用いて、生物起源のマグネシウム方解石の溶解の閾値、及び溶解速度と飽和度Ω_aの関係を、室内溶解実験によって明らかにすると共に、
（２）フィールドにおける自然条件下でのサンゴ礁砂地の溶解速度を、流速可変チャンバーを使った実験によって測定した。
（３）さらに、渦相関法による水柱-堆積物境界層における酸素フラックスの観測と、微小電極をつかった堆積物中での溶存酸素の鉛直プロファイルから、水柱-堆積物境界層における酸素の拡散係数を求め、この酸素の拡散係数をアルカリ度の拡散係数に適用して、堆積物中の間隙水から求めた炭酸系鉛直プロファイルから、水柱-堆積物境界層でのアルカリ度フラックスを見積もった。
全てのフィールドでの実験及び観測は石垣島の白保サンゴ礁で実施し、室内実験で用いたサンプルも同場所で採取した生物起源のものを用いた。

（１）室内実験

生物起源のマグネシウム方解石の溶解の閾値を求めたところ、堆積物全体のマグネシウム方解石については$\Omega_a \fallingdotseq 3.8$、有孔虫及び紅藻殻のマグネシウム方解石は $3.0 < \Omega_a < 3.2$、サンゴから採取したアラゴナイト鉱物については$\Omega_a \fallingdotseq 1.0$ の溶解閾値をもつことが明らかになり、Ω_a が低下するにつれ、溶解速度は増加することがわかった。この結果、サンゴ礁域における夜間の炭酸塩溶解は、砂地堆積物中の有孔虫や紅藻が持つマグネシウム方解石によって引き起こされることが明らかになった。また、今回の結果を先行研究と比較したところ、Plummer and Mackenzie(1974)で求められた生物起源マグネシウム方解石の溶解閾値に近いことが分かった。

（２）流速可変チャンバー実験

流動可変チャンバーを用いて、様々な CO_2 条件下で砂地での溶解速度と水柱のΩ_aの関係を求めた。その結果、昼・夜を問わず、流速の変化が砂地の溶解速度に与える影響はみられなかった。また、海水中に人工的に CO_2 を添加した場合、溶解速度が自然条件下に比べ、過小に見積もられている可能性が示唆された。これはチャンバー実験では、実験時間が短く、さらに模擬的な高 CO_2 海水が間隙水全体量に対して少ないため、堆積物表層のみが高 CO_2 条件になったに過ぎず、堆積物内部の間隙水まで影響が及ばなかったことが原因と考えられる。このことから、マグネシウム方解石の溶解による水柱のアルカリ度の増加を見積もる上で、堆積物中間隙水の炭酸系鉛直プロファイルと、それによる堆積物-水柱境界層でのアルカリ度フラックスを把握することが重要といえる。

（３）溶存酸素及び炭酸系成分の鉛直プロファイルと渦相関法による酸素フラックスの観測

溶存酸素及び pH 微小電極と間隙水の採水から、溶存酸素と炭酸系の堆積物-水柱鉛直プロファイルを観測した。その結果、溶存酸素については、堆積物中の深度 0-10㎜間で昼間は光合成の影響で増加、夜間は呼吸の影響で減少する特徴が顕著にみられた。また pH もそれに対応するように変動していた。そしてそれより深い深度では昼夜を問わず、酸素が完全に枯渇している様子が明らかになった。一方、炭酸系成分については、5㎜ 以深では常に$\Omega_a \fallingdotseq 3.0$ であることがわかった。これは（１）で求めた生物起源の有孔虫に対する飽和度（Ω_{fora}）の溶解閾値（$\Omega_{fora} \fallingdotseq 1$）に相当する。よって堆積物中では、生物の呼吸や脱窒によって生産された二酸化炭素を、マグネシウム方解石の溶解反応により消費することで、Ωが一定に保たれていると考えられる。

一方、同時に渦相関法を用いて水柱-堆積物境界面の酸素フラックスを観測したところ、夜間には生物の呼吸の影響を受け 5.0-5.7 $mmol\,m^{-2}\,hr^{-1}$ の酸素の吸収が、昼間には光合成の影響を受け 14.4-24.0 $mmol\,m^{-2}\,hr^{-1}$ の酸素の放出が確認された。さらに、酸素プロファイルの傾きの平均値を用いて拡散係数を求めたところ、水柱-堆積物境界面での拡散係数は $4.9\times10^{-4}\ cm^2\ s^{-1}$ と見積もられた。これは酸素の分子拡散の約 30 倍に相当しており、水柱-堆積物境界面では分子拡散ではなく、海水の流れや波、潮位変化による水圧の変化といった物理的プロセスや堆積物中の生物活動による生物的プロセスが、拡散係数の変化に起因していると考えられる。

この拡散係数と堆積物の間隙水の炭酸系鉛直プロファイルから、夜間の水柱-堆積物境界層でのアルカリ度フラックスは、堆積物から水柱方向に 1.0-2.6 $mmol\,m^{-2}\,hr^{-1}$ と見積もられた。

（４）考察

採取した間隙水と水柱の炭酸系成分をアルカリ度-全炭酸ダイアグラム上にまとめた。その結果、水柱のアルカリ度の上昇は、従来の研究で言われていた水柱-表層堆積物のマグネシウム方解石の溶解反応として起きているわけではなく、堆積物表面から 10㎜ の深度間での生物的な呼吸とそれに伴う非生物的なマグネシウム方解石の溶解によって高いアルカリ度の間隙水が生じ、それと水柱のアルカリ度との勾配から水柱-堆積物境界層でのアルカリ度フラックスが励起されているという理解に至った。さらに、いちど海水のΩ_{fora}が 1.0 を切り、溶解の閾値を過ぎてしまった場合、堆積物から水柱に向けてのアルカリ度フラックスが劇的に大きくなることが示唆された。

本研究によって初めて、水柱で観察されるアルカリ度の増加が堆積物中の炭酸系鉛直プロファイルと拡散係数の関係から明らかにされた。今後、生態系自らの影響が蓄積される特殊なサンゴ礁生態系条件下において、面積的に大部分を占め、且つ海洋酸性化の影響が最初に出るであろうサンゴ礁砂地溶解の効果を、サンゴ礁生態系全体スケールの炭酸系モデルに組み込むことが求められる。

Abstract

The ocean is a large carbon reservoir and more than 30% of the CO_2 emitted into the atmosphere by human activities is taken up by the oceans (Sabine et al., 2004), lowering the pH of surface water and decreasing the saturation state of minerals (Kleypas et al., 2006). Future uptake of CO_2 by the ocean is predicted to reduce seawater pH by 0.3 to 0.5 units by 2100 (Caldeira and Wickett, 2003), which is called ocean acidification. Previous studies have mainly investigated the effects of elevated pCO_2 on the net production and calcification of marine organisms. On the other hand, carbonate dissolution is predicted to occur only in polar regions and in the deep sea where saturation state with respect to aragonite (Ω_a) will be <1 by 2100. Recent reports demonstrate nocturnal carbonate dissolution of reefs, despite a Ω_a value of > 1 (Yates and Halley, 2006; Cyronak et al., 2013). This is probably related to the dissolution of reef carbonate (Mg-calcite), which is more soluble than aragonite. However, the threshold value of Ω_a for the dissolution of natural sediments has not been clearly determined. Moreover, Mg-calcite dissolution at sand area in coral reefs under natural conditions (such as tidal change, current, photon flux and temperature so on) have not been understood. Originally, previous studies considered that total alkalinity (A_T) increase in water column was caused by a reaction between seawater in the water column and surface of the sediment. However, A_T increase in water column should be determined by the A_T profile in the sediment and diffusion coefficient caused by physical factor such as current and tidal change. Thus, it is important to understand the mechanism that controls the profiles of O_2 and A_T, and to estimate diffusion coefficient under natural hydrodynamic condition. In this study, (1) the dissolution system with conditions reproducing those of a natural coral reef was designed, and the dissolution rates of aragonite in corals and of Mg-calcite excreted by other marine organisms were measured, under conditions of $\Omega_a > 1$, with controlled seawater pCO_2, (2) the *in-situ* Mg-calcite dissolution rate under natural condition was measured by flow-controlled chamber

experiment, (3) diffusion coefficient at sediment-water interface was determined by using eddy covariance (EC) technique and O_2 profile in sediment and, (4) A_T flux at sediment-water interface was estimated according to the diffusion coefficient and the gradient in A_T in sediment,.

All field observation was conducted at Shiraho Reef, Ishigaki Island, and samples used by laboratory experiment were also collected at the same site.

1. Laboratory Experiment

By laboratory experiment, dissolution of bulk carbonate sediments at Shiraho reef occurs at Ω_a values of 3.7 to 3.8. Mg-calcite derived from foraminifera and coralline algae dissolves at Ω_a values between 3.0 and 3.2, and aragonite starts to dissolve when Ω_a = 1.0. Dissolution rate increased with the decreases of Ω_a. Nocturnal carbonate dissolution of coral reefs occurs mainly by the dissolution of foraminiferans and coralline algae in reef sediments. The solubilities of foraminiferans and coralline algae obtained by this study agreed with those measured by Plummer and Mackenzie (1974).

2. Flow-controlled chamber experiment

In order to understand relationship between dissolution rate and Ω_a in water column, chamber experiment, which can control flow rate, were designed and conducted at Shiraho reef sand area. Data showed that there were no significant differences in dissolution/calcification rate between high-flow and low-flow condition. While dissolution rate increases as Ω_a decreased in laboratory experiment, dissolution rate measured by flow-controlled chamber did not change. It would mean that carbonate profiles in sediment was not affected by high pCO_2 in water column because of short duration of experiment or a little amount of water column in chamber relative to sediment pore water. Therefore, understanding of pore water sediment profile under natural condition and estimation of A_T flux at sediment-water interface is

important.

3. A_T flux estimated by sediment pore water profiles and eddy covariance

O_2 and carbonate profiles in sediment were measured by microelectrode and pore water analysis. Between 0 and 10 mm depth, respiration by organisms consumed oxygen and produced CO_2 and decreased pH at night. On the contrary, O_2 increased by the photosynthesis during day time. Deeper than at least 10 mm, O_2 was depleted even during day time. On the other hand, saturation state of biogenic foraminifera (= Ω_{fora}), which was determined by my laboratory experiment, was always constant at the value of 1.0. Both organic reaction such as respiration and inorganic Mg-calcite dissolution occur in the sediment and keep Ω_{fora} constant.

At the same time, DO fluxes measured by EC were 4.95-5.66 mmol m^{-2} hr^{-1} uptake at night and 14.44-23.99 mmol m^{-2} hr^{-1} production during day time. This is because that photosynthesis by microalgae on the upper part of sediment produced O_2, and on the contrary, respiration during nighttime consumed O_2. Also, diffusion coefficient at night was calculated from DO flux observed by eddy covariance and O_2 profile, and night average diffusion coefficient was as 4.9×10^{-4} cm^2 s^{-1}. This value was 30-100 times higher than molecular diffusion. Diffusion coefficient observed by this study was nearly equal to previous studies and diffusion coefficient was mainly caused by physical condition such as flow rate and current and biological condition in the sediment.

According to diffusion coefficient and A_T profile in sediment, A_T flux at sediment-water interface at night was calculated as 1.6- 2.6 mmol m^{-2} hr^{-1}.

4. Discussion

Carbonate chemistry in pore water and water column were summarized on the A_T-C_T diagram. The exact estimation on Mg-calcite dissolution can be achieved not by the reaction between water column and surface of the sediment but by A_T profile in the sediment and diffusion coefficient. Both organic reaction such as respiration and inorganic Mg-calcite dissolution occur in the sediment and keep Ω_{fora} constant. Moreover, once saturation level of seawater in water column passed the threshold of Mg-calcite dissolution, estimated A_T flux increases drastically.

A_T increase in the water column can be more properly estimated by diffusion coefficient and A_T profile in the sediment. It is essential to consider diagenetic processes within sediments in reef-scale carbon cycle models and the quantitative evaluation of the buffering capacity of reef sand areas containing Mg-calcite sediments.

Contents

Chapter 1.

Introduction

1-1. Ocean acidification and carbonate dissolution

The ocean is a large carbon reservoir that absorbs atmospheric CO_2, which then equilibrates with bicarbonate (HCO_3^-) and carbonate (CO_3^{2-}) ions. More than 30% of the CO_2, which is emitted into the atmosphere by human activities, is taken up by the oceans, lowers the pH of surface water, and decreases the saturation state of carbonate minerals (Sabine et al., 2004; Kleypas et al., 2006). Future uptake of CO_2 by the ocean is predicted to reduce seawater pH by 0.3 to 0.5 units over the next few decades (Caldeira and Wickett, 2003), which is called ocean acidification.

The fundamental chemistry of inorganic carbon in seawater has been described by Zeebe and Wolf-Gladrow (2003), and Millero (2006). Dissolved inorganic carbon in seawater occurs mainly in three inorganic forms: free aqueous carbon dioxide ($CO_2(aq)$), bicarbonate (HCO_3^-), and carbonate (CO_3^{2-}) ions, which are related to each other as follows:

$$CO_2 + H_2O \leftrightarrow HCO_3^- + H^+ \leftrightarrow CO_3^{2-} + 2H^+ \quad (1\text{-}1)$$

The sum of the dissolved forms CO_2, HCO_3^-, and CO_3^{2-} is called total dissolved inorganic carbon (C_T), and total alkalinity (A_T) is a measure of the capacity of water to neutralize acids. They can be described as follows:

$$C_T = [CO_2] + [HCO_3^-] + [CO_3^{2-}] \quad (1\text{-}2)$$

$A_T = [HCO_3^-] + 2[CO_3^{2-}] + [B(OH)_4^-] + [OH^-] - [H^+]$ + minor components ($[HPO_4^{2-}] + 2[PO_4^{3-}] + [H_3SiO_4^-] + [NH_3] + [HS^-] - [HSO_4^-] - [HF] - [H_3PO_4]$) (1-3)

Ocean acidity is measured as pH (pH = -log10 $[H^+]$) and can be reported on different scales: National Bureau of Standards (pH_{NBS}), seawater (pH_{SWS}), free (pH_F), and total (pH_T). The total scale is used in this study as recommended by Dickson (2010).

Future projected changes in calcification and carbonate dissolution resulting from ocean acidification could be drastic and sufficiently large so that coral reef communities and carbonate ecosystems in general could become subject to a net loss of $CaCO_3$ material (Kleypas et al., 1999; Andersson et al.,2009; Gattuso and Hansson, 2011).

In order to discuss the acidity index of seawater for a given mineral, saturation state is used. It is a measure of the thermodynamic potential of the mineral to precipitate or dissolve; the saturation state of calcium carbonate (Ω) is defined as follows:

$$\Omega = [Ca^{2+}] \times [CO_3^{2-}]/K^*_{sp} \quad (1\text{-}4)$$

where K^*_{sp} is the product of the equilibrium concentrations of Ca^{2+} and CO_3^{2-}, which differs among mineralogies of calcium carbonate such as aragonite, calcite and Mg-calcite.

Calcium carbonate formation is thermodynamically favorable when $\Omega > 1.0$, but is unfavorable when $\Omega < 1.0$. Oceanic uptake of CO_2 causes an increase in hydrogen ion concentration $[H^+]$ and a decrease in carbonate ion concentration $[CO_3^{2-}]$, leading in turn to a decrease in Ω.

Carbonate dissolution is described as follows:

$$CaCO_3 + CO_2 + H_2O \rightarrow Ca^{2+} + 2HCO_3^- \quad (1\text{-}5)$$

This indicates that carbonate dissolution would cause increases in A_T, C_T, and Ω values. This carbonate–bicarbonate system buffers atmospheric CO_2 levels and ocean acidification, indicating that carbonate dissolution causes an increase in the buffer capacity of seawater (i.e., an increase in alkalinity). These links indicate that an accurate understanding of this buffer system is needed to correctly predict future changes in the carbon balance between the atmosphere and the ocean, and the resulting degree of ocean acidification.

1-2. $CaCO_3$: aragonite, calcite, and Mg-calcite

1-2-1. Property of Mg-calcite organisms

The most important carbonate minerals in seawater reactions are the $CaCO_3$ polymorphs of aragonite and calcite, and marine calcite may contain variable amounts (6 to 30 mole %) of $MgCO_3$ as solid solution, generically termed Mg-calcite or high Mg-calcite (Morse et al. 2007). In this study, "Mg-calcite" indicates high Mg-calcite. Aragonite is both denser and more soluble than calcite, and when the Mg content in calcite is > 8-12 mole%, Mg-calcite dissolves more readily than aragonite (Plummer and Mackenzie, 1974; Bischoff et al., 1987; Morse et al., 2006). Thus, Mg-calcite is the first mineral phase to undergo dissolution as a result of undersaturated conditions caused by ocean acidification, which makes it "the canary in a coal mine" (Morse et al., 2006; Andersson and Mackenzie 2012).

Mg-calcite is mainly formed by foraminifera and coralline algae. Mg components of coralline algae are 6-21 mole% (Goldsmith et al., 1955; Borowitzka, 1982), and the foraminifera as a group display a very large variability in the Mg content of their carbonate shells, ranging between more than 20 mole% to less than 0.1 mole% of $MgCO_3$ (Figure1-1). Frequently, foraminifera that share the same habitat display significant differences in their Mg concentration, indicating that the Mg content is predominantly determined by biological factors (Blackmon and Todd, 1959). Blackmon and Todd (1959) concluded that the Mg variability in foraminifera shells is related to their taxonomy and phylogenetic relationships. While planktonic foraminifera are members of the low-Mg calcite group (<4 mol % $MgCO_3$), benthic foraminifera especially in shallow environment such as coral reefs are mainly member of Mg-calcite group.

Over the course of geologic time, there is considerable evidence that change in seawater chemistry has profoundly influenced biomineralization by marine organisms (Stanley 2008).

A calcite sea is one in which calcite and low-Mg-calcite are the primary inorganic marine calcium carbonate precipitate, whereas an aragonite sea is the alternate seawater chemistry in which aragonite and Mg-calcite are the primary inorganic carbonate precipitates. The Cambrian through the Mississippian and the Jurassic through the Paleogene were predominantly calcite seas, whereas the Mississippian through the Jurassic and the Neogene (including today) are characterized by aragonite seas (Figure1-2).

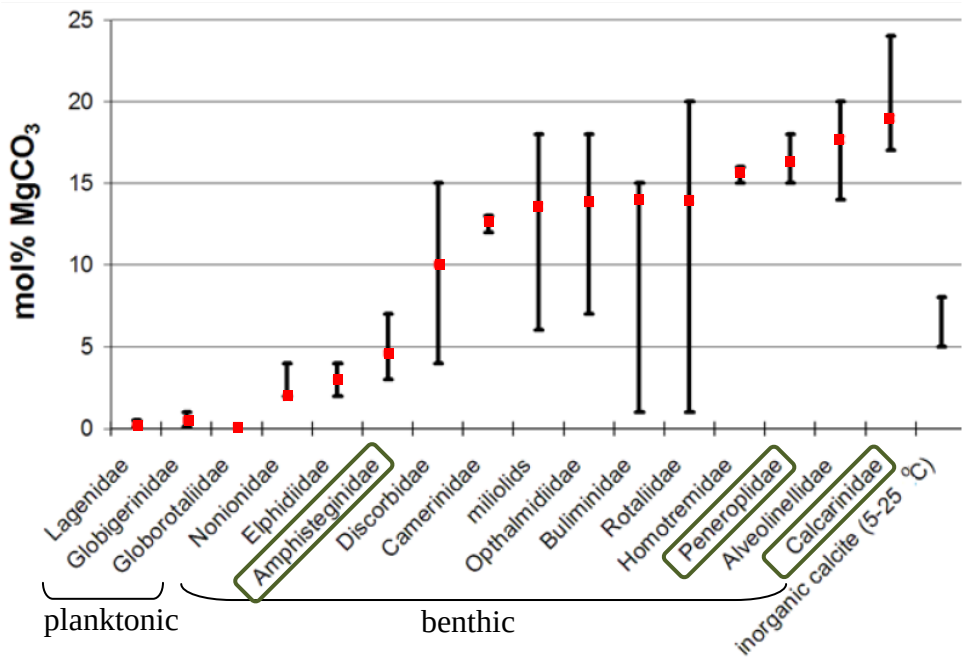

Figure1-1. Mg content of various foraminifera groups cited from Bentov and Erez (2006). The average values are marked by red squares and the ranges are shown by vertical bars. At the right column, the range of values expected for inorganic precipitation of calcite from seawater based on values at 5 and 25 °C is shown. Amphisteginidae, Peneroplidae and Calcarinidae are found at coral reef community.

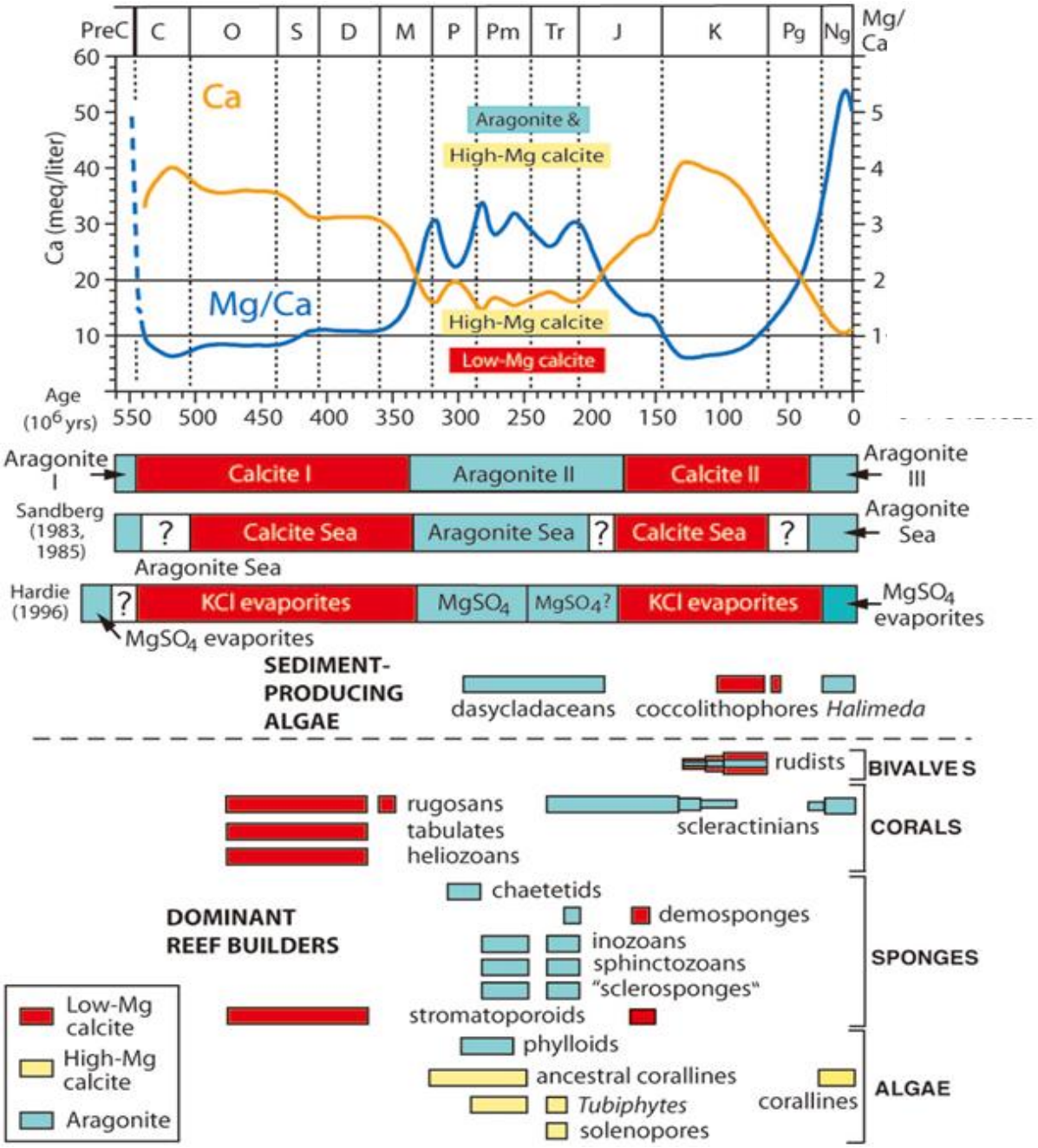

Figure 1-2. Comparison of the temporal distribution of mineralogies and producers of marine sediment cited from Stanley (2008). The large upper diagram shows nonskeletal precipitation of low-Mg calcite, high-Mg calcite, and aragonite as a function of the Mg/Ca molar ratio of seawater. The lowermost broad horizontal bar shows temporal oscillations observed in the geologic record between calcitic and aragonitic nonskeletal carbonates and between KCl and $MgSO_4$ marine evaporates. Shown below are temporal distributions of the carbonate-producing taxa.

1-2-2. The relationship between ocean acidification and biogenic calcification

Saturation state of aragonite is defined as Ω_a according to equation (1-4), and Figure 1-3 shows the changes in Ω_a that are predicted to occur as atmospheric CO_2 concentrations (ppm) increase. Today, in the high latitude region, the value of Ω_a ranges from 1 to 2. On the other hand, in the low latitude such as coral reefs, the value of Ω_a ranges from 3 to 4.5. When pCO_2 rises to the level of 650 ppm, in the coral reef, the value of Ω_a is still higher than one. Therefore, chemical dissolution of biogenic carbonate such as coral reef at the low latitude had not been expected, and previous studies have mainly investigated the effects of elevated pCO_2 on the net production and calcification of marine organisms by laboratory experiments.

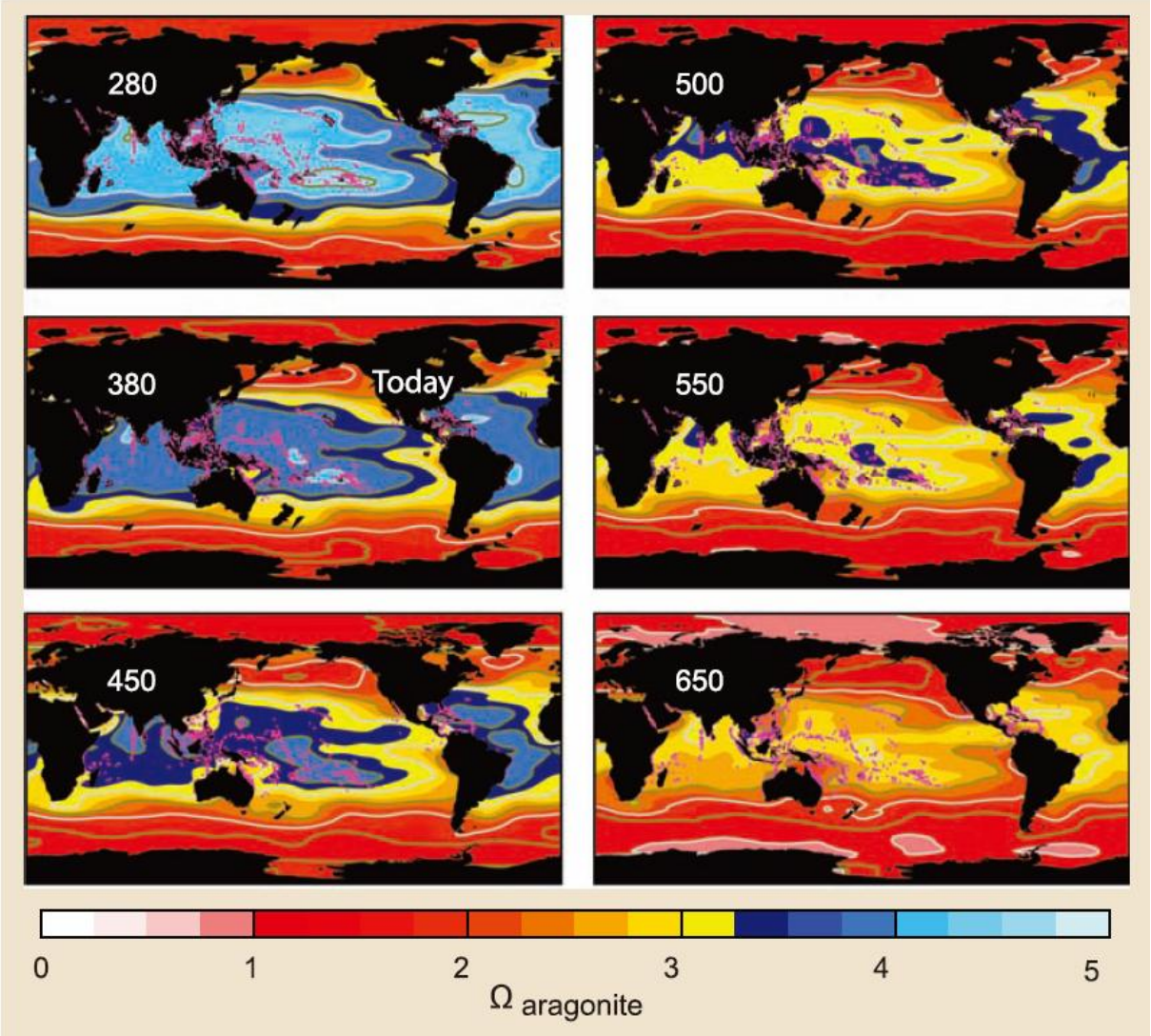

Figure 1-3. Changes in Ω_a that are predicted to occur as atmospheric CO_2 concentration (ppm) increases (number at top left of each panel) plotted over shallow-water coral reef locations shown as pink dots. Before the Industrial Revolution (280 ppm), nearly all shallow-water coral reefs had $\Omega_a > 3.25$ (Hoegh-Guldberg et al., 2007, Figure 4).

Ries et al. (2009) presented the results of 60 days laboratory experiments in which they investigated the effects of CO_2-induced ocean acidification on calcification in 18 benthic marine organisms. They showed that 10 of the 18 species studied exhibited reduced rates of net calcification and, in some cases, net dissolution under elevated pCO_2. However, in seven species, net calcification increased under the intermediate and/or highest levels of pCO_2, and one species showed no change at all (Figure 1-4).

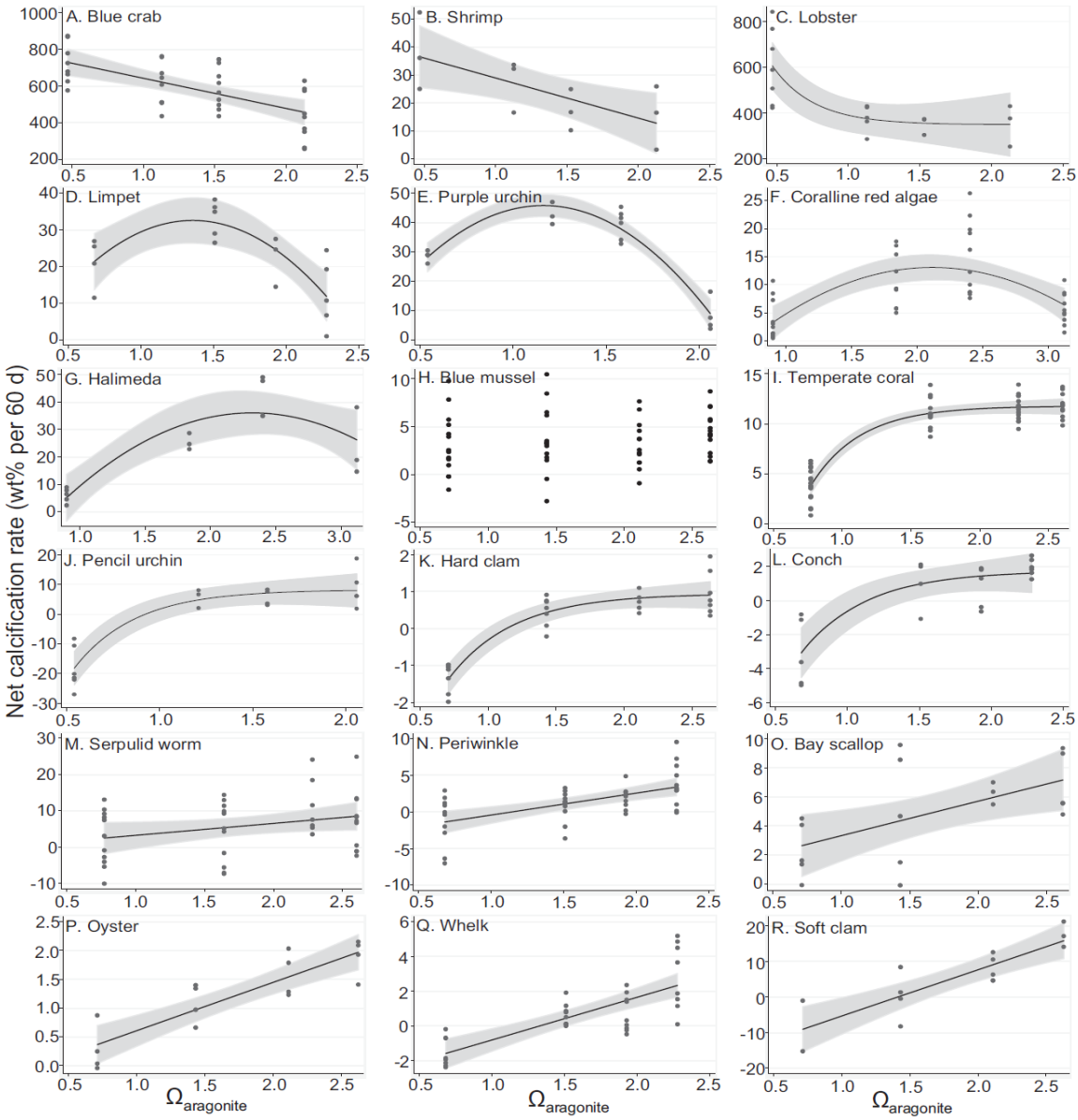

Figure 1-4. Calcification response patterns for 18 species of calcifying organisms subjected to 60 days of CO_2-induced reductions in $CaCO_3$ saturation state of seawater. Net rates of calcification(+)/dissolution(–) were estimated from buoyant weighing (verified with dry weight measured after harvesting) and are expressed as a percentage of the organisms' initial buoyant weight cited from Ries et al. (2009).

Doney et al. (2009) and Kroeker et al. (2013) summarized the biological responses to increasing pCO_2 (Figure 1-5). The results reveal decreased survival, calcification, growth, development and abundance in response to acidification when the broad range of marine organisms is pooled together. However, the magnitude of these responses varies among taxonomic groups, suggesting there is some predictable trait-based variation in sensitivity. Furthermore, the results suggest that other factors, such as nutritional status or source population, could cause substantial variation in organisms' responses.

For coralline algae, which excrete Mg-calcite, calcification rate decreased with increasing CO_2 condition (Kuffner et al., 2008, Comeau et al., 2013). On the other hand, for benthic foraminifera in coral reefs, both negative and positive effects of calcification against ocean acidification were reported. While calcification rate and growth rate decreased when pCO_2 increased (Kuroyanagi et al., 2009; Hikami et al., 2011; and Uthicke and Fabricius, 2013), calcification of *Calcarina gaudichaudii* and *Baculogypsina sphaerulata* generally increased with increased pCO_2 (Hikami et al., 2011; Fujita et al., 2011; and Vogal and Uthicke, 2012). They probably reflect different sensitivities among the species to carbonate chemistry, which may be due to different metabolisms of their symbiotic algae.

Physiological response	Major group	Species studied	a	b	c	d
Calcification						
	Coccolithophores[1]	4	2	1	1	1
	Planktonic Foraminifera	2	2	–	–	–
	Molluscs	4	4	–	–	–
	Echinoderms[1]	3	2	1	–	–
	Tropical corals	11	11	–	–	–
	Coralline red algae	1	1	–	–	–
Photosynthesis[2]						
	Coccolithophores[3]	2	–	2	2	–
	Prokaryotes	2	–	–	1	–
	Seagrasses	5	–	–	–	–
Nitrogen Fixation						
	Cyanobacteria	1	–	1	–	–
Reproduction						
	Molluscs	4	4	–	–	–
	Echinoderms	1	1	–	–	–

1) Increased calcification had substantial physiological cost; 2) Strong interactive effects with nutrient and trace metal availability, light, and temperature; 3) Under nutrient replete conditions.

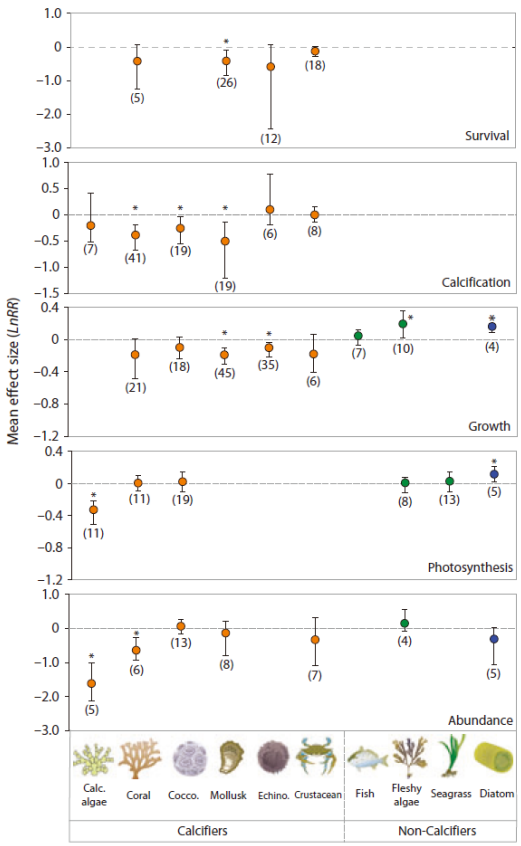

Figure 1-5. The relationship between biological responses and ocean acidification for several species: the left table was summarized by Doney et al. (2009) and the right table was summarized by Kroeker et al.(2013). Variation in effect sizes among key taxonomic groups, divided by major response variables. Means are from a weighted, random-effects model with bootstrapped bias-corrected 95% confidence intervals. The number of experiments used to calculate the means is given in parentheses. *denotes a significant difference from zero.

Future projected changes in calcification and carbonate dissolution resulting from ocean acidification could be sufficiently large so that coral reef communities and carbonate ecosystems could become subject to a net loss of $CaCO_3$ material (Yates and Halley, 2006; Andersson et al., 2007; Silverman et al., 2009; Andersson and Gledhill, 2013). In spite of the fact thatcarbonate dissolution will increase in response to ocean acidification, the effect of ocean acidification on carbonate dissolution rates has received relatively little attention compared to the effect on the ability of organisms to calcify (Andersson et al., 2009). Since Mg-calcite will be the first responder to ocean acidification, the dissolution of Mg-calcite should be precisely evaluated. Problems of Mg-calcite dissolution will be described in the following section.

1-3. Solubility experiment of Mg-calcite

The solubility of Mg-calcite varies according to the magnesium content. Figure 1-6 shows the solubility of Mg-calcite cited from Morse et al.(2007). $IAP_{magnisian\ calcite}$ is the ion activity product of the solution in equilibrium with Mg-calcite, and it indicates thermodynamic equilibrium. In general, carbonate minerals with a higher Mg content show higher solubility, but the solubility of synthetic and biogenic Mg-calcite varies under laboratory conditions, and there is variability in the solubility of biogenic Mg-calcite from different organisms.

Morse et al. (2007) divided the solubilities of Mg-calcite into three major categories: (A) synthetic Mg-calcite solubilities (Bischoff et al., 1987; Mucci and Morse, 1984); (B) the ‘‘best-fit’’ biogenic Mg-calcite solubilities (Bischoff et al., 1987; Walter and Morse, 1984); and (C) “Plummer and Mackenzie (1974) solubility” (Figure 1-6). Of these, category (C) has the highest values for Mg-calcite solubility, with the solubility of 12% to 15% mole Mg-calcite exceeding aragonite solubilities by a factor of five. Category (B) shows significantly higher solubilities than category (A) due to the heterogeneity and instability by biogenic factors, although the overall trend in category (B) is similar to that in category (A). While categories (A) and (B) reflect the thermodynamic solubilities of biotic and abiotic Mg-calcite, it is likely that category (C) may reflect the influence of kinetic, rather than thermodynamic, factors, including the retention of reactive surface particles after minimal sample cleaning and lack of annealing but may also reflect reactivity in nature (Morse et al., 2007).

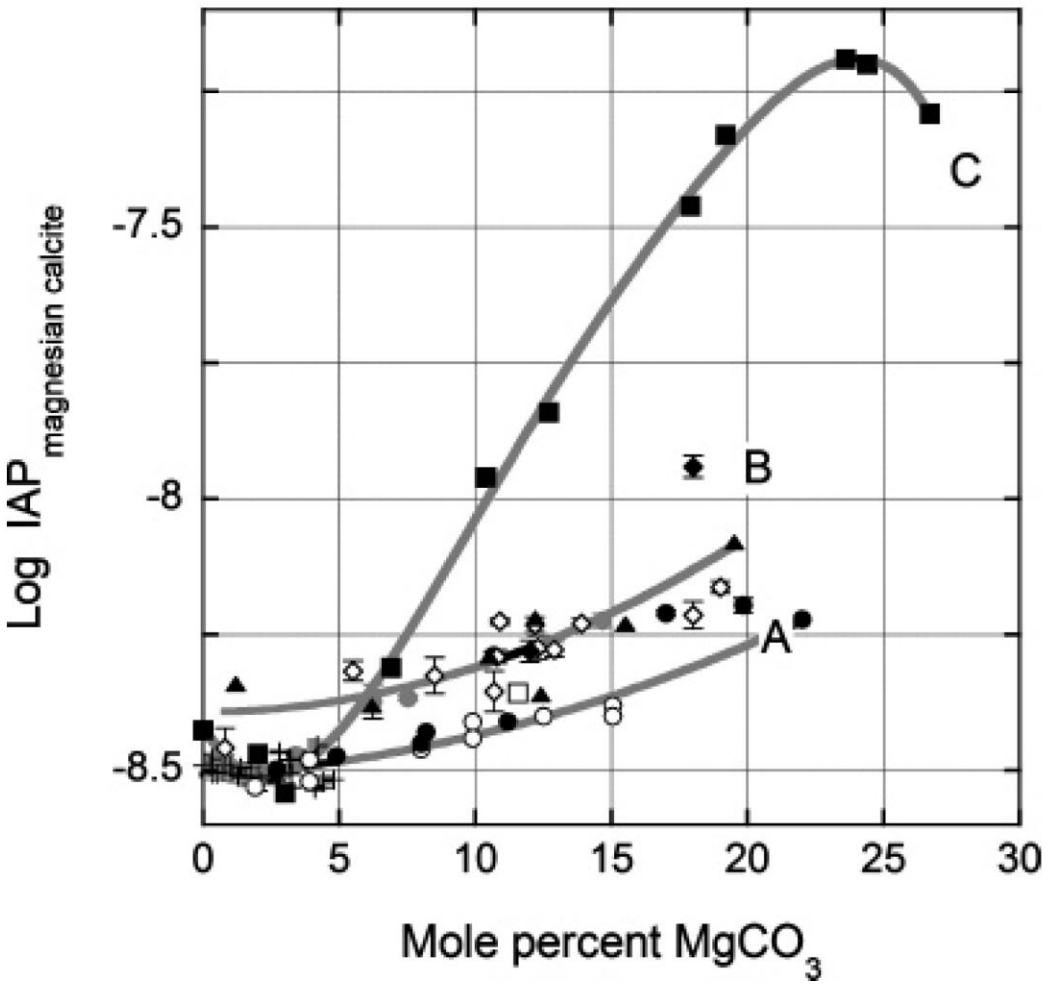

Figure 1-6. Solubility of Mg-calcite cited from Morse et al. (2007): Data are from synthetic (gray solid circles, Busenberg and Plummer, 1989; open circles, Bischoff et al., 1987; black solid circles, Mucci and Morse, 1984, open squares, Lafon, 1990), natural inorganic (crosses, Busenberg and Plummer, 1989), and biogenic phases (open diamonds, Busenberg and Plummer, 1989; closed triangles, Bischoff et al., 1987; closed diamonds, Walter and Morse, 1984; solid squares, Plummer and Mackenzie, 1974, recalculated by Thorstenson and Plummer, 1977). $IAP_{magnisian\ calcite}$ is the ion activity product of Mg-calcite, which indicates thermodynamic equilibrium. Trends (A) is "synthetic Mg-calcite solubilities", (B) is the ''best-fit'' biogenic Mg-calcite solubilities, and (C) is "Plummer and Mackenzie (1974) solubility"

The relationship between Ω and the dissolution rate of synthetic and biogenic calcium carbonates in the laboratory was studied by Keir (1980). Hales and Emerson (1997) reviewed the result of Keir (1980) and made corrections to the original measurements. The dissolution of $CaCO_3$ is usually described by this equation:

$$R = k \times (1 - \Omega)^{n} \qquad (1\text{-}6)$$

where k is the dissolution rate constant ($time^{-1}$), n is the reaction order, and R is the dissolution rate (% $time^{-1}$). Published estimates of n range from 1 to 4.5 (Keir 1980; Hales and Emerson 1997) based on laboratory studies. However, these dissolution rates are not consistent with those obtained from field observations (Gehlen et al. 2005). Moreover, no Mg-calcite dissolution experiments have been performed by using natural seawater, suggesting inhibitors in seawater can not be reproduced. Indeed, it is pCO_2 that alters Ω_a under human induced ocean acidification. Consequently, laboratory studies need to set Ω_a values using pCO_2 to attain consistency with the environment. Although relationship between dissolution rate and Ω is variable depending on water conditions such as temperature, pressure, salinity and flow rate condition, it is essential to determine the relationship between biogenic Mg-calcite dissolution rate and Ω under typical coral reef conditions with respect to pCO_2 and flow rate for example, in order to understand and estimate natural buffering systems.

1-4. Dissolution of carbonate sand in the field

Dissolution of carbonate sand has been discussed in relation to the saturation state of water column (Figure. 1-3) based on the assumption that dissolution would occur on the surface of the sediment. A few model studies, which featured the Mg-calcite dissolution, calculated dissolution rate as the reaction between seawater in water column and surface sediment (Andersson et al., 2003; Morse et al., 2006). These studies did not consider the early diagenetic processes such as respiration and denitirification in the sediment. On the other hand, carbonate dissolution rate in the actual environment are mostly measured by chamber experiment (Nakamura and Nakamori, 2009; Cyronak et al., 2013). This method also does not consider processes in sediment either. A_T change in water column was considered to occur by the reaction between carbonate minerals on surface of the sediment and seawater in water column.

However, seawater in water column was also changed by the biogenic reaction such as respiration and denitirification in sediment. Pore water is definitely different from seawater in water column. Consequently, we need to understand the Mg-calcite dissolution mechanism not as the simple reaction between surface sediment and seawater in water column, but as the processes in sediment. In this section, chamber experiment method will be introduced at first, and then general understanding of flux at sediment-water interface will be explained. Lastly, Eddy Covariance (EC) method, by which DO flux at sediment-water interface under natural condition can be measured, will be described as a feasible approach to measure A_T flux between sediment and water column.

1-4-1. Chamber experiment

In this chapter, chamber experiment method conducted by previous studies will be introduced. In order to estimate community metabolism involving dissolution at coral reef, *in-situ* chamber experiments were conducted. By a chamber experiment, the target community was closed by a chamber, and net photosynthesis and net calcification rates of the community were estimated based on the changes in the chemical composition of seawater in the chamber. Photosynthesis/respiration and calcification/dissolution rates of each ecosystem component, such as sand area or sea grass area etc., were estimated based on chamber experiments. Figures 1-7, 8 and 9 show the chamber experiment system used at coral sand area (Yates and Halley, 2006; Nakamura and Nakamori, 2009; Cyronak et al., 2013), and Table 1-1 summarizes the information of each chamber experiments.

With the systems shown in Figures 1-7 and 1-8, sand area was covered by a chamber and submarine pump was used to keep seawater homogeneous in the chamber. Thus, flow condition in actual environment can not be reproduced. With the system in Figure 1-9, although flux at sediment-water interface under several current conditions were observed, the simple relationship between carbonate dissolution and ocean acidification was not revealed due to ground water, which has higher A_T relative to seawater in water column. Also, actual natural hydrodyanamics caused by tidal and wave change can not be reproduced even if submarine pump was used to change advection in the chamber. Moreover, as all chamber experiments did not consider processes in sediment, it is hard to understand and estimate carbonate dissolution in sediment. Therefore, firstly, by using flow-controlled chamber experiment, dissolution rate under several flow conditions without ground water should be observed at several CO_2 levels. Secondly, another approach by which we can measure flux under natural condition and observation of vertical profiles of solutes should be challenged.

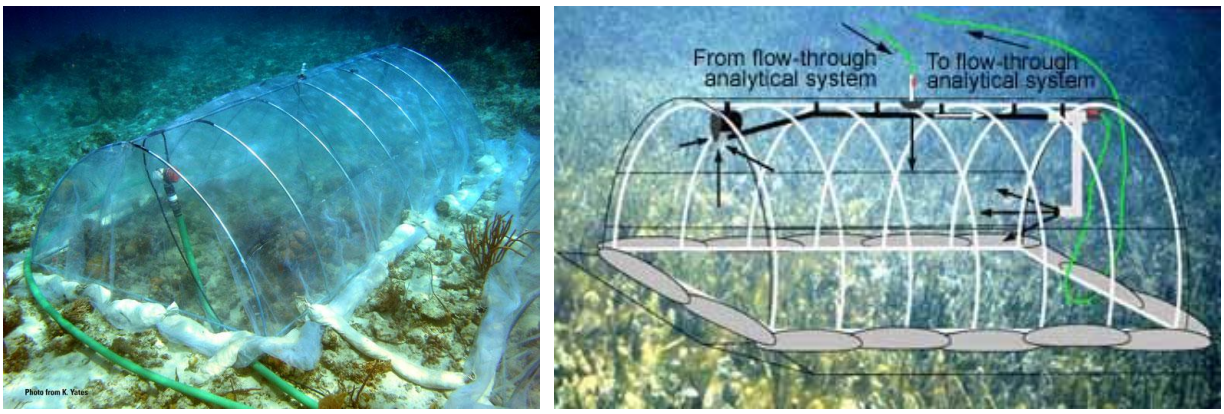

Figure 1-7. “SHARQ” (the Submersible Habitat for Analyzing Reef Quality) chamber system: Yates and Halley (2003, 2006) established “SHARQ” chamber system. “SHARQ” is a large, 4.9 (l) x 2.4 (w) x 1.2 (h)-meter, portable benthic incubation chamber designed to isolate a mass of water over the underlying substrate. A flow through analytical system enables continuous, 24-h monitoring of water chemistry resulting from benthic community processes. They conducted 24-h chamber experiments at Molokai reef, Hawaii. These pictures are cited from http://gulfsci.usgs.gov/tampabay/reports/

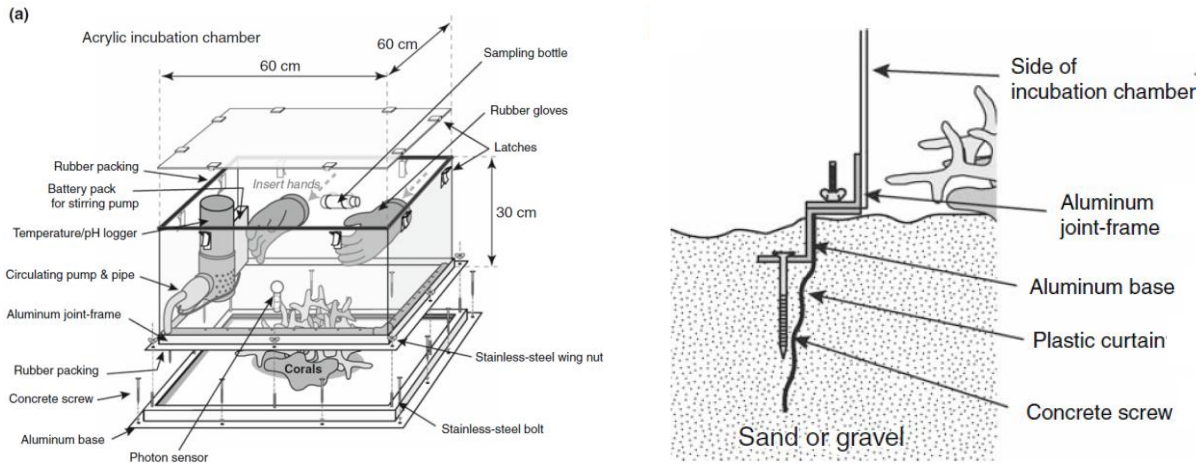

Figure 1-8. Schematic diagram of the incubation chamber (Nakamura and Nakamori, 2009): They measured dissolution/calcification and photosynthesis/respiration rate at Shiraho sand area, which is about 1000 m north to our study site.

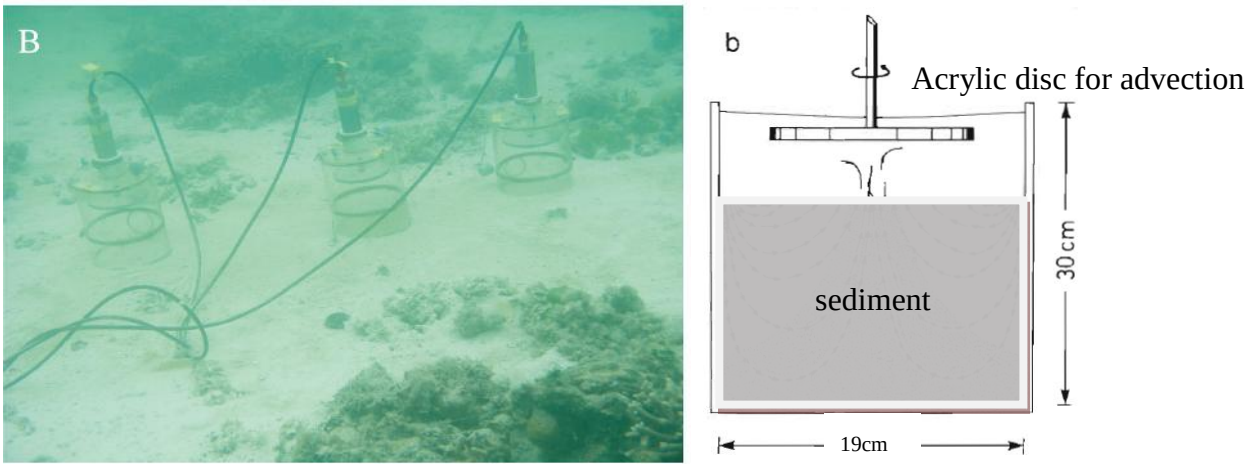

Figure 1-9. A photograph and schematic diagram of the incubation chamber (Cyronak et al., 2013): Chambers with an internal diameter (i.d.) of 190 mm and a height of 150 mm (Huettel and Gust 1992) were inserted into the carbonate sands distributed between outcrops of coral to retain a water column height of 190 to 240 mm. Advection was induced within the chambers based on the spinning rate of the acrylic disk within each chamber (diffusive, 40 rotation per minute (RPM), and 80 RPM). In order to maintain a homogeneous distribution of solutes within the diffusive chamber it was operated with the disk slowly spinning clockwise for one rotation, then, after a pause, spinning counterclockwise for the other rotation and repeating (Glud et al. 2008).

Table 1-1. Information of previous chamber experiment studies

Reference	Location	from the shore line (ground water effect)	flow change	hydrodynamics caused by tidal and wave change
Yates and Halley (2006)	Molokai reef	800m (no effect)	×	×
Nakamura and Nakamori (2009)	Shiraho	300m (less?)	×	×
Cyronak et al. (2013)	Heron Island	75m (large)	○	×

1-4-2. General theory of flux at sediment-water interface

The usual approach to calculate the flux of a dissolved species at the sediment-water interface is to treat all mixing processes in terms of diffusion coefficients in combination with Fick's First Law of diffusion for sediments (Berner, 1980), which is expressed as follows:

$$F = - D_T \, dC/dz + v \, C$$

, where F is the total (diffusive plus advective) flux, C is the concentration, z is the depth within the sediment, v is the unidirectional vertical flow relative to the sediment-water interface, and D_T is the total diffusion coefficient, which is defined as: $D_T = D_S + D_B + D_I + D_{wc}$ (i.e., the molecular diffusion (D_S), biodiffusion (D_B), irrigation (D_I), and wave and current induced diffusion (D_{WC}) coefficients, respectively; Figure 1-10).

In shallow water sediments, D_S is 10-100 times smaller than other diffusion coefficients (Berner, 1980), and the advection term vC can be ignored if no unidirectional strong flow such as ground water intrusion exists. This indicates that the dC/dz slope and the total diffusion coefficient D_T need to be evaluated in order to estimate the total flux (=F) at sediment-water interface, which requires field observations under natural hydrodynamic conditions. Since all chamber experiments did not consider processes in sediment as shown in the previous section 1-4-1, dC/dz slope and the total diffusion coefficient D_T under natural hydrodynamic conditions can not be estimated. Thus, field observation technique should be adopted. In the following section, Eddy Covariance technique (EC), which enables to measure oxygen flux at sediment-water interface under natural hydrodynamic conditions, will be introduced.

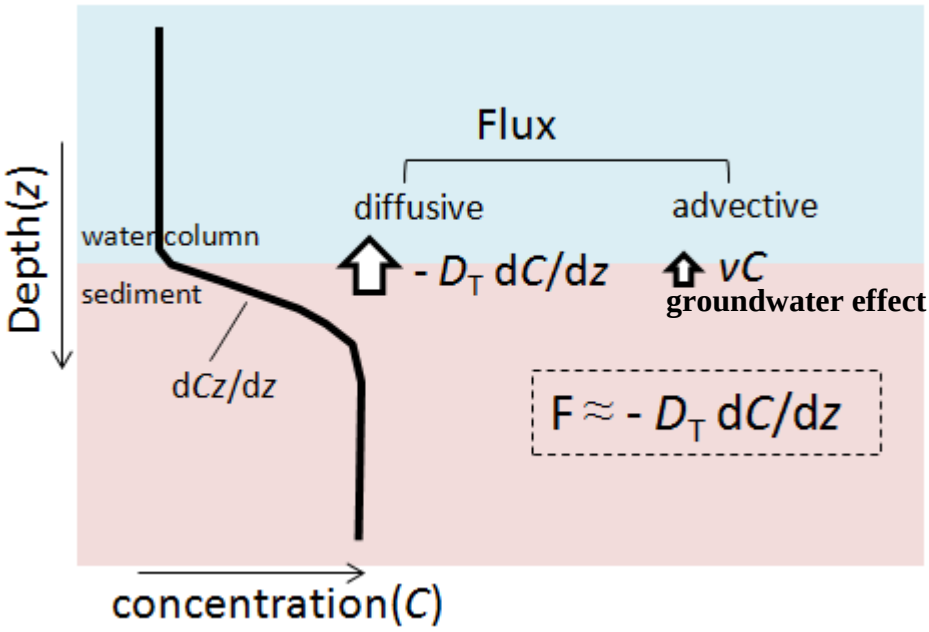

Figure 1-10. Illustration of fluxes of dissolved species at the sediment-water interface

1-4-3. Eddy Covariance and vertical profile of solutes in sediment

1-4-3-1. Outline of Eddy Covariance

Another technique to determine fluxes under natural condition is Eddy Covariance (EC). The method analyzes high-frequency current and scalar aquatic concentration data series, and yields values of fluxes of these high-frequency data (theory of EC will be explained in the following section). The EC technique has been employed previously to determine continuous CO_2 and water vapor fluxes within the atmosphere over an area of forest (Verma et al. 1986, Wofsy et al., 1993; Vermetten et al., 1994; Baldocchi et al., 2001), and to study O_2 dynamics within a shallow river bed, two lakes, a variety of near shore marine environments, a deep marine bay, and a coral reef (Berg et al., 2003, 2009; Kuwae et al., 2006; McGinnis et al., 2008; Brand et al., 2008; Berg and Huettel, 2008; Glud et al., 2010; Hume et al., 2011; Long et al., 2013). The advantages of EC are that (1) measurements can be made under natural light and hydrodynamic conditions, (2) sediments are not enclosed or disturbed, and (3) the fluxes derived using the EC method reflect the benthic O_2 exchange processes that occur over sediments with large surface areas (tens of square meters; Berg et al., 2007).

Berg et al. (2003) first applied EC to measure O_2 uptake fluxes under aquatic sediment conditions, and they compared fluxes with those measured by two different methods; *in-situ* chamber experiment and micro-profile method at muddy marine sediment (Aarhus Bay, Denmark). With micro-profiles method, flux at sediment-water interface was calculated by multiplication of gradient and molecular diffusion coefficient. The calculated O_2 uptake by the EC technique is shown in Figure 1-11, as with the result from the *in situ* chambers and from O_2 micro-profiles using the gradients in the diffusive boundary layer. Their data show that the significantly higher O_2 uptake was determined by EC technique than by chamber experiments and micro-profiles methods. Since these two methods tend to underestimate the

O_2 flux, they concluded that EC can overcome the disadvantages of the two conventional methods because of its (1) applicability for *in situ* measurements without creating artifacts (no alterations of in situ environment) and (2) lack of limitations regarding the nature of seabed characteristics such as sediment permeability, topography, and vegetation. The method is analogous to the measurement of near-bottom, turbulence induced heat and momentum fluxes often undertaken by physical oceanographers (e.g., Shaw and Trowbridge, 2001).

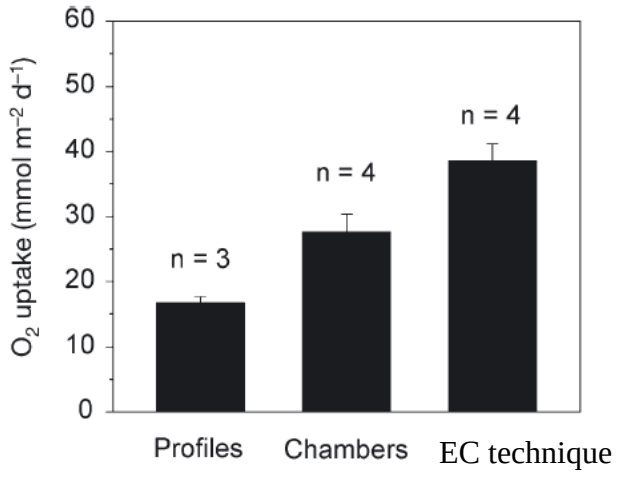

Figure 1-11. Mean (+1 SE) O_2 uptake by muddy marine sediment (Aarhus Bay, Denmark) determined by O_2 micro-profiles, *in situ* chambers and the EC cited from Berg et al. (2003)

1-4-3-2. Theory of Eddy Covariance

The theory of eddy covariance (EC) was explained by previous studies (Berg et al. 2003, Kuwae et al. 2006, Burba and Anderson 2010). The mathematical expression for advection and molecular diffusion used to evaluate vertical O_2 flux at sediment-water interface is expressed as follows:

$$O_2 \text{ Flux} = U_z \times C - D_s \, dC/dz \quad (1\text{-}7)$$

where U_z is the vertical velocity of water, C is the concentration of O_2 in water, D_s is the molecular diffusivity of O_2 in water, and z is the vertical coordinate (e.g. Berner 1980, Boudreau1997). Figure 1-12 shows the illustration of vertical flux and each parameter. In almost all natural aquatic environments, turbulent advection mainly caused by bioturbation, irrigation, wave and current is the dominant mode of vertical transport within the water column relative to the molecular diffusion at sediment-water interface, meaning that the second term in Eq. (1-7) about molecular diffusion, can be neglected. In addition, modeling of turbulent motions commonly separates instantaneous values of Uz and C into two components: $\overline{U_z} + U'_z$, and $\overline{C} + C'$, where $\overline{U_z}$ and $\overline{C}$ are the mean vertical velocity and concentration of O_2, respectively, and U'_z and C' are the vertical turbulent fluctuating velocity and turbulent fluctuating concentration of O_2 (e.g. Reynolds 1895, Boudreau 1997), respectively. This means that equation (5-1) can be converted to

$$O_2 \text{ Flux} = \overline{(\overline{Uz} + Uz')(\overline{C} + C')} \quad (1\text{-}8)$$

which expands to

$$O_2 \text{ Flux} = \overline{\overline{Uz}\,\overline{C} + \overline{Uz}\,C' + Uz'\overline{C} + Uz'C'} \quad (1\text{-}9)$$

As the averaged deviations from the average are removed (because averaged deviation from an average is zero), equation (1-9) can be simplified to

O_2 Flux = $\overline{\overline{Uz}\,\overline{C} + Uz'C'}$ (1-10)

which, combined with a negligible mean vertical current for a horizontal homogeneous field without divergence or convergence, means that equation (1-10) can be simplified as:

O_2 Flux = $\overline{Uz' \times C'}$ (1-11)

Consequently, the O_2 flux can be estimated by measuring these two fluctuating components, meaning that high-temporal-resolution Uz' and C' data are needed, ideally at a frequency of 15-25 Hz (Berg et al. 2003).

If A_T flux at sediment-water interface can be observed by EC directly, it is simple and appropriate because carbonate dissolution increases A_T while other typical reactions such as photosynthesis or respiration do not change A_T. However, EC cannot be directly applied to A_T values, primarily because there is no available A_T sensor that is able to detect such a high time resolution variations although high-resolution temporal variations in oxygen abundances can be determined using micro-electrodes. In this study, I consider diffusion coefficient measured by DO can be applied to that of A_T, because it is mainly determined by hydrodynamics such as current or flow and bioturbation. This means that estimation of A_T fluxes under natural flow conditions requires the determination of oxygen diffusion coefficients using the flux and concentration profile of O_2 within the sediment. This must be performed with determining the A_T profile through the sediment and applying this profile to the diffusion coefficient, thereby enabling the estimation of A_T fluxes under natural flow conditions.

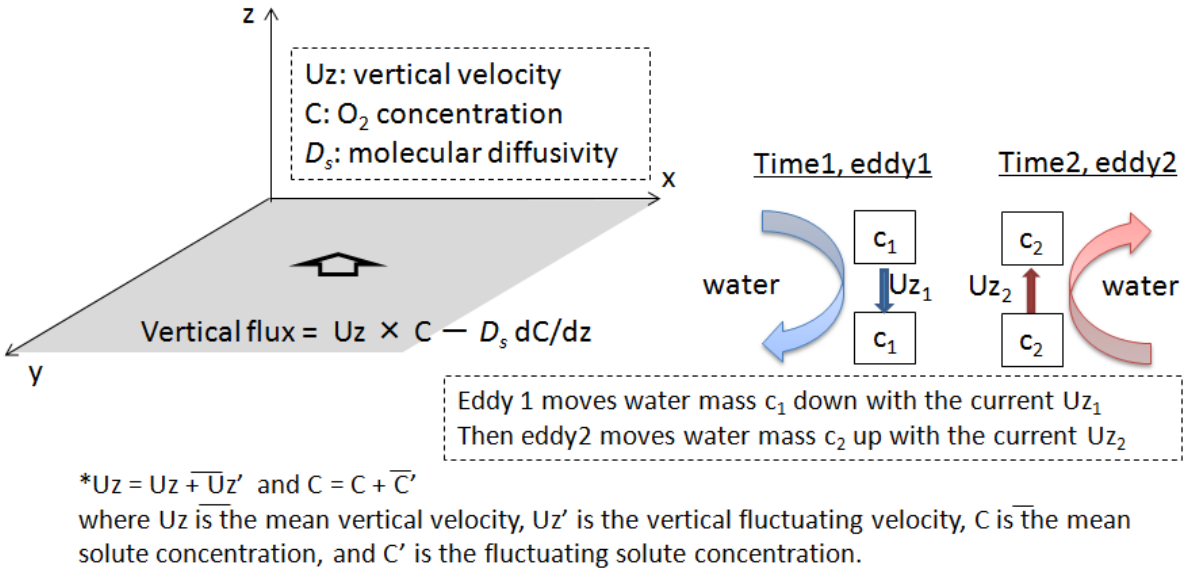

*Uz = Uz + $\overline{Uz}$' and C = C + $\overline{C}$'
where Uz is the mean vertical velocity, Uz' is the vertical fluctuating velocity, C is the mean solute concentration, and C' is the fluctuating solute concentration.

Figure 1-12. Illustration of vertical flux and parameters

1-4-3-3. Vertical profile of solutes in sediment

Figure 1-13 shows a schematic vertical profiles of pore water chemistry on continental margins (Sarmiento and Gruber, 2006). Remineralization of organic matter by aerobic respiration consumes oxygen and proceeds through a series of steps that produce several remineralized inorganic chemicals, including nitrate. The production of nitrate increases concentration of nitrate in the pore water with depth in the zone where oxygen decreases. However, at about the depth in the sediments where oxygen runs out, the nitrate concentration begins to decrease. Properties of pore water are altered by remineralization of organic matter and dissolution/precipitation and adsorption/desorption of chemicals. These chemical and biological processes create large concentration gradients of O_2, NO_3^-, etc. between the pore water and the overlying seawater, and those gradients varied depending on flow condition, permeability, mineral composition, organisms in sediment and time.

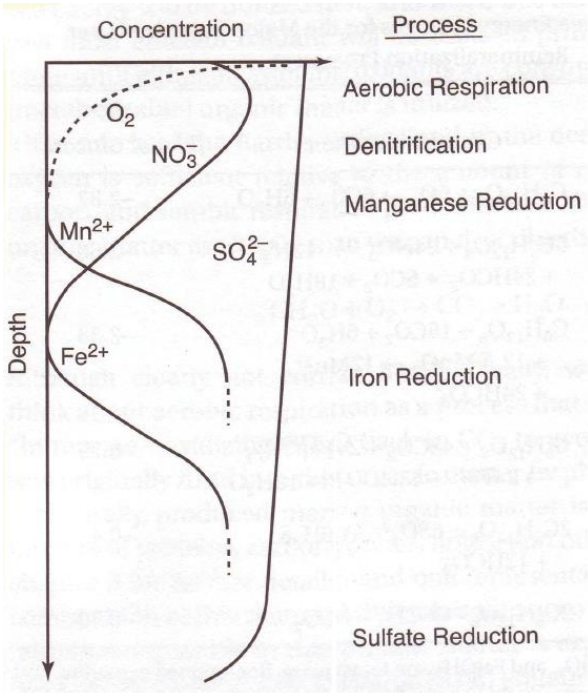

Figure 1-13. Schematic vertical profiles of reactants and products of remineralization reactions in sediments. Also shown are the reduction process zones cited from Sarmiento and Gruber (2006)

Carbonate profiles in coral reefs were measured by previous studies (Alongi et al., 2006; Hu and Burdige, 2007; Burdige et al., 2008; Rao et al., 2012). For permeable sand area in a coral reef, Rao et al. (2012) showed pH, O_2, calcium, and A_T profiles in sediment at Heron Reef, Australia (Figure 1-14). Oxygen and pH profiles were measured by micro electrode, and calcium and A_T were measured by pore water sampling. They revealed the vertical profile of those parameters, and discussed the photosynthesis and respiration rate. However, time series changes in O_2 and A_T were not discussed because there were few *in-situ* profiles data. Moreover, Mg-calcite dissolution was not focused on at all. In order to estimate Mg-calcite dissolution, vertical and time series change in A_T must be revealed.

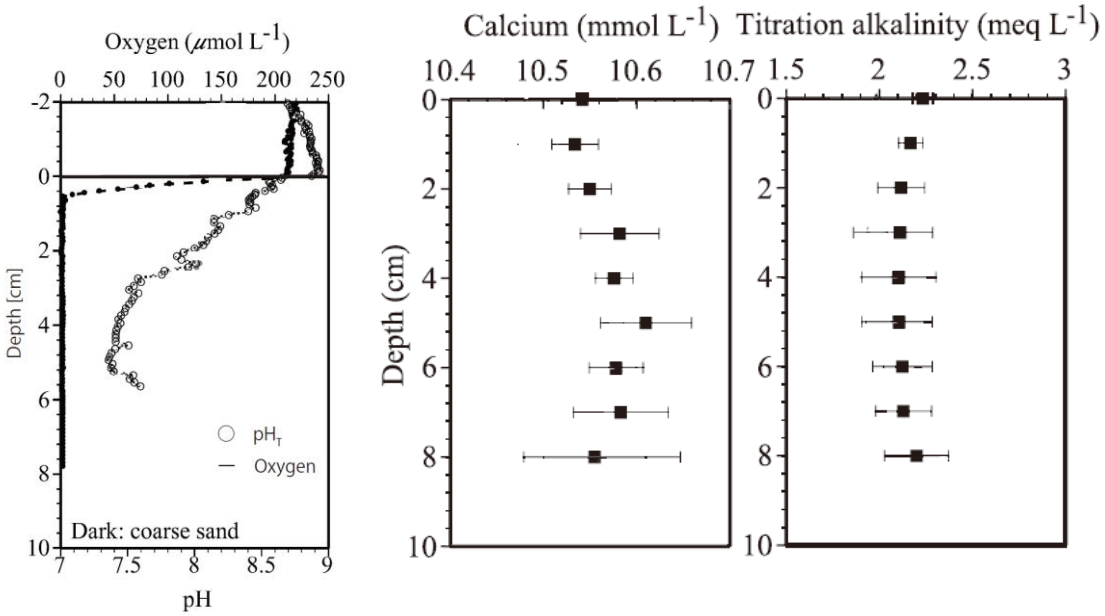

Figure 1-14. Oxygen and pH profiles measured by micro electrode, and calcium and A_T measured by pore water sampling in Heron Reef sediments cited from Rao et al. (2012). Oxygen and pH were measured at night. Symbols of calcium and A_T were the mean $\pm$ 1 SD of replicate profiles of calcium and A_T (n = 3).

1-5. Purposes of this study

In order to evaluate Mg-calcite dissolution in coral reef, which will be the first reactor to the ocean acidification, threshold of various biogenic Mg-calcite dissolution and the relationship between kinetic dissolution rate and Ω_a must be resolved in laboratory experiment at first. Then, exact dissolution rate at sand area under natural condition should be understood because sand area in coral reefs consists mainly of biogenic Mg-calcite, which occupies large proportion in coral reef. To achieve this purpose, two approaches are taken. One is a chamber experiment which can reproduce flow condition. The other is the measurement of A_T profile in sediment and the estimation of diffusion coefficient based on O_2 profile and O_2 flux observed by EC. At last, the mechanism of Mg-calcite dissolution at coral sand area will be examined and future impact against ocean acidification will be predicted.

In Chapter 2, study site and the characterization of sand were described. All field observations were conducted at the Shiraho reef, Japan, and samples used by laboratory experiments also were collected at Shiraho reef. In Chapter 3, laboratory experimental system was established, and threshold of biogenic Mg-calcite dissolution and relationship between kinetic dissolution rate and Ω_a was clarified. In Chapter 4, a flow-control chamber system constructed to measure dissolution rate under reproduced *in-situ* flow conditions was explained. Closed chamber experiments were conducted under several flow rates and pCO_2 levels. In Chapter 5, diffusion coefficient of O_2 at sediment-water interface was calculated from O_2 flux measured by EC and concentration profile of O_2 in sediment. Using this value and A_T profile in sediment, A_T flux at sediment-water interface was estimated. In Chapter 6, results of laboratory experiment and field observation were summarized and mechanism of Mg-calcite dissolution at sand area was discussed.

Chapter 2.

Study site and property of sediment

2-1. Study site

Field observations, experiments and sampling were conducted at Shiraho reef (24°22′N, 124°15′E) on the southeast coast of Ishigaki Island, SW Japan (Figure 2-1) in 2007, 2010, 2011 and 2012. The study area is a fringing reef with a reef flat 850 m wide from the shore to the reef edge, with reef crests exposed during low tides, separating seawater on the reef from the outer ocean and resulting in a semi-closed system for 2-5 hours each tidal cycle.

Kayanne et al. (1995) first reported diel patterns of CO_2 changes within reef water at the Shiraho reef, indicating that the reef flat area is a net sink for atmospheric CO_2. They also studied CO_2 dynamics in this area for a year, showing that pCO_2 levels in the reefs were governed by seasonal changes in sea surface temperature (SST) and metabolic processes, as well as by the status of coral reefs (as represented by coral coverage; Kayanne et al. 2005). Nakamura and Nakamori (2009) measured diurnal variations in photosynthesis and respiration (organic production) and calcification and dissolution (inorganic production) within sandy areas, seagrass meadows and coral areas using a closed chamber at the Shiraho reef. These data enabled Watanabe et al. (2013) to develope a carbonate system dynamics (CSD) model for the Shiraho reef; this model indicated large spatiotemporal differences in CO_2 sinks and sources. The abundant carbonate chemistry data for the Shiraho reef means that this area has become a representative site for the study of coral reef carbonate systems.

The organic and inorganic productivity in sandy parts of the study area has yet to be measured, primarily as these areas have low productivity values relative to coral or seagrass areas; however these areas have highly sensitive to ocean acidification, primarily as they are dominated by biogenic Mg-calcite (Andersson et al., 2009). In addition, these sandy areas are three times as large as the coral habitats (Kayannne et al., 2005), indicating that the inorganic dissolution within sandy areas must be considered in order to understand and evaluate carbon cycles within the Shiraho reef.

Suzumura et al. (2002) measured chlorophyll a (Chl a) concentrations in surface carbonate sediments at Shiraho reef sandy area, and reported that sediments had an enriched population of Bacillariophyta (diatoms). Also, they clarified that diatoms were dominant, particularly representatives of the genera *Amphora*, *Nitzschia*, and *Navicula* by microscopic observation of the sediment sample. From my observation conducted on July 2013, polychaete and nematode were observed with a dry weight of 1.2 g in 800 g of bulk sediment. Surface of the sediments were usually flat except soon after typhoon. Our sampling and observation were not affected by typhoons.

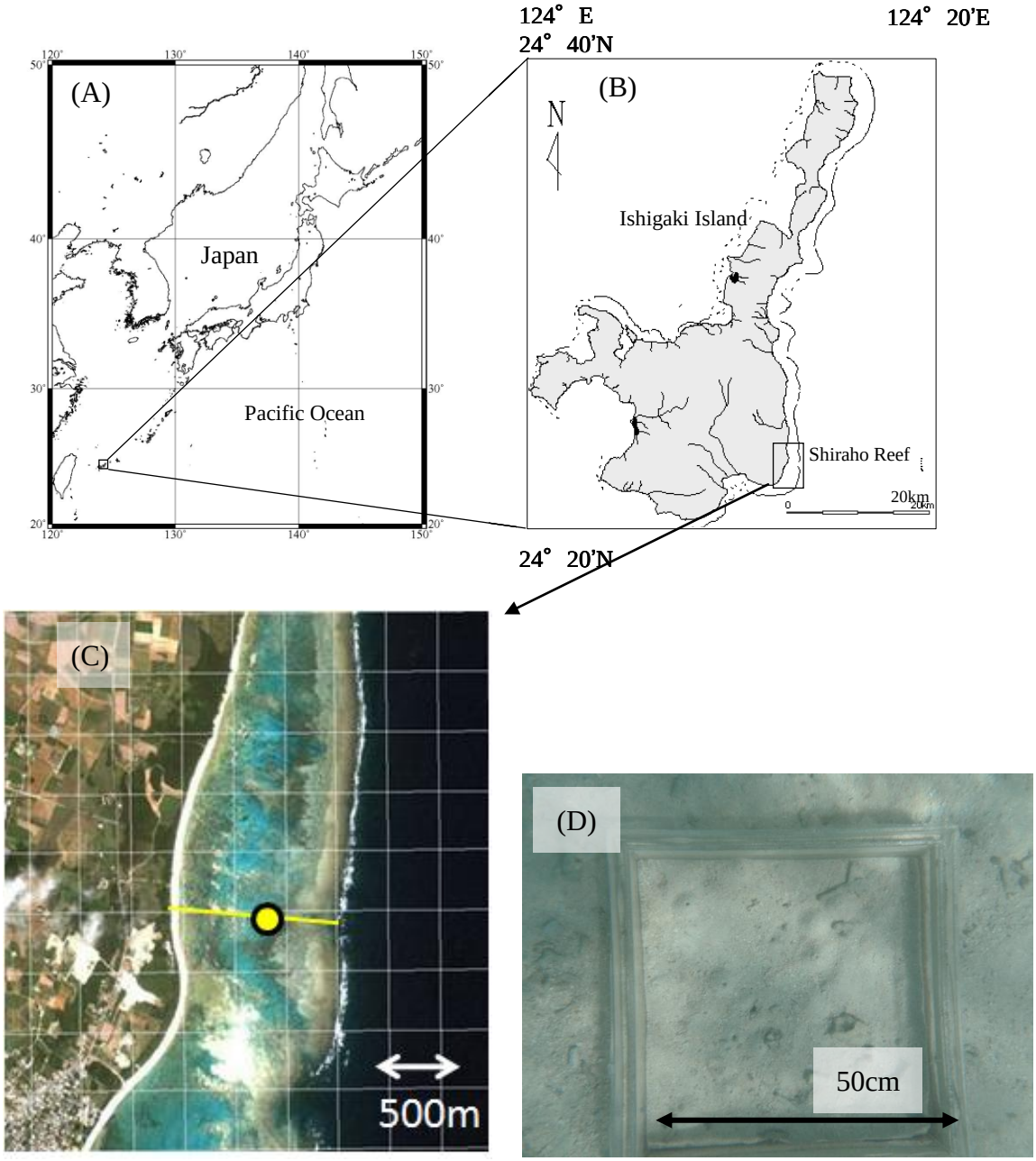

Figure 2-1. Location and aerial photograph of the study site: All field observations were conducted at yellow point. (D) No sea grass and no coral lived in sand area .

2-2. Property of sediment

All the observations, experiments and sampling were conducted at the point 600 meters to the east from the shoreline, in the center of a typical sand area of the shallow lagoon (yellow point in Figure 2-1), where the effect of ground water is minor and neglected.

2-2-1. Size fraction, permeability and porosity

Figure 2-2 shows the composition of size fraction, which were measured by using -2~3 ϕ sieves. The error bars indicate the standard error (SE) for seven dry sieve measurements. The dominant size fraction of the coral reef sediment in the study area is from –1.0 to 0.0 ϕ (1-2 mm), forming 45.6 % of the overall sediment (Figure 2-2). The permeability and porosity of these sediments are 2.88 ± 0.01 × 10^{-3} m s^{-1} (n = 3) and 0.354 ± 0.001 (n = 4) respectively. The permeability was measured based on constant head method and the porosity was calculated by water content and sediment density. These two analyses were performed at Port and Airport Research Institute in Kurihama.

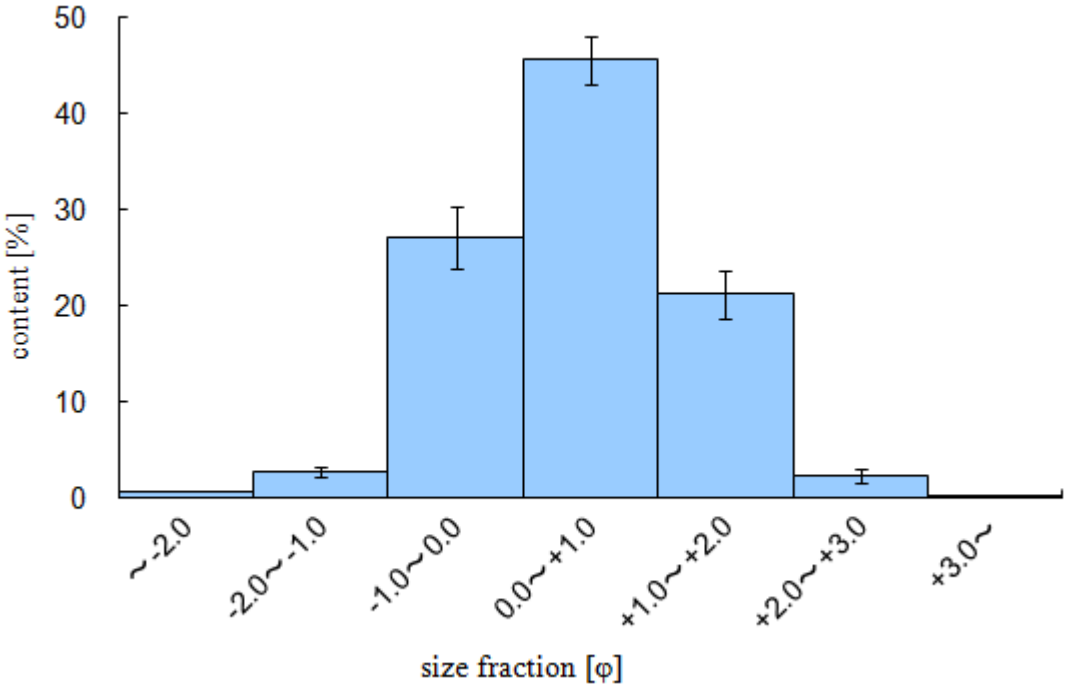

Figure 2-2. Result of size fraction of bulk sediment. Bulk sediments were collected at Shiraho reef sand area and were measured by using -2~3 ϕ sieves.

2-2-2. Mineralogy

The mineralogy was identified by dyeing method and X-ray diffraction (XRD) analysis. These two analyses are explained as follows.

The composition of the sediment samples was determined for 837 sand grains with sizes between 1.0-2.0 mm. Firstly they were boiled and dyed with $Co(NO_3)_2$ for 20 minutes. Since only aragonite crystal becomes redpurple, it is easy to identify aragonite (Friedman 1959). After sand grains were identified by using a stereoscopic microscope, the compositions were calculated by weight, which was measured by an electronic balance (MC5, Sartorius KK). Table 2-1 and Figure 2-3 show the results. More than 40 % of the sediment samples consisted of foraminifera.

The $MgCO_3$ contenst for foraminifera and coralline algae were estimated by the position of the peak X-ray strength (Goldsmith and Graf, 1958), which was measured by the X' Part Pro X-ray diffractometer (Panalitycal) with Cu target. The tube voltage of 45 kV, the tube current of 40 mA, the scanning interval of 20 to 35° 2θ, the time per step(s) of 19.685, and scan speed (°/s) of 0.0167 were used. Table 2-2, Figures 2-4, 5 and 6 show the result of XRD. Foraminifera and coralline algae are calcite crystal system, whose peaks are between calcite and dolomite, suggesting that they are Mg-calcite. The magnesium contents of the coralline algae and foraminifera were 16.5 ± 0.4 and 13.3 ± 0.4 mole%, respectively, and the coral was pure aragonite.

Table 2-1. Resuls of weight and grain number: 837 sand grains with sizes between 1.0-2.0 mm were counted and weighted. Measured weight had ±0.0001g.

	weight[g]	count	[%]
Coral	0.5901	120	16.9
Shell	0.2648	60	7.6
calcareous algae	0.0650	25	1.9
other aragonite	0.0653	11	1.9
Foraminifera	1.4592	415	41.7
coralline algae	0.1809	40	5.2
sea urchin	0.0949	16	2.7
Others	0.7758	150	22.2
Total	3.4960	837	100

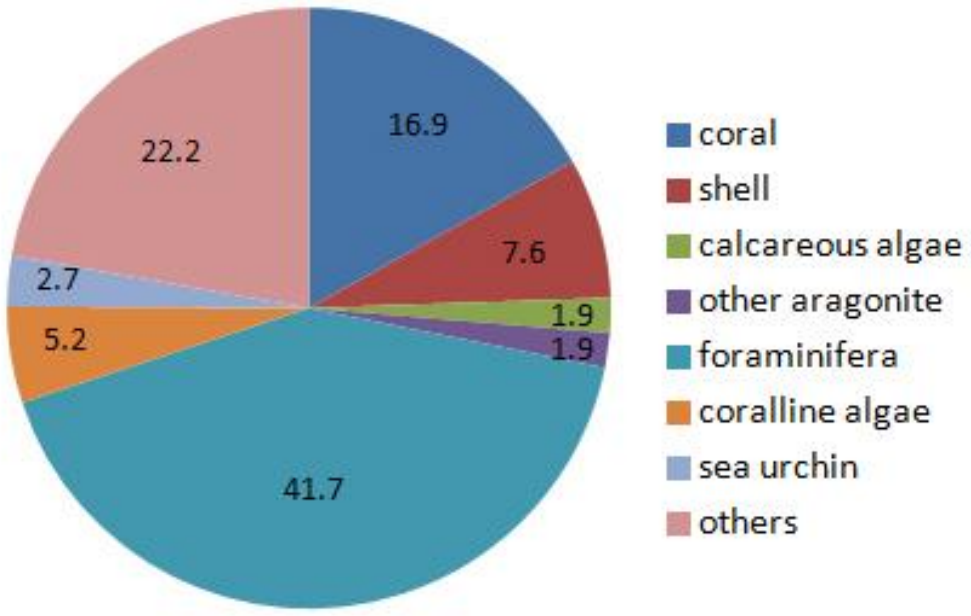

Figure 2-3. Weight composition of sediment samples (%). Sand granis were indentified by dyed with $Co(NO_3)_2$ and using a stereoscopic microscope

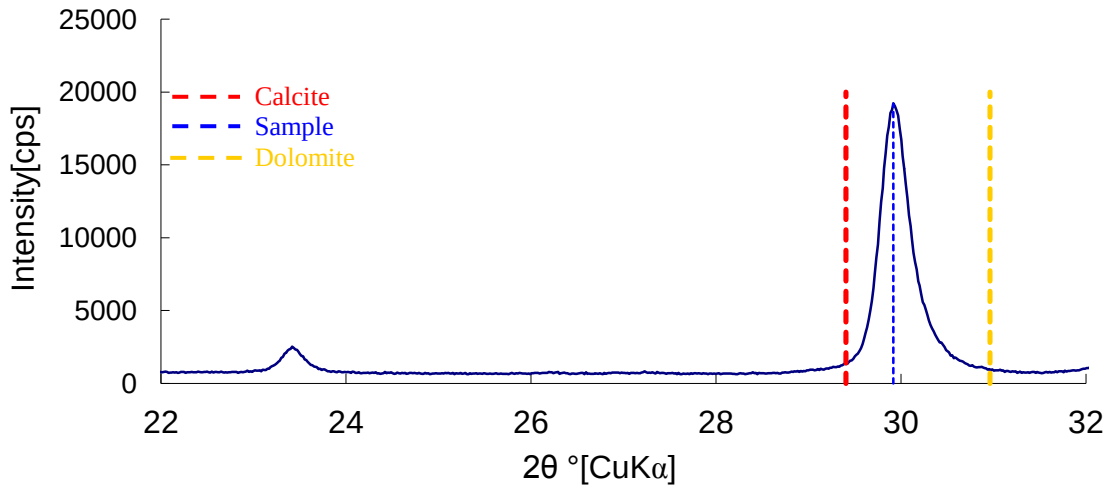

Figure 2-4. Result of XRD (coralline algae). Blue solid line shows the coralline algae result, blue dashed line shows peak position of coralline algae, yellow dashed line shows dolomite peak position, and red dashed lines shows calcite peak position. Mg content was calculated by these three peak positions.

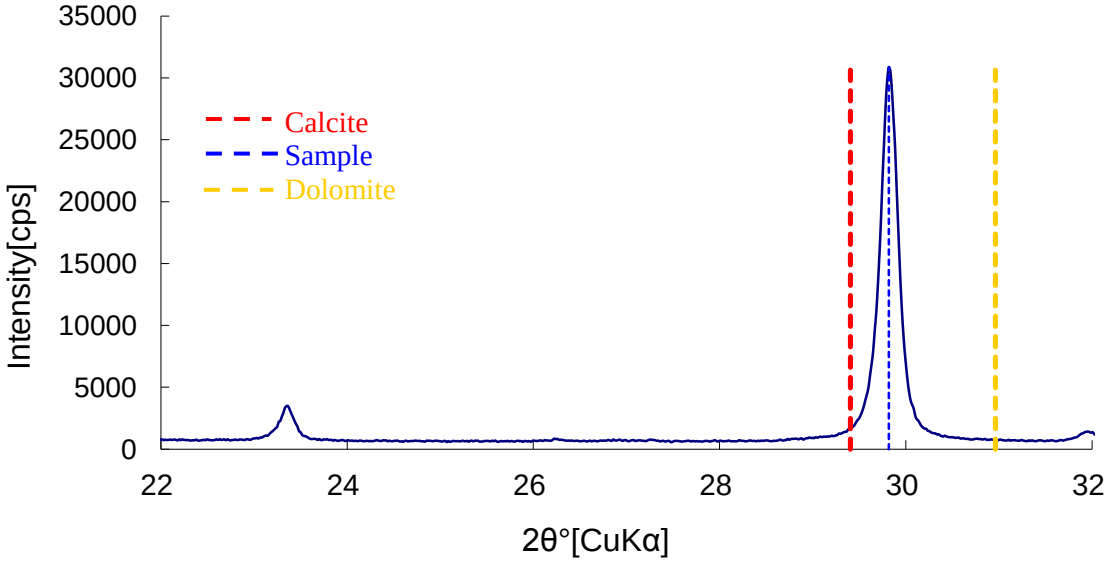

Figure 2-5. Result of XRD (foraminifera). Blue solid line shows the foraminifera result, blue dashed line shows peak position of foraminifera, yellow dashed line shows dolomite peak position, and red dashed lines shows calcite peak position. Mg content was calculated by these three peak positions.

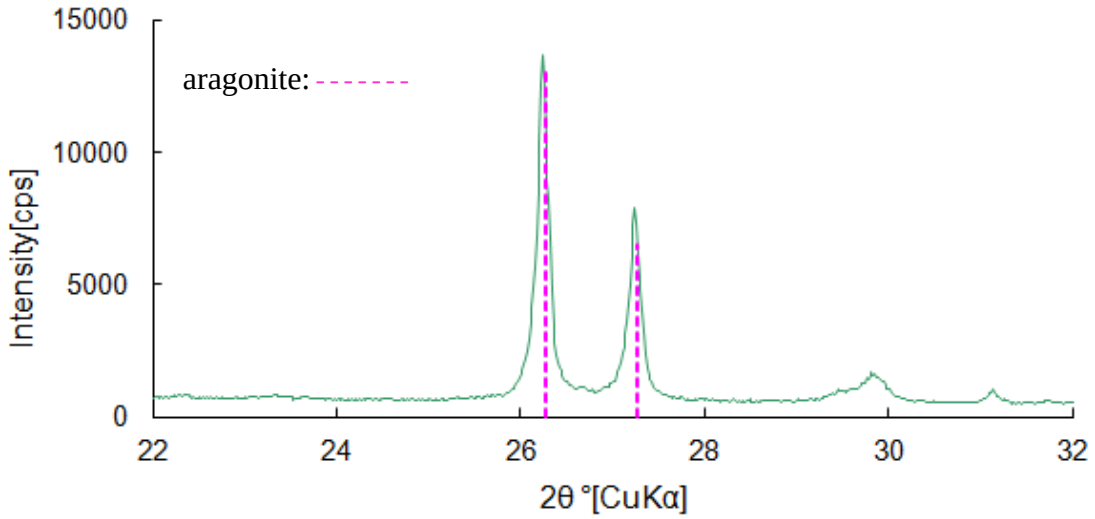

Figure 2-6. Result of XRD (coral). Green line shows the result of coral sample. Two purple dashed lines show aragonite peak positions, suggesting that coral sample is pure aragonite

Table 2-2. $MgCO_3$ content for coralline algae and foraminifera, which were calculated by calcite and dolomited peak positions.

sample	2θ	$MgCO_3$ content
coralline	29.918	16.5±0.4mole%$MgCO_3$
foraminifera	29.818	13.3±0.4mole%$MgCO_3$
Calcite	29.407	0mole%$MgCO_3$
Dolomite	30.961	50mole%$MgCO_3$

2-2-3. Specific surface area

Specific surface area (SSA) was analyzed by Brunauer–Emmett–Teller (BET) method using Gas Adsorption Appratus (BELSORP 28SA, BELL Japan INC) at National Institute of Advanced Industrial Science and Technology in Tsukuba. The BET method is widely used for the calculation of surface areas of solids by physical adsorption of gas molecules (Brunauer et al. 1938). Physical adsorption of gas molecules were calculated by the difference of pressure, and high-resolution capacitance manometer was used to measure it. SSA of bulk sediment, foraminifera, coralline algae, coral (before experiment), and coral (after dissolution experiment) were 0.72, 0.93, 2.10, 1.50, and 1.30 m^2 g^{-1} respectively. Errors of SSA measurements were better than 1%.

Chapter 3.

Threshold of Mg-calcite dissolution determined by laboratory experiment

3-1. Introduction

The dissolution of $CaCO_3$ is usually described by higher-order reaction rate law with respect to undersaturation: (1-Ω) and Ω_a is generally used for index of ocean acidification (Gattuso and Hansson, 2011). In order to clarify the relationship between Ω_a and the rate of Mg-calcite dissolution, I measured the dissolution rate of aragonite from a coral (*Porites* sp) and Mg-calcite excreted by several organisms under conditions of $\Omega_a > 1$, using an experiment system that controlled pCO_2 in seawater. Ω_a threshold of biogenic Mg-calcite dissolution calculated by total alkalinity (A_T) and dissolved inorganic carbon (C_T) was measured.

3-2. Methodology

3-2-1. Experimental design

In order to predict the effect of Mg-calcite dissolution against ocean acidification, knowledge of the relationship between biogenic Mg-calcite dissolution rate and Ω_a is essential. Most of the previous studies focused not on biogenic Mg-calcite in nature but on pure minerals (Morse et al. 2007). Moreover, the experimental conditions such as flow rate, the way how to add pCO_2 in seawater, sample treatment and mineralogy were differed from actual environment. Here, I designed an experimental system with conditions matching those of a natural coral reef. Carbonate sediments were collected from Shiraho reef and prepared with minimal treatment (ultrasonic cleaning and drying). Natural seawater was used for the dissolution experiment and the Ω_a value of the seawater was controlled by CO_2, rather than by HCl or NaOH.

The experimental system (Figure 3-1) consists of four components: a seawater tank, a dissolution chamber, a CO_2 gas unit, and a flow-through analyzer for A_T and C_T. The experimental procedure is described below.

First, CO_2 gas (420 to 2210 ppm) levels were prepared using the CO_2 gas unit, imitating CO_2 conditions similar to those close to the present day (420 ppm), 2 × pre-industrial levels (~560 ppm), 4 × pre-industrial levels (~1120 ppm), and 8 × pre-industrial levels (~2240 ppm). Seawater in the tank was circulated through the seawater line (bypass line) for 10 to 12 hours to allow the seawater and introduced CO_2 to equilibrate. The pCO_2 in seawater in the tank was checked with a non-dispersive infrared gas analyzer (NDIR, LI-COR, LI-820) during the experiment. After the pCO_2 had stabilized, A_T and C_T were determined using the flow-through analyzer (Kimoto Electric Company Limited) before the experiment began. About 10g of samples were placed in the dissolution chamber (600ml), and seawater was circulated through

the seawater line (dissolution line). The flow rate was about 5 cm s^{-1}. A_T and C_T were measured again after several hours, both in the middle and at the end of the experiment. The experiment was performed as a time series, and A_T and C_T were analyzed periodically through its duration (~1.5 h).

The conditions for each experiment are listed in Table 3-1. Temperature in the incubator was maintained at 26 °C and the dissolution experiment was performed at seven different pCO_2 levels for bulk sediment, four levels for coralline algae and foraminiferans, and three levels for coral.

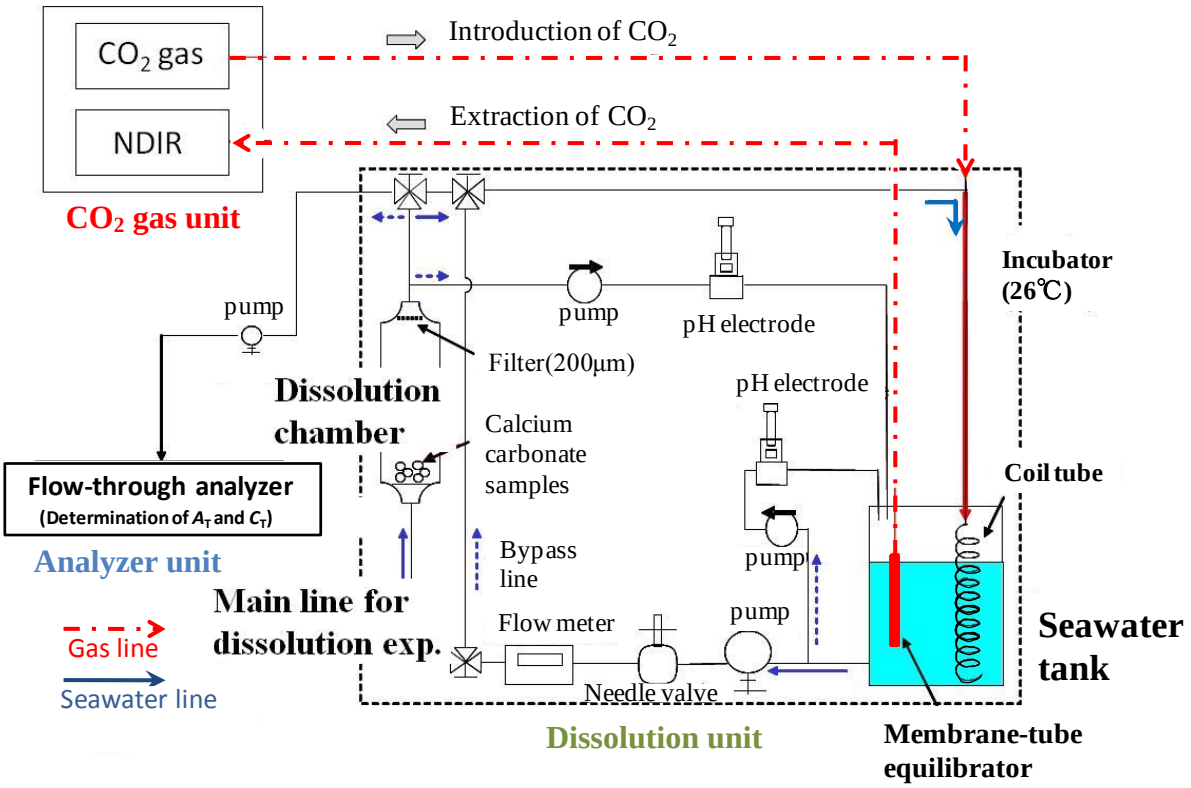

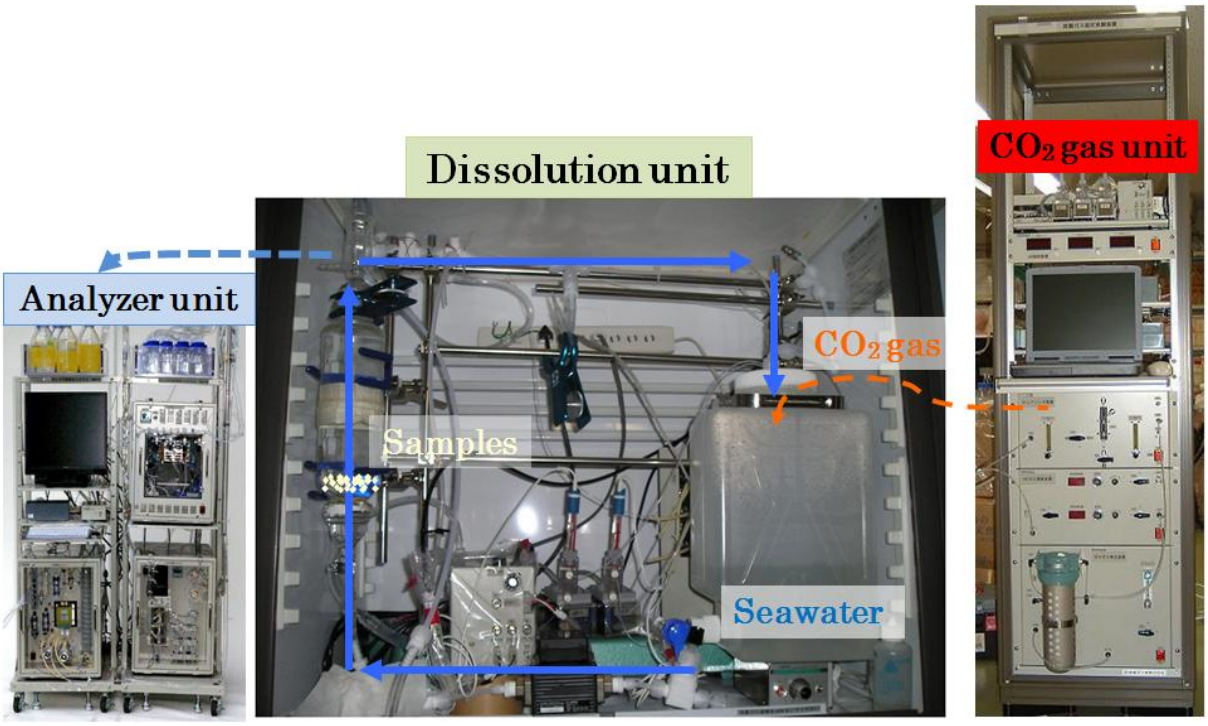

Figure 3-1. Schematics and photographs of laboratory experiment. Experiment systems consist three units: CO_2 gas unit, dissolution unit, and analyzre unit.

Table 3-1. Condition for each experiment

Samples	Incubator temperature	seawater : sample ratio (by weight)	pCO_2 [ppm]	Ω_a
Bulk sediment	26°C	310:1	420 , 590 , 750 , 820 , 1110 , 1290 , 2030	3.5 , 2.9 , 2.5 , 2.4 , 1.9 , 1.7 , 1.2
Coralline algae	26°C	310:1	570 , 830 , 1070 , 2000	2.9 , 2.3 , 1.8 , 1.2
Foraminifera	26°C	310:1	510 , 570 , 1240 , 2210	3.2 , 2.9 , 1.7 , 1.1
Coral	26°C	310:1	1070 , 1550 , 2100	1.9 , 1.6 , 1.1

3-2-2. Specification of system components

Seawater tank: CO_2 gas was introduced to the seawater by using a 3.5 m coiled tube with a single small hole to allow for bubbling and equilibration (Figure 3-1). The coiled tube is made of fluorocarbon polymers and is a closed system. Seawater pCO_2 in the tank was monitored continuously by using a membrane tube and NDIR (Non Dispersive InfraRed) similar to the system used by Saito et al. (1995).

Dissolution chamber: By using a pump, seawater was introduced to the dissolution chamber (600 ml) from the seawater tank. Carbonate samples for dissolution experiments were placed in this chamber. Mesh filters (200 μm) were affixed to both sides of the chamber to prevent loss of samples.

CO_2 gas unit: Gas mixtures of CO_2 at concentrations between 420 and 2210 ppm were prepared by mixing CO_2 free gas, which passed through soda lime traps to remove trace CO_2, with pure CO_2 using two mass flow controllers, and then dissolved in seawater. The gas flow rate monitored in CO_2 gas unit was 400 ml min^{-1} in all experiments.

Flow-through analyzer: The sample seawater was introduced directly to the flow-through analyzer (Kimoto Electric Company Limited) by switching the flow line (Kimoto et al., 2001; Watanabe et al., 2004). Certified reference materials (A. Dickson, University of California) were used to calibrate the system. Sodium carbonate solutions were used for the C_T calibration. The analytical accuracies of A_T and C_T were within 3 μmol kg^{-1} and standard deviations of A_T and C_T were 1.1 μmol kg^{-1} and 2.1 μmol kg^{-1} respectively (Kimoto et al., 2002; Watanabe et al., 2004). Since seawater was removed to measure A_T and C_T, water volume during experiment decreased as experiment went on. The seawater volume during the experiment was reported in Supplementary Table 1, and was taken into account for calculating dissolution rate.

3-2-3. Sample treatment

For the dissolution experiment, commercially available seawater (Nihon-Aquarium-Service Co., Ltd.) collected from a depth of 500 m at 34.7°N, 139.4°W (near Izu Islands, Japan) and sterilized by UV rays was used for preservation. The seawater was filtered using a 0.45 μm capsule filter. Carbonate samples used were coral, foraminifera, coralline algae, and bulk sediment sampled from Shiraho reef. The sediments were collected from the surface sediment layer using a scoop in August 2007, and the coral, foraminifera and coralline algae in October 2007. Samples were cleaned in an ultrasonic bath sonicator and dried at 40 °C for about 12 h. Chemical sterilization was not conducted so as not to destroy the micro structure.

3-2-4. Calculation

The A_T of seawater increases by 2 moles for every 1 mole of calcium carbonate dissolution. The carbonate dissolution rate is measured by analyzing the change in A_T. Salinity changes also affect the A_T. Salinity change was caused by the evaporation due to (1) dry gas introduced from CO_2 gas unit and (2) decrease in seawater volume in the dissolution unit. Figure 3-2 shows time series of A_T without and with two salinity correction models. Since there were no samples and only seawater in dissolution unit, no A_T change should have been observed. However, A_T without salinity correction increased with time. Thus, salinity correction should be made. Dry gas flow calibration was calculated according to the relationship between gas flow and salinity change (Table 3-2). Seawater volume calibration was conducted assuming that no A_T changes were occurred with time in Figure 3-2. Seawater volume calibration was simply calculated by duration time because seawater volume was considered to decrease with duration time. Figure 3-3 shows the both calibration results and there are no significant differences. Since seawater volume were variable among each experiment condition and the change in nA_T (normalized total alkalinity) according to dry gas flow calibration was about 2 to 3 μmol kg^{-1}, a value within the error range of the measurement as mentioned in 3-2-2, dissolution rate in this study was calculated by gas flow correction. Using equation (3-1), A_T was standardized to a constant salinity, and the dissolution rate was then calculated:

$$nA_T = A_T \times S_{average}/S_{sample} \qquad (3\text{-}1)$$

where nA_T is the normalized total alkalinity (μmol kg^{-1}), representing the total alkalinity standardized to the salinity; $S_{average}$ is the average salinity during all the experiments; and S_{sample} is the calibrated salinity according to Table 3-2. C_T was also standardized to salinity, and nC_T (normalized dissolved inorganic carbon, μmol kg^{-1}) was obtained. Salinity was

measured using a salinometer (PORTASAL 8410A, Guildline Instruments Limited). IAPSO (International Association for Physical Sciences of the Ocean) standard seawater was used for calibration. The precision of salinity analysis is ± 0.003.

Dissolution rates were calculated as follows:

$$R = \Delta n A_T/2 \times m_W \times M \times 100/(m_s \times t) \qquad (3\text{-}2)$$

where $\Delta n A_T$ is the difference in $n A_T$ over the course of the experiment, m_W is the weight of seawater, M is the molecular weight of calcium carbonate (=100), m_s is the average weight of the carbonate sample over the course of the experiment, and t is the duration of the experiment. Due to the design of the system, a small amount of seawater remains in the pump and tubes at the end of each run. However, only a small amount of seawater (10 ml = less than 0.5% of total volume) was remained in the pump at the end of each experiment, and this was corrected for when determining the mass balance of A_T.

Seawater fugacity of CO_2 (fCO_2) and Ω_a values were calculated from A_T, C_T, seawater temperature, and salinity, using the calculation program CO2sys (http://cdiac.esd.ornl.gov/oceans/co2rprt.html; DOE, 1994). The total scale for pH was used in all calculations, employing the equilibrium constants (K_1 and K_2) reported by Mehrbach et al. (1973; refit by Dickson and Millero, 1987).

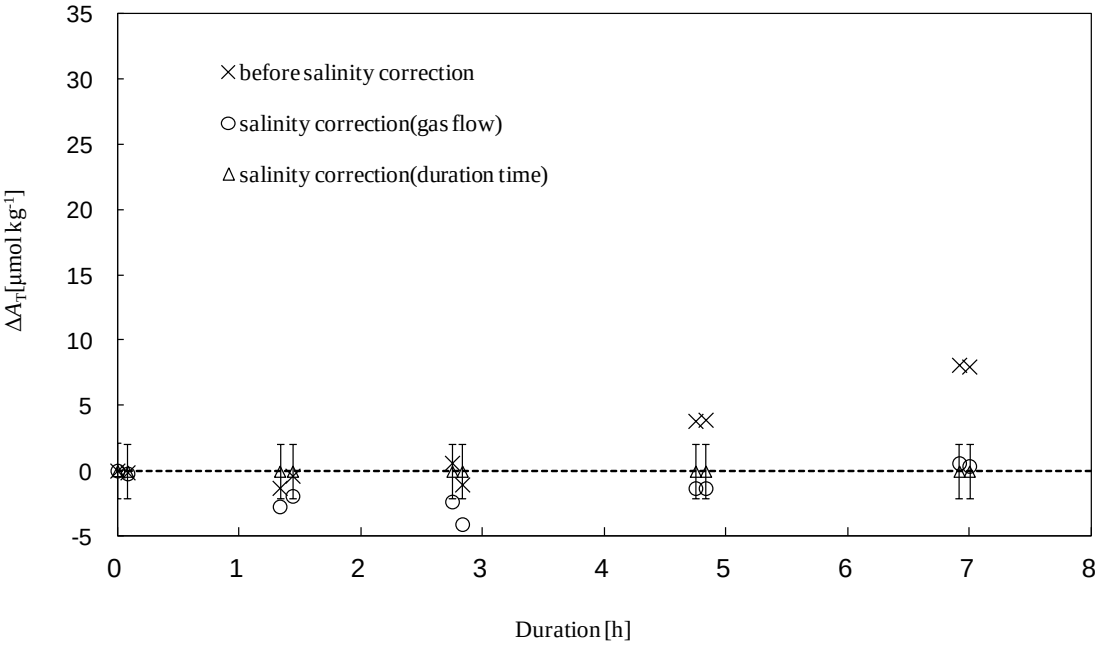

Figure 3-2. Results of blank experiment. X symbols show A_T changes before salinity correction, circle symbols show A_T changes after salinity correction according to gas flow, and triangle symbols show A_T changes after salinity correction according to duration time.

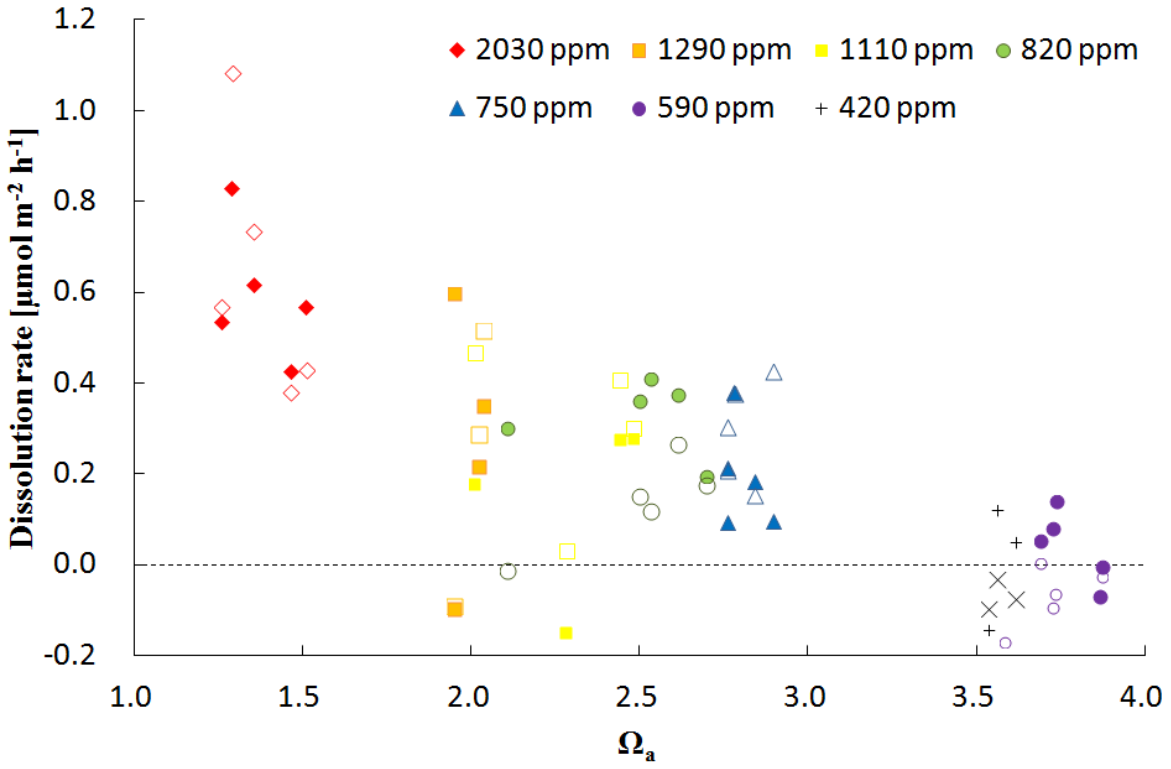

Figure 3-3. The relationship between average dissolution rate and average Ω_a for bulk experiment. Solid symbols show gas flow calibration and open symbols show duration time calibration. There are no significant differences between two corrections. Calculated dissolution rate has about 0.3 µmol m^{-2} h^{-1} error bar

Table 3-2. Relationship between change of gas flow, salinity and A_T

Gas Flow[ml min^{-1}]	ΔSalinity [h^{-1}]	ΔA_T [µmol kg^{-1} h^{-1}]*
50	0.0045	0.308
300	0.0085	0.584
500	0.0264	1.803

*Assuming that initial A_T = 2350 µmol kg^{-1}

3-3. Results

The conditions for each experiment are listed in Table 3-1 and the results of all experiments are listed in Supplementary Table 1. The results of the bulk dissolution experiment are shown in Figure 3-4. During the experiments, nA_T varied between 6 and 25 μmol kg^{-1}. No increase in nA_T was observed when pCO_2 was 420 ppm, and the change in nA_T was highest when pCO_2 was 2030 ppm.

Figure 3-5 shows the average dissolution rates during each interval, calculated from nA_T changes, plotted against averaged Ω_a. Although Ω_a in seawater varied during experiment, the constant dissolution rate was considered during each interval for analytical limit. The unit of dissolution rate was converted to [μmol m^{-2} h^{-1}] by specific surface area measured in Chapter 2 with the assumption that specific surface area did not change during experiment. However, specific surface area of coral sample decreased from 1.5 m^2 g^{-1} to 1.3 m^2 g^{-1} before and after the dissolution experiment. The effect of specific surface area for calculating dissolution rate should be considered in the future. The average dissolution rate was fastest (0.56 μmol m^{-2} h^{-1}) when Ω_a was 1.3 and slowest when Ω_a was 3.7.

Similarly, Fig. 3-6 shows the results of dissolution experiments on coralline algae, foraminiferans, and coral, together with those of the bulk sediment. In all cases, the dissolution rate increases as Ω_a decreases. Dashed lines indicate standard errors for dissolution rate, and Ω_a calculated from A_T and C_T has an error of 0.05. Since the analytical accuracies of A_T were 3 μmol kg^{-1}, calculated dissolution rate has about 0.3 μmol m^{-2} h^{-1} error bar, suggesting that range of threshold of each Mg-calcite dissolution was basically contain analytical error. The threshold value of foraminiferan and coralline algal dissolution is $3.0 < \Omega_a < 3.2$, and that of the bulk sediment is $3.7 < \Omega_a < 3.8$ by using linear fit, and these values

are used for the following discussion chapter. The dissolution rate of the coral shows no significant change when $1.5 < \Omega_a < 2.0$.

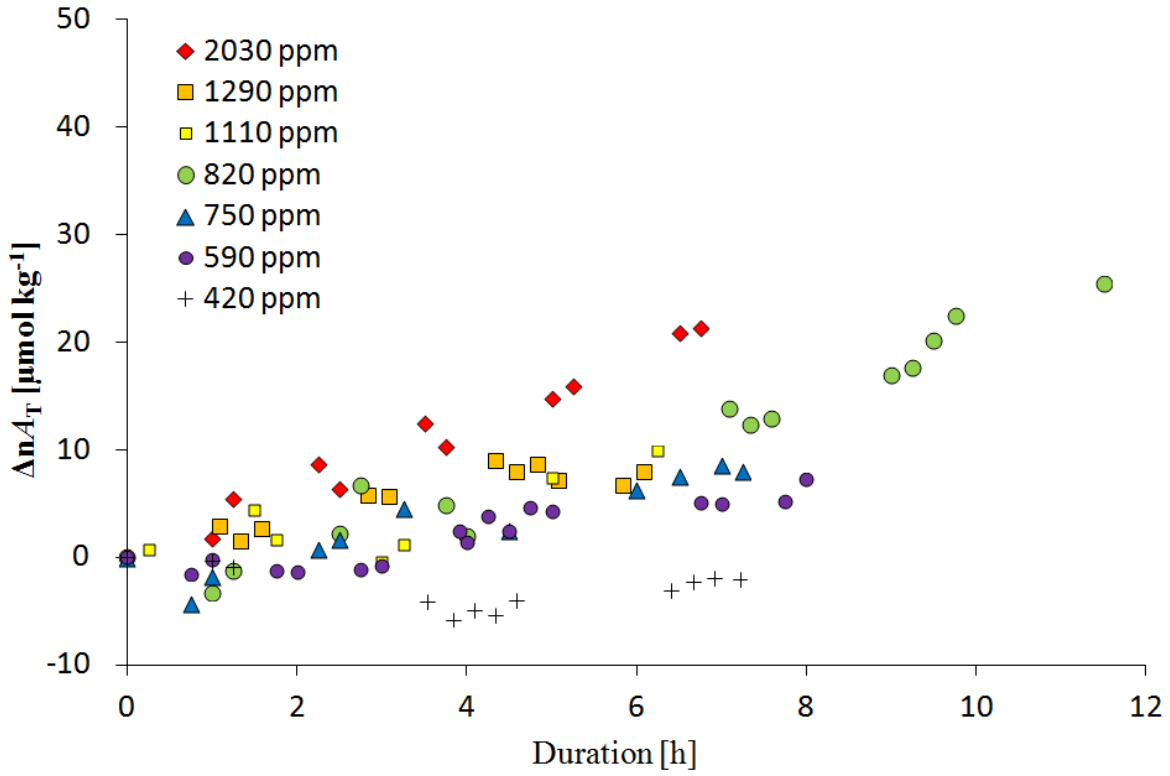

Figure 3-4. The result of bulk dissolution experiment (nA_T and duration).

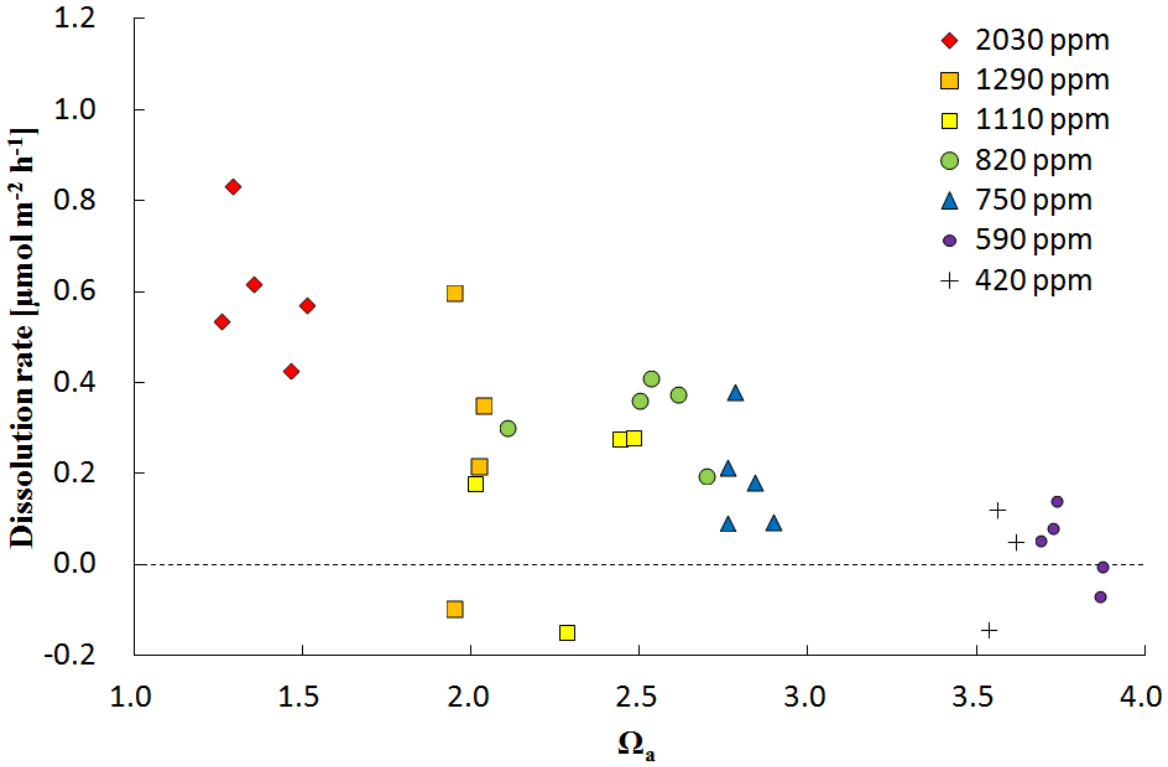

Figure 3-5. The relationship between average dissolution rate and average Ω_a (bulk).

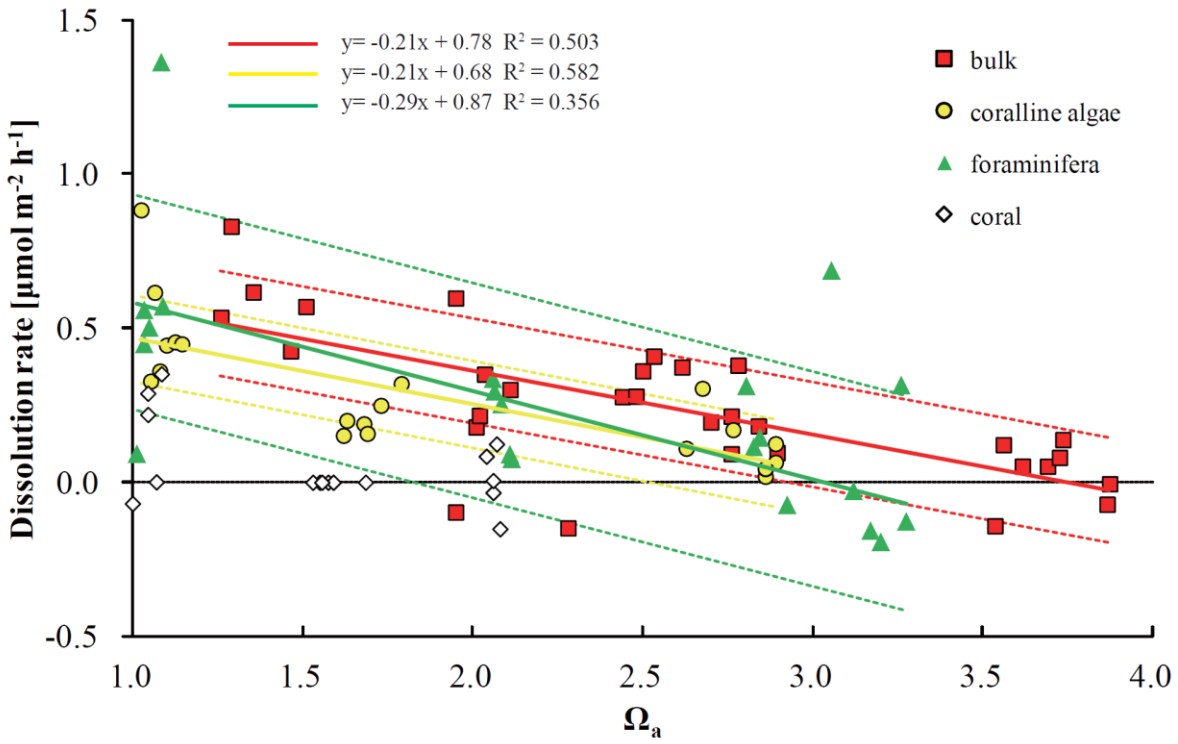

Figure 3-6. The relation between average dissolution rate and average Ω_a (for all samples): Solid lines indicate linear regression of dissolution rate on Ω_a, and dashed lines indicate each standard errors.

3-4. Discussion

As in earlier studies (Bischoff et al., 1993; Morse et al., 2006, 2007), the dissolution rate differences among samples are presumably resulted from the solubility differences of minerals with varying Mg content and specific surface area.

3-4-1. Relationship between solubility and Ω_a

I compared the Mg-calcite solubilities obtained in this study with those measured previously (Morse and Mackenzie, 1990) using the Ω_a threshold of coralline algae and foraminifera dissolution. The solubilities of biogenic Mg-calcite obtained by foraminifera are calculated using the results of two different types of experiments: Plummer–Mackenzie solubility (Plummer and Mackenzie, 1974) and biogenic best-fit solubility (Walter and Morse, 1984; Bischoff et al., 1987) as mentioned in Chapter 1. The Ω value of Mg-calcite (16 mole % Mg) is 0.2 based on the former method and 0.8 based on the latter, when Ω_a = 1.0. This discrepancy originates from differences in pretreatment and the experimental method (Bischoff et al., 1993; Morse et al., 2006). For example, in the Plummer–Mackenzie method, carbonate samples were washed in an ultrasonic bath and then dried, whereas for the biogenic best-fit solubility they were not only washed in an ultrasonic bath, but were chemically treated with H_2O_2 to remove organic matter. That is why solubilities of biogenic Mg-calcite are different among researches, and it is difficult to determine which solubilities should be adopted when evaluating the effect of Mg-calcite dissolution in nature (Morse et al., 2007; Andersson et al., 2009).

In the present work, the $-\log(K^*_{sp})$ values of coralline algae (16.5 ± 0.4 mole % Mg) and foraminiferans (13.3 ± 0.4 mole % Mg) are 7.80 and 7.82, respectively, and according to Plummer and Mackenzie (1974), $-\log(K^*_{sp})$ value of 12.7 mole % Mg is 7.82 (Figure 3-7). Samples used in this study were cleaned only in an ultrasonic bath and dried at 40°C for about

12 h, following Plummer and Mackenzie (1974). The foraminifera and coralline algae solubilities calculated in this study are similar to those reported by Plummer and Mackenzie (1974). On the other hand, a significant dissolution rate of coral was obtained even when Ω_a = 1.1. Since Ω_a (calculated from A_T and C_T) has an error of 0.05, biogenic aragonite starts to dissolve where $1.05 < \Omega_a < 1.15$. Alternatively, biogenic aragonite may be slightly more soluble than synthetic aragonite because of its heterogeneity and instability.

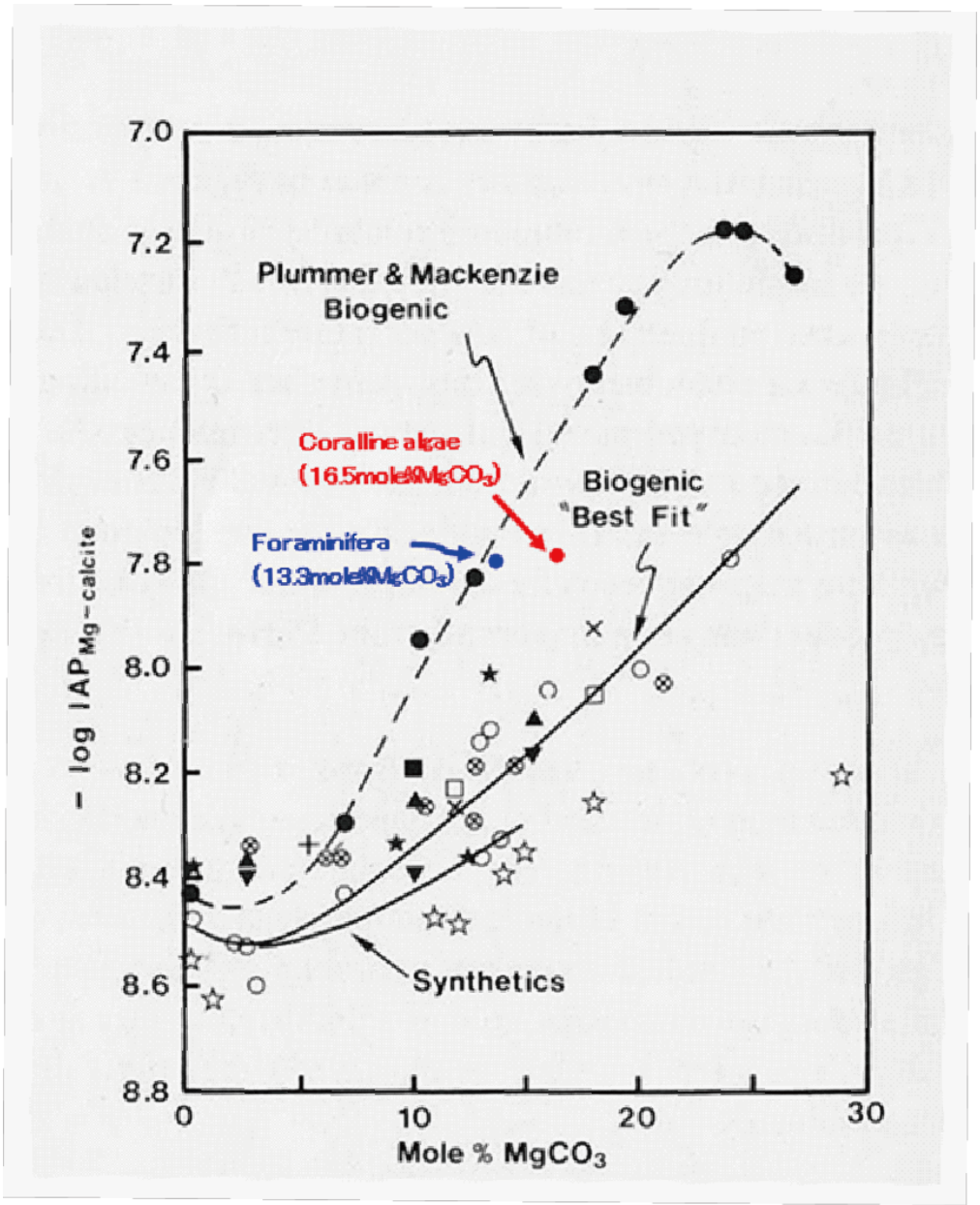

Figure 3-7. Solubility of Mg-calcite cited from Morse et al. (2007): Data from the present experiment are shown by red and blue circles. Logarism of ion acitivity product (log IAP) is calculated by threshold of foraminifera and coralling algae dissolution and Morse et al. (2007).

3-4-2 Evaluation of Mg-calcite dissolution

The relationship between dissolution rate and Ω_a, as obtained from the present experiments (Figure 3-6) and surface sediment area (Chapter 2-2-3), is as follows:

Bulk sediment: Dissolution rate (i.e. DR_{bulk}) [$\mu mol\ m^{-2}\ h^{-1}$] = $-0.21 \times \Omega_a + 0.78$ (3-3)

Foraminifera: Dissolution rate (i.e. DR_{Fora}) [$\mu mol\ m^{-2}\ h^{-1}$] = $-0.29 \times \Omega_a + 0.87$ (3-4)

Coralline algae: Dissolution rate (i.e. DR_{CA}) [$\mu mol\ m^{-2}\ h^{-1}$] = $-0.21 \times \Omega_a + 0.68$ (3-5)

Correlation coefficient is R = -0.710 for bulk sediment, R = -0.596 for foraminifera, and R = -0.763 for coralline algae, and relationship between duration rate and Ω_a had statistically significant correlation (α=0.01) by test for no correlation. According to equations (3-3) to (3-5), the net dissolution of bulk sediment was zero at $3.7 < \Omega_a < 3.8$ whereas those of foraminifera and coralline algae were zero at $3.0 < \Omega_a < 3.2$.

In order to discuss the validity of each estimated Mg-calcite dissolution rate and bulk sediment dissolution rate, total calculated dissolution rate (i.e., the dissolution rate of foraminifera + coralline algae; DR) are considered, and DR is defined as follows:

$DR = DR_{fora} \times$ (Foraminifera/Bulk) + $DR_{CA} \times$ (Coralline algae/Bulk) (3-6)

The composition ratio is derived from Figure 2-3; and in the case that DR < 0, DR=0 was used, assuming no precipitation of calcium carbonate. If foraminiera and coralline algae are the only dissolving grains in the bulk sediment, DR_{bulk} should be equal to the total calculated dissolution rate (DR). Figure 3-8 shows DR plotted against the DR_{bulk} (equation 3-3). Dashed line in Figure 3-8 indicates the 1:1 line for DR and DR_{bulk}. When $1.9 < \Omega_a < 3.7$ values assign to equation (3-3) and (3-6), dotted lines are obtained. The result suggests that DR is smaller than DR_{bulk}, especially when $\Omega_a > 3.0$.

The sediment samples consist of 75% foraminifera, coralline algae, coral, and other aragonite; 3% echinoids, and 22% “indiscernible other minerals”; the latter two components were not included in the calculations because echinoid test is composed of Mg-calcite with a low $MgCO_3$ content (8.0 mole % Mg), corresponding to a relatively small contribution to the bulk dissolution rate, and the “indiscernible other minerals” are considered to be calcite or Mg-calcite, because they did not acquire coloration when dyed with $Co(NO_3)_2$ (aragonite colors red-purple), and over 95% of the sediment in the Shiraho reef is carbonate. Any minerals in the minor fraction such as biogenic heterogenic Mg-calcite or organisms appear to be much more soluble than the foraminiferans and coralline algae, meaning that we may underestimate the dissolution rate. On the other hand, dissolution can be generally explained from foraminiferan and coralline algal dissolution when $\Omega_a < 3.0$ (Figure 3-8), and this finding is applicable to reef environments where sediment grains consist mainly of these biogenic carbonates.

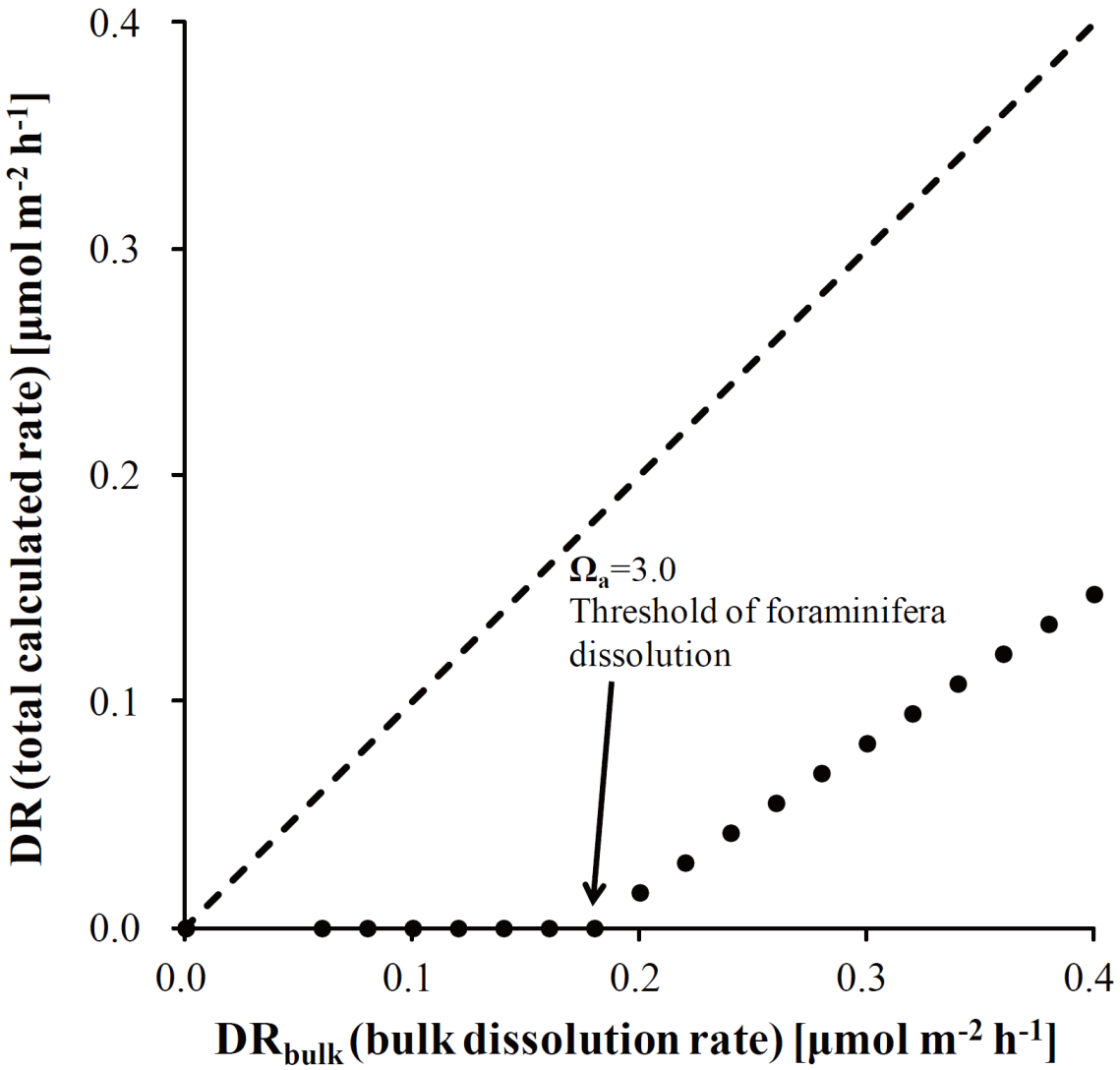

Figure 3-8. Relationship between bulk dissolution rate (DR_{bulk}) and total calculated dissolution rate (DR): If bulk dissolution rate is equivalent to total calculated dissolution rate at any Ω_a values, the plots should be on dashed line. However, the relationship between bulk dissolution rate and total calculated dissolution rate is shown by dotted line, suggesting that bulk dissolution rate is always higher than total calculated dissolution rate.

Chapter 4.

Dissolution/calcification rate at sand area determined by chamber experiment

4-1. Introduction

In order to estimate *in situ* net dissolution/calcification rate at sand community, two types of chamber experiments were conducted. Flow-controlled chamber was operated under both flow and non-flow conditions. On the other hand, non-flow-controlled chamber was easier to operate but could be used only under non-flow condition. The results of non-flow-controlled chamber experiment and evaluation of both flow chamber experiments are described in appendix. In this section, I discuss net dissolution/calcification rate at sand area obtained by flow-controlled chamber.

4-2. Methodology

4-2-1. Experimental design for flow-controlled chamber

In order to estimate net dissolution/calcification rate *in situ* at a sand area under flow condition, a flow-controlled chamber was constructed and placed on the bottom (Figure 4-1). The flow-controlled chamber was 0.8 × 0.5 × 0.3 m, and consisted of five parts: an aluminum baseboard, clear acrylic side panels with aluminum frame, a clear acrylic top, connected vinyl chloride hose (8 cm diameter, 5m length), and a submerged pump (65 DWT 62.2, Ebara Co., Ltd). The submerged pump was controlled by an inverter (FR-D720-3.7K, Mitsubishi Electric Co., Ltd) on the boat, and flow rate inside the chamber was able to be changed up to about 15 cm s^{-1}. To increase pCO_2 in seawater inside the chamber, a vinyl chloride large syringe (1.5 L size) was used. This syringe was connected to the chamber by two flanges. Seawater sampling procedure and the curtain to prevent mixture of seawater outside was the same as the non-flow-control chamber.

A photon flux sensor (ALW-CMP, JFE Advantech Co., Ltd), an electromagnetic current meter (INFINITY-EM, JFE Advantech Co., Ltd), and a temperature logger (CO-U22-001, Climatic Co., Ltd) were placed inside the chamber. They were recorded at 10-mins intervals. The procedure of experiments were as follows: (1) closing the chamber and a large syringe filled with CO_2 saturated seawater was connected to the chamber and injected, (2) turning pump on, (3) after more than 5 min, a sample of seawater in the chamber was collected by a connected tube and syringe. (4) Seawater in the sealed chamber was re-sampled after about 3h. (5-1) When we wanted to continue experiment, procedure (4) was repeated. (5-2) When we wanted to change CO_2 condition in seawater, the chamber was opened and seawater in the chamber was exchanged with the surrounding water, and (6) after waiting more than 15 min, the procedure (1) was repeated. Seawater samples were collected into 300-mL borosilicate

glass bottles (Duran, Schott) with 0.2 ml of saturated mercuric chloride ($HgCl_2$) solution for preservation.

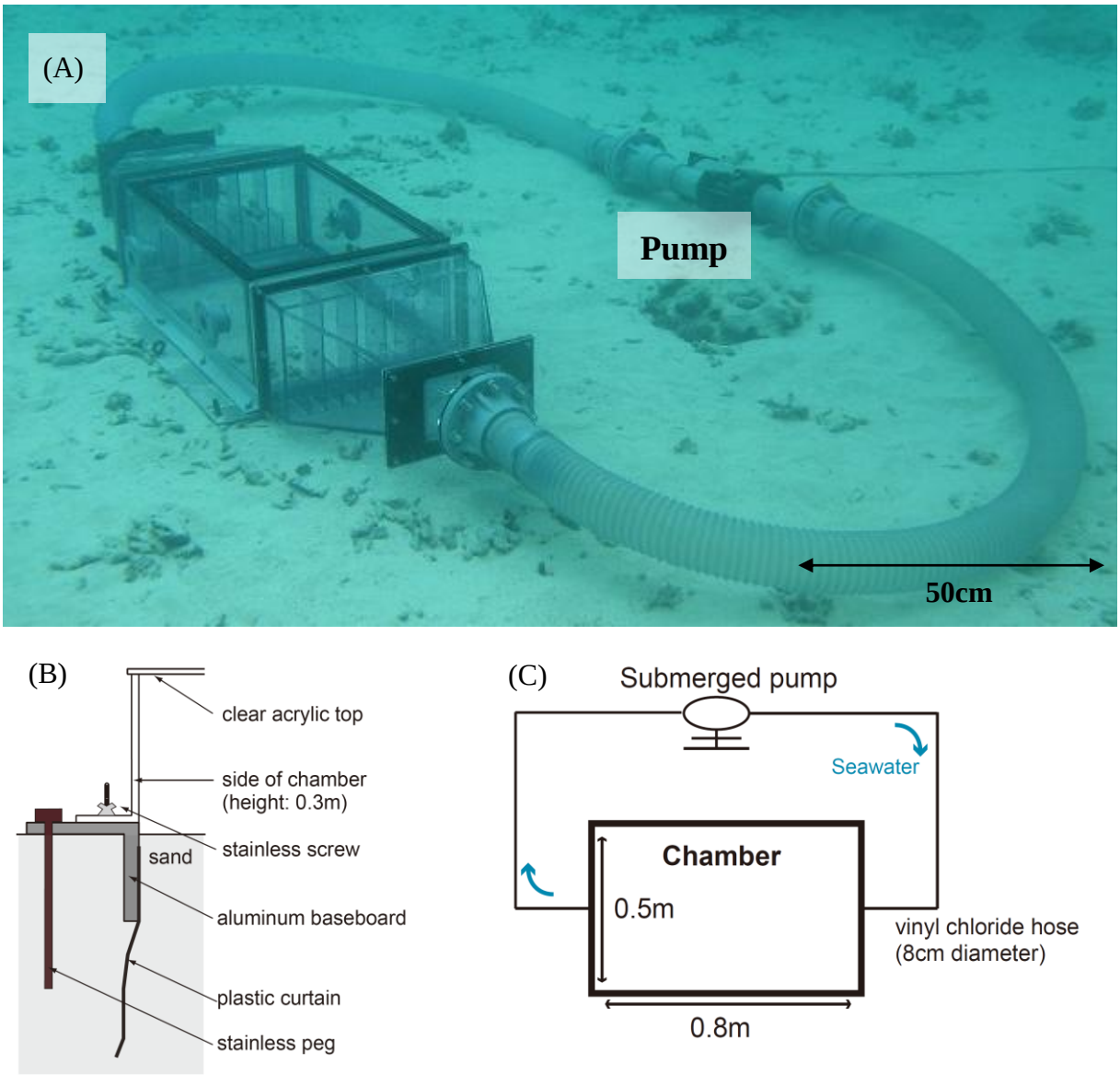

Figure 4-1. (A) Picture of flow-controlled chamber (0.8 × 0.5 × 0.3 m) (B) Aluminum baseboard with plastic curtain was fixed by stainless peg, and was jointed with chamber by stainless screw. Top of chamber can be removed and it was attached to the chamber. (C) Schematic design of flow-controlled chamber: Sand area was enclosed by chamber, and seawater in chamber was circulated by submerged pump.

4-2-2. Calculation

Net dissolution/calcification rate of the sand area was estimated based on the changes in the chemical composition of seawater in the chamber. The A_T of seawater increases by 2 moles for every 1 mole of calcium carbonate dissolution. A_T, C_T, and salinity (S) of the samples were measured at the University of Tokyo within two months after the sampling date. A_T and C_T were obtained by the flow-through analyzer (Kimoto Electric Company Limited). The analytical accuracies of A_T and C_T were within 3 μmol kg^{-1} and standard deviations of A_T and C_T were 1.1 μmol kg^{-1} and 2.1 μmol kg^{-1} ,respectively (Kimoto et al., 2002; Watanabe et al., 2004), which were checked against certified reference materials (CRMs) distributed by A. Dickson (Scripps Institution of Oceanography). Salinity was determined using a salinometer (PORTASAL 8410A, Guildline Instruments Limited). The precision of salinity analysis is ± 0.003.

Dissolution rates were calculated as follows:

$$R = \Delta A_T/2 \times m_W \times M \times 100/ (S_A \times t) \quad (4\text{-}1)$$

where ΔA_T is the difference in A_T between start and end of the experiment, m_W is the weight of seawater calculated on each chamber volume, M is the molecular weight of calcium carbonate (=100), S_A is the enclosed area by each chamber, and t is the duration of the experiment.

4-3. Results

4-3-1. Relationship between dissolution rate and flow rate

Figure 4-2 shows the average dissolution/calcification rates plotted against averaged Ω_a conducted by flow-controlled chamber experiment, and Supplementary Table 3 summarized the experimental conditions. Diamond data indicate under flow condition of 15 cm s^{-1} (fast), square data indicate under flow condition of 5 cm s^{-1} (middle), and circle data indicate under flow condtion of 2 cm s^{-1} (slow). The experiments under fast flow conditions were conducted only in winter, and those under slow flow conditions were conducted under natural CO_2 conditions (i.e. no CO_2 added conditions). Although it was expected that dissolution rate increased with the decrease in Ω_a, dissolution/calcification rate did not show a significant correlation with Ω_a. In order to evaluate multiple effects such as flow rate, CO_2 addition or natural condition, and Ω_a for dissolution/calcification rate, analysis of covariance (ANCOVA) was conducted. Table 4-1 shows the result of ANCOVA test for net dissolution/calcification rate compared by the covariate factors of CO_2 addition/Natural × Ω_a × Flow rate. There were no significant differences in dissolution/calcification rate between high-flow, middle flow, and low-flow conditions.

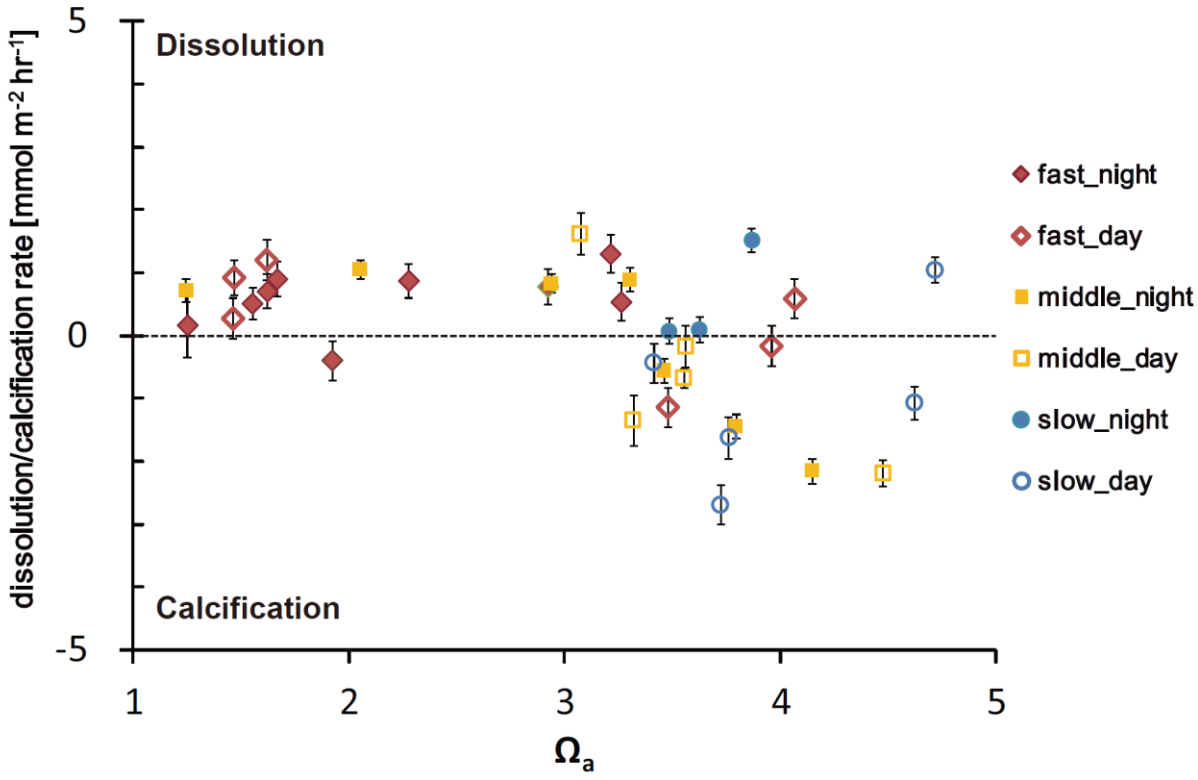

Figure 4-2. The relationship between average dissolution rate and Ω_a conducted by flow-controlled chamber: "fast" corresponds to 15 cm s^{-1} flow rate in chamber, "middle" 5 cm s^{-1}, and "slow" 2 cm s^{-1}

Table 4-1. *F*-statistics and *p*-values for the results of the analysis of covariance showing the influence on net dissolution/calcification rate for CO_2 addition or natural, Ω_a, and flow rate, and their netsted effects (*$p < 0.01$). Only the combination effect of CO_2 addition/natural and Ω_a had an influence on net dissolution/calcification rate.

Night	F	Pr (>F)
CO_2 addition / Natural	0.376	0.552
Ω_a	0.026	0.875
Flow rate	1.101	0.317
(CO_2 addition /natural) × Ω_a	6.327	0.029*
(CO_2 addition/ natural) × Flow rate	0.263	0.618
Ω_a × Flow rate	0.007	0.937
(CO_2 addition/natural) × Ω_a ×Flow rate	2.092	0.176

Day time	F	Pr (>F)
CO_2 addition / Natural	1.122	0.314
Ω_a	0.393	0.545
Flow rate	1.173	0.304
(CO_2 addition /natural) × Ω_a	1.584	0.237
(CO_2 addition/ natural) × Flow rate	0.227	0.644
Ω_a × Flow rate	0.074	0.792
(CO_2 addition/natural) × Ω_a ×Flow rate	0.442	0.521

4-3-2. Comparison between natural condition and CO_2 addition condition

While biogenic calcification rate during day time varied with temperature and light intensity, inorganic dissolution rate relatively did not vary by those effects. Thus, nighttime data were used to compare between natural condition and CO_2 addition condition. Figure 4-3 shows the nighttime average dissolution/calcification rates plotted against averaged Ω_a under all flow conditions with ambient CO_2 and CO_2 addition. Net dissolution rate varied between -2.15 and 1.53 mmol m^{-2} hr^{-1}, and each green shade represented linear fit and its standard error range. The relationship between dissolution rate and Ω_a under natural condition was different from that under CO_2 addition condition (analysis of covariance (ANCOVA): F = 6.327, P = 0.029 and Table 4-1). While net dissolution rate did not increase with Ω_a decrease under CO_2 addition conditions, negative correlation between dissolution/calcification rate and Ω_a was observed under natural conditions.

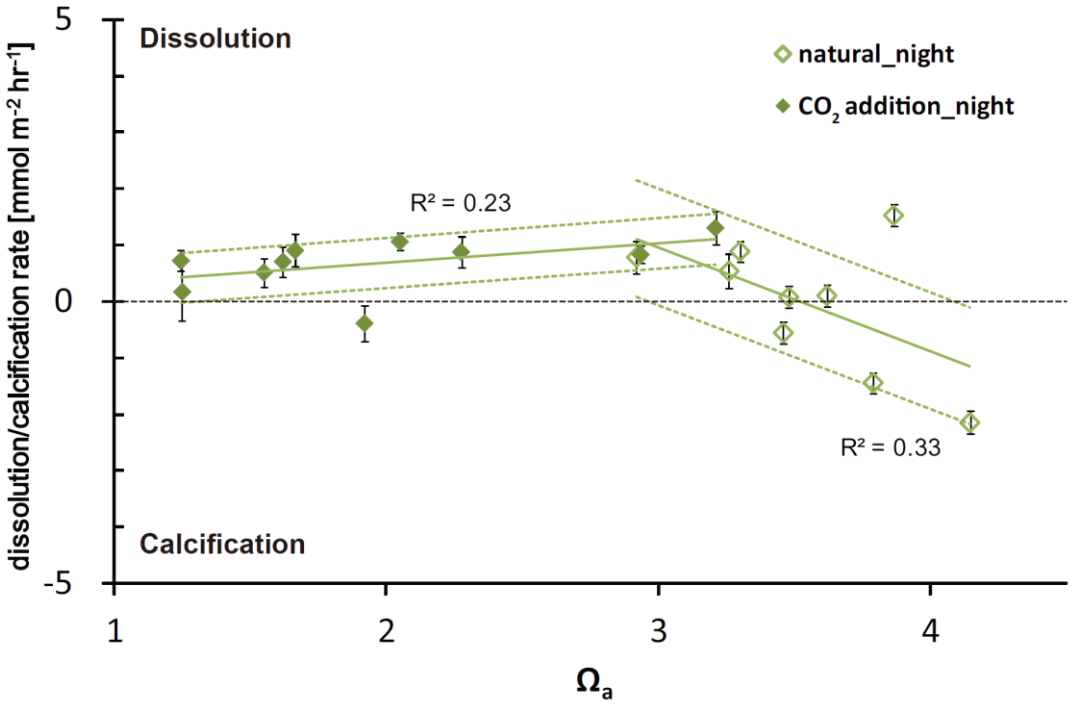

Figure 4-3. The relationship between average dissolution/calcification rate and Ω_a under flow condition, comparing natural condition and CO_2 addition: Dashed lines indicate each standar errors

4-4. Discussion

Since previous studies mainly measured a diurnal carbonate changes in a whole coral reef community, relationship between Ω_a and dissolution rate especially at sand area has been taken into account in only few studies. Figure 4-4 summarizes the relationship between Ω_a and dissolution rate at night. All of data were estimated by chamber experiment. Table 4-2 lists the information of previous studies sauch as, dissolution rate at sand area, location, and experiment type. In Yates and Halley (2006) and Nakamura and Nakamori (2009) chamber system, a submersible pump was mounted in the chamber to mix seawater and flow rate could not be changed. On the other hand, the chamber systems of our study and Cyronak et al. (2013) could change flow rate. Mean dissolution rates observed at each site are as follows: 0.3 $\pm$0.2 mmol m^{-2} hr^{-1} in Yates and Halley (2006), 0.6 $\pm$ 0.3 mmol m^{-2} hr^{-1} in Nakamura and Nakamori (2009), 1.4 $\pm$ 0.9 mmol m^{-2} hr^{-1} in Cyronak et al. (2013), 0.3 $\pm$ 1.7 mmol m^{-2} hr^{-1} in this study. Dissolution rate did not show a significant correlation with Ω_a ($R = 0.09$, $p > 0.01$), and similar to the results in this study (4-3-1). Cyronak et al. (2013) showed that flow rate change did not influence dissolution rate.

In general, biogenic calcification rate under flow condition increased as compared to those under zero-flow condition because the mass transfer rate between the ambient seawater and inside the calcifiers increased under the high-flow rate (Veron 1995; Nakamura and Yamasaki 2006; Nakamura et al., 2013). On the other hand, chamber experiment results showed that there was no significant correlation between flow condition and dissolution rate, suggesting that A_T increase observed in water column was not caused by surface dissolution but by reactions and pore water profiles in sediment. It would mean that carbonate profiles in sediment were not affected by high pCO_2 in water column because of the short-time experiment or a little amount of water column in chamber. Therefore, understanding of pore

water sediment profile under natural condition and estimation of A_T flux at sediment-water interface is important.

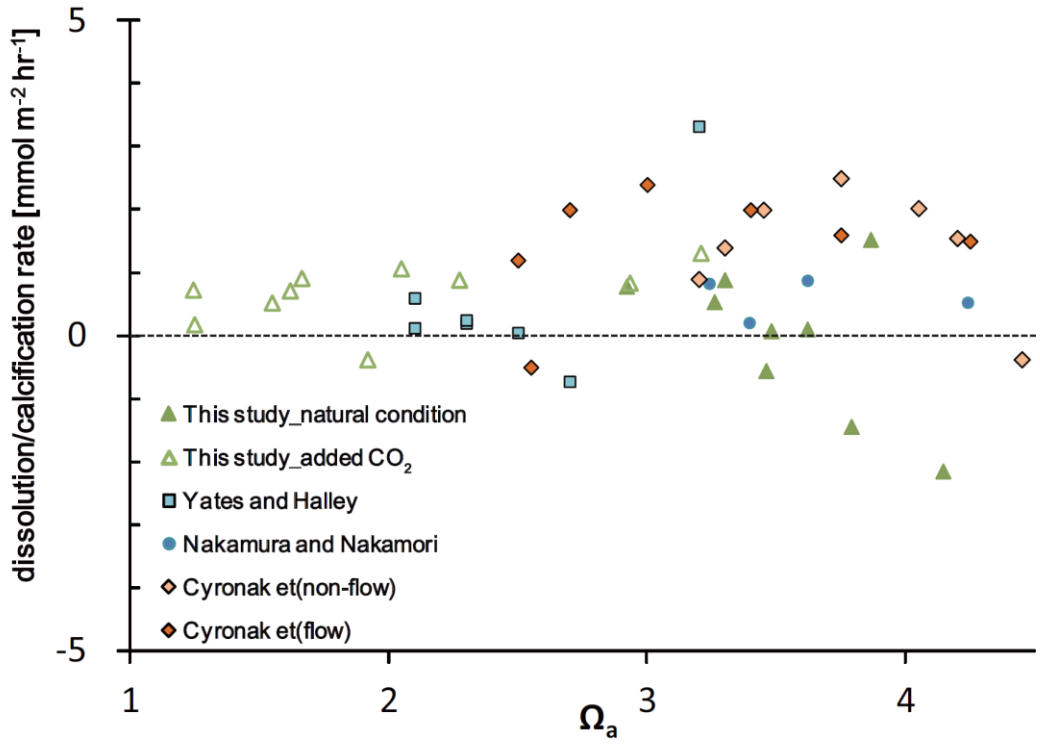

Figure 4-4. The relationship between average dissolution/calcification rate and Ω_a at night estimated by chamber experiment: Light bule symbols indicate Yates and Halley (2006), blue symbols indicate Nakamura and Nakamori (2009), light and dark orange diamonds indicate Cyronak et al. (2013) and green symbols indicate this study. Cyronak et al. (2013) showed that there were no diffirences in dissolution rate between flow condition and no-flow condition.

Table 4-2. Nighttime dissolution rate at sand area estimated by chamber experiment

Reference	Location	Mg-calcite proportion	from the shore line (ground water effect)	flow change	Dissolution rate [mmol m^{-2} hr^{-1}]
Yates and Halley (2006)	Molokai reef	40%	800m (no effect)	×	−0.7−3.3
Cyronak et al. (2013)	Heron Island	33.1%	75m (large)	○	−0.4−2.5
Nakamura and Nakamori (2009)	Shiraho	46.9%	300m (less?)	×	0.2−0.9
This study	Shiraho	46.9%	600m (none)	○	−2.1−1.5

Chapter 5.

A_T flux estimated by sediment pore water profiles and eddy covariance

5-1. Introduction

In this chapter, profiles of chemical parameters in pore water of the carbonate sediment and oxygen flux between sediments and water under natural flow condition determined by eddy covariance technique (EC) will be reported. O_2, pH, carbonate and nutrient profiles in the sediment pore water were measured by micro electrode and pore-water sampling. At the same time, O_2 flux was estimated by EC. From O_2 profile and O_2 flux, diffusion coefficient was determined. Using the diffusion coefficient and A_T profile in sediment, A_T flux under natural hydrodynamic condition was estimated.

5-2. Methodology

5-2-1. Measurements of pore water profiles in sediment

5-2-1-1. Micro sensor profiling

In situ O_2 and pH profiles for pore water of the carbonate sediment at Shiraho reef sand area (Figure 2-1) were measured using Unisense A/S OX-N and pH-N micro-electrode sensors mounted on an analogue profiling instrument (Figure 5-1). These micro-sensors were thick-walled with 1.1-mm tip diameters, and a 90% response time of less than 5 s (O_2) and 1 s (pH). The profiling instrument was placed on the sediment with the micro-sensors initially positioned 1-2 cm above the sediment surface. O_2 and pH profiles to a sediment depth of 4-5 cm were measured at intervals of 0.5 mm per 30 seconds during both night and day with measurements about every two hours over a 12-h period. While O_2 and pH profiles measured by microelectrodes reflected just one stuck profile, their data had high resolution for depth. O_2 and pH profiles at night were obtained on 4 October 2012, those during day time were obtained on 6 October 2012, with conditions on both dates being clear and calm.

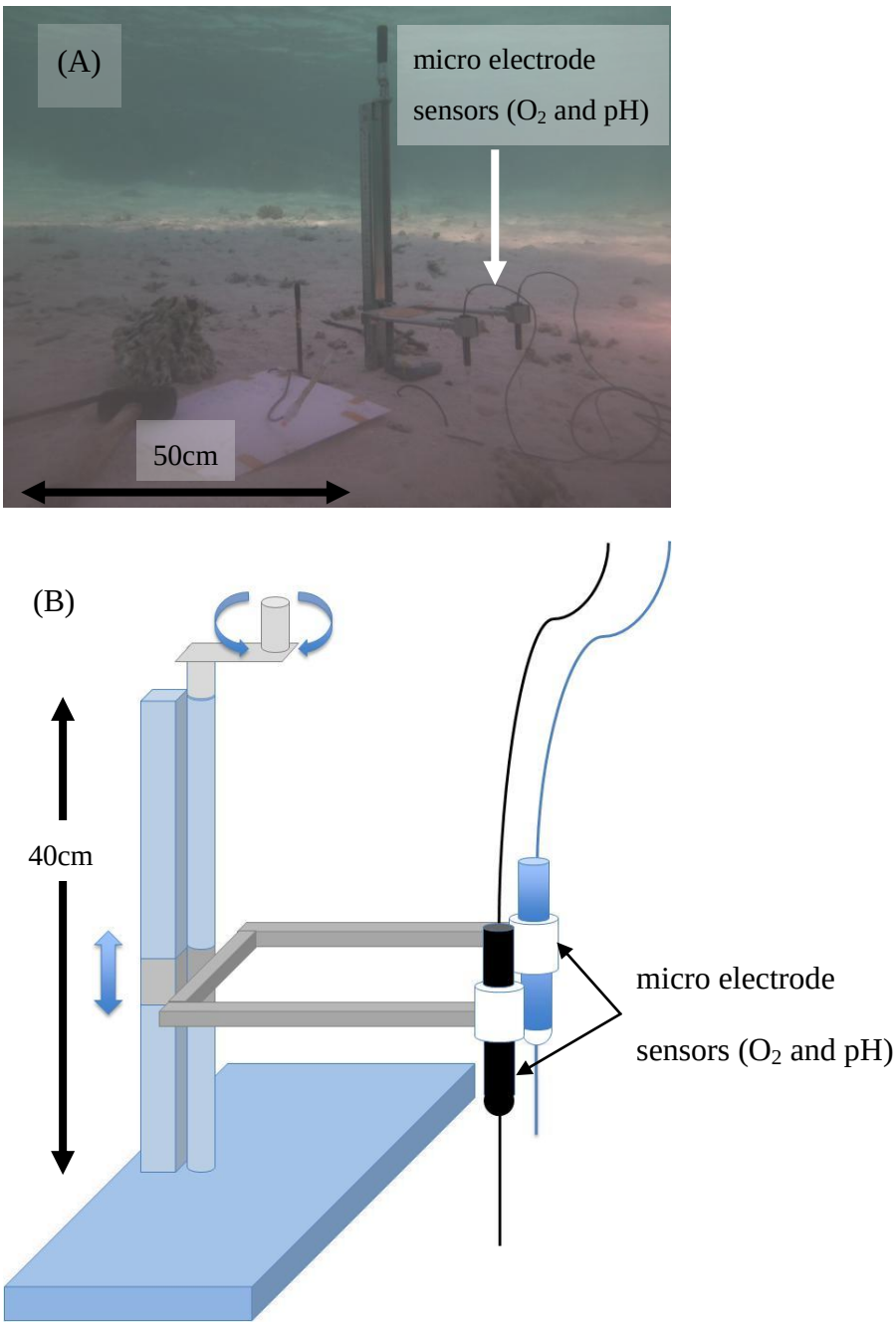

Figure 5-1(A) Underwater photo of analogue profiling instrument and (B) schematic design of analogue profiling instrument: arms can be moved by turning the handle.

5-2-1-2. Pore-water sampling

Carbonate and nutrient analysis of pore waters within the sediments was undertaken on five or six acrylic cores (80 mm diameter, 150 mm depth) by diving at Shiraho reef sand area (Figure 2-1). Both ends of the core were sealed with rubber stoppers, and seawater above the sediments was extracted on the boat based on the principle of siphon by using a tube (Figure 5-2-1). The wet sands were sampled using stainless spoon at 10-mm intervals, then they were preserved in a plastic bag to prevent air contact (Figure 5-2-2). Pore water was extracted on the boat using a syringe; the extracted water was passed through a 0.45 μm filter before bottling (Figure 5-2-3). Their profiles were considered to reflect typical or average profiles in sand area because several cores were used to collect pore water.

Carbonate chemistry analysis was conducted for pore waters that were collected using 30-ml bottles after mixing with 0.02 ml of saturated mercuric chloride ($HgCl_2$) solution for preservation. A_T and pH_T values were analyzed using a autoburette titrator (ATT-05, Kimoto Electric; Kimoto et al., 2001). Nutrient analysis was conducted on 10-ml samples that were frozen at -20°C after sampling, then concentrations of nitrate (NO_3^-), nitrite (NO_2^-), ammonia (NH_4^+), silica (SiO_2) and phosphate (PO_4^{3-}) were determined colorimetrically using an autoanalyzer (QuAAtro 2HR, BLTEC).

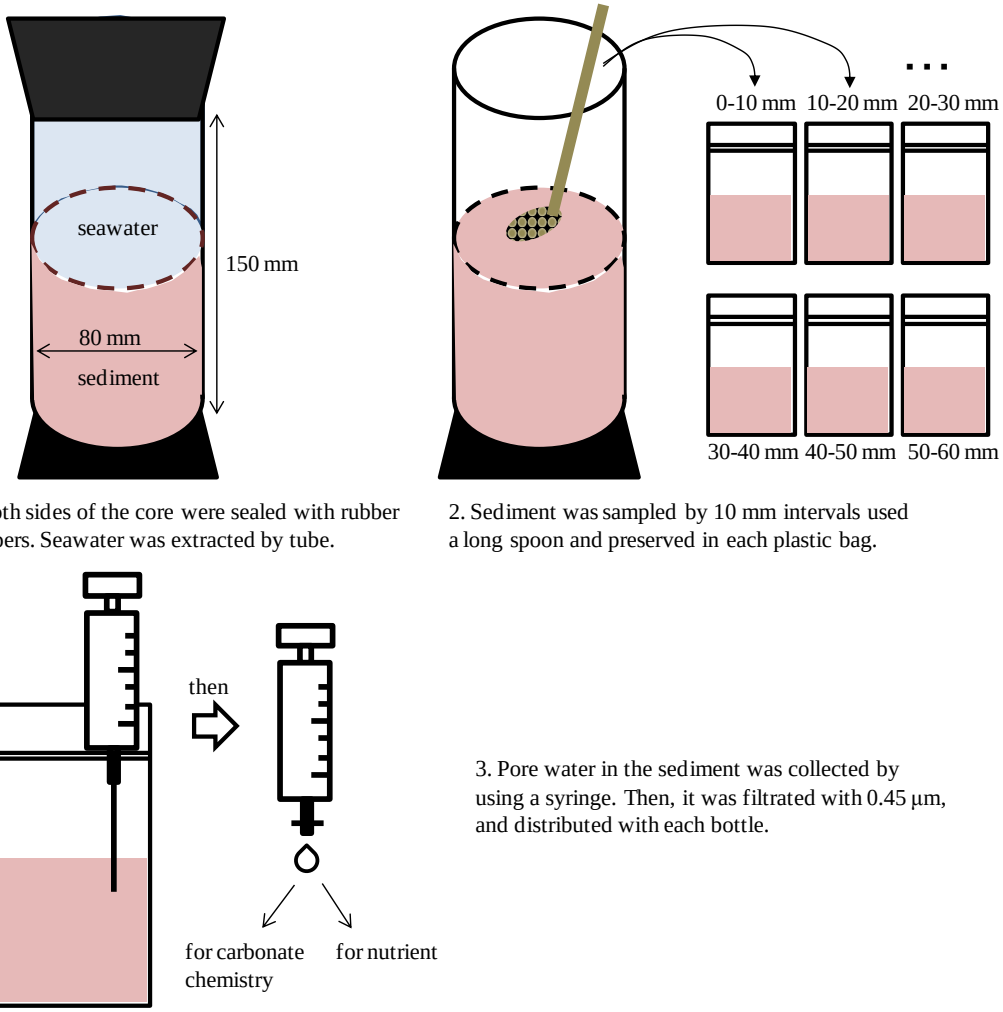

Figure 5-2. Illustration showing how to collect pore water from sediment

5-2-2. Eddy covariance

Current velocity was measured in this study using an acoustic Doppler velocimeter (Vector, Nortek) that measures 3-D velocity using a cylindrical measurement (14 mm height, 14 mm diameter) located on the centerline of the pipe, 157 mm from the surface of the sediment (Figure 5-3). The EC system employed during this study used metallic pipes (~1.5 m height, 1.2 m width) oriented perpendicular to the main direction of tidal currents in order to avoid artifacts in flux estimates during current field disturbances. Velocities were corrected against variations in the speed of sound related to temperature and ambient seawater salinity, and the manufacturers have accuracies of ± 0.1 cm s^{-1} (Kuwae et al., 2006). Oxygen concentrations were measured using a Clark-type oxygen microelectrode (OX-10, Unisense) with contemporaneous measurements of ambient DO values using a phosphorescent DO sensor (Rinko I, JFE Advantech) for calibration during observation. Figure 5-4 shows the temporal changes of DO concentration measured by micro electrode and phosphorescent sensor. DO in water column varied from 100 to 450 μmol l^{-1}. DO increased due to photosynthesis during day time, and decreased due to respiration during nighttime. From initial to 18:00 on 6 Oct., both results had similar fluctuation, however after that time, time lag between DO measured by phosphorescent sensor and by microelectrode was observed. This means micro electrode was out of order caused by debris or biofouling such as benthic microalgae. Also, from 6:00 to 7:40 on 5 Oct. and from 5:00 to 7:40 on 6 Oct., steep DO change was observed. Watanabe et al. (2013) reported that the reef crest becomes exposed to the atmosphere during low tide and rapid flow transition occurred from peak ebb tide to flood tide. Thus, these data were excluded for calculation because horizontal homogeneity of DO was not established. A photon flux sensor (ALW-CMP, JFE Advantech) and a temperature logger (CO-U22-001, Climatic) were deployed near the EC observation system that recorded data at 10-min intervals from 4 to 7 October 2012.

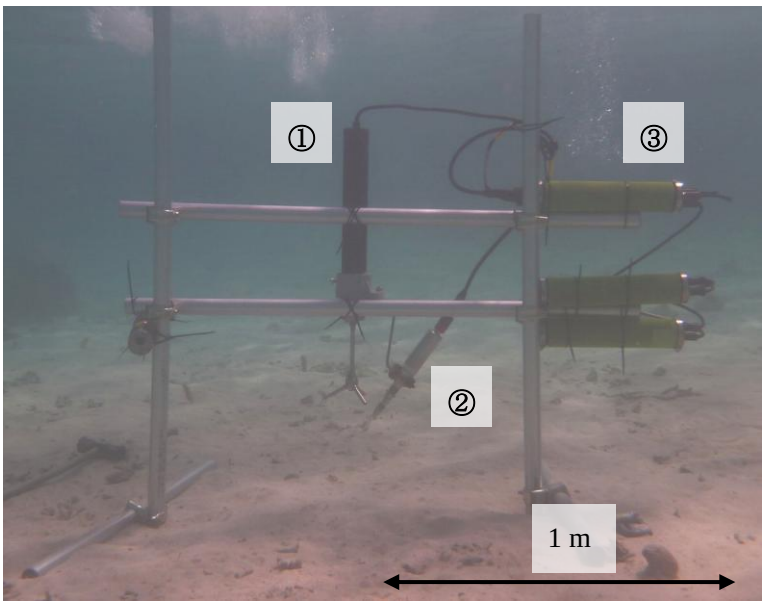

① Doppler velocimeter (ADV)

② O_2 microelectrode

③ battery for ADV and O_2 microelectrode

Figure 5-3. Underwater photo of eddy covariance measurement conducted at Shiraho reef. Doppler velocimeter, O_2 microelectrode, and their batteries were located on the pipe.

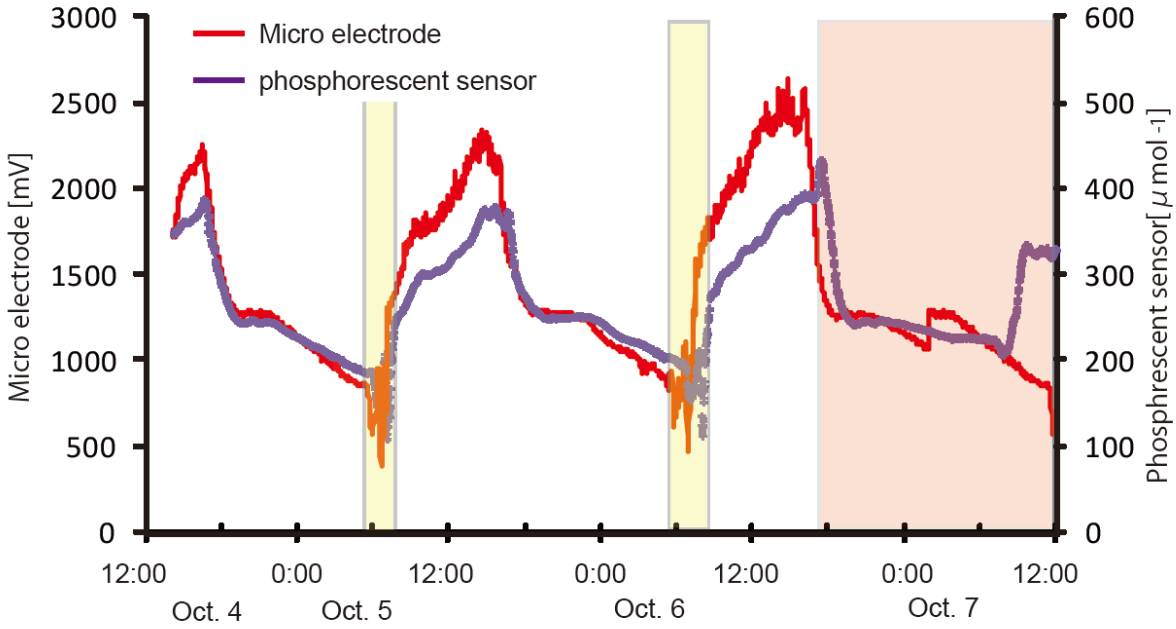

Figure 5-4. DO concentration during EC observation measured by micro electrode and phosphorescent sensor (Rinko I, JFE Advantech Co., Ltd): Yellow area shows steep DO change, and red area shows time lag between microelectrode and phosphorescent sensor.

5-3. Results

5-3-1. Seawater and environment condition in water column

Figure 5-5 shows the temporal changes of light intensity, water temperature, water depth, DO measured by phosphorescent sensor and microelectrode, as well as A_T and C_T in water column. DO measured by microelectrode, A_T, and C_T data were obtained only during micro sensor profiling and pore water sampling (as mentioned in 5-2-1) while other data were continuous data. During day time, temperature and DO increased, and A_T and C_T decreased because of metabolic community photosynthesis and calcification. On the other hand, during nighttime, temperature and DO decreased, and A_T and C_T increased. DO measured by microelectrode were consistent with that measured by phosphorescent sensor.

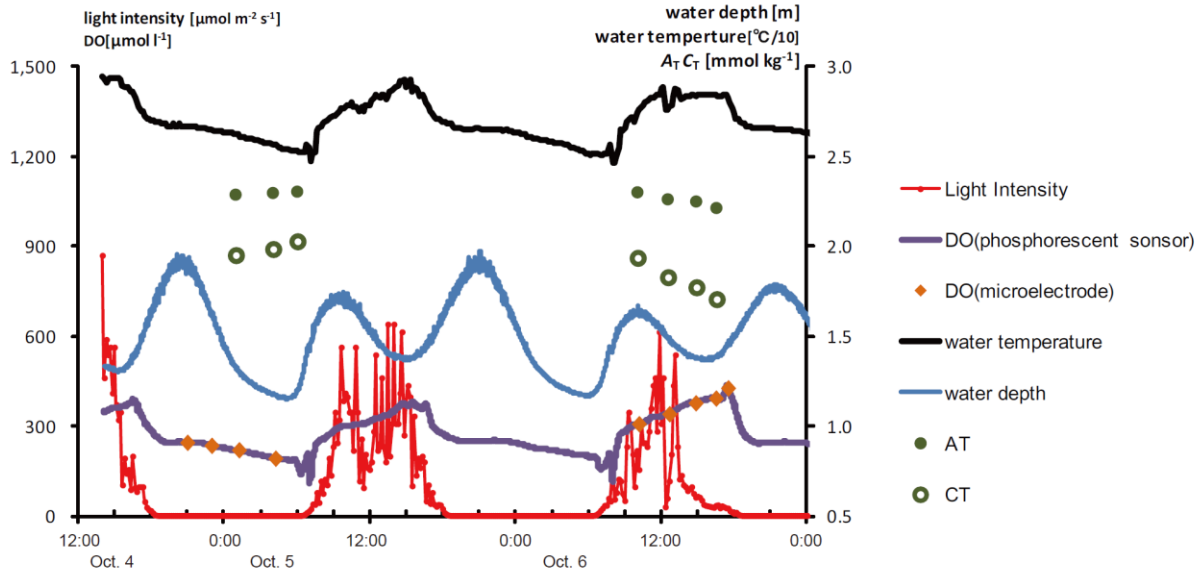

Figure 5-5. Daily changes in environment condition in water column during observation: Light intensity, water temperature, water depth, DO concentration were measured by phosphorescent sensor and microelectrode. A_T, and C_T were measured by pore water sampling.

5-3-2. Sediment profiles

5-3-2-1.DO and pH_T profiles

In situ O_2 and pH_T profiles within the upper ~60 mm of sediments measured by microelectrode within the Shiraho Reef sands are shown in Figures 5-6 (A), (B) and 5-7 (A), (B) with zero positions representing the sediment-water interface determined by naked eyes when the microelectrode touched the sediment.

Nighttime DO values and pH values within the water column decreased with time, whereas DO and pH values in the water column were constant throughout bottom 20 mm. DO values within the sediment decreased drastically in the upper 10 mm of the sediment before reaching zero at the depth of 10 mm. In comparison, sediment pH values show a two-step decrease between depths of 0 and 20 mm before reaching an almost constant value at depths of 20 mm especially for data on 21:00 and 1:30.

Daytime DO values and pH values within the water column increased with time, and brighter daytime conditions yielded maximum DO and pH values at a depth of 2–9 mm, although peak DO and pH depths varied with time. Namely, maximum peak observed at 10:30, peak decreased with time, suggesting photosynthesis in the sediment changed in response to light intensity (Figure 5-6). Pore water DO and pH values decreased with the increase in depth within sediments until reaching constant values at depths of 20 mm.

5-3-2-2. A_T, Ω_a, C_T and pH_T profiles

A series of 10–mm-average pore water profiles of A_T, Ω_a, C_T and pH_T profiles are shown in Figures 5-6 (C), (D), (E), (F) and 5-7 (C), (D), (E), (F). Standard errors of all data are so small that they are within each symbols (e.g. within $\pm$ 5 μmol l^{-1} for A_T). Results of all observation are listed in Supplementary Table 4.

Nighttime A_T and C_T values within the water column increased with time, whereas Ω_a and pH values within the water column decreased. Pore water A_T and C_T values reached the maximum at a depth of 5 mm, before remaining constant or undergoing a slight decrease at depths of >15 mm, whereas pore water Ω_a and pH values reached the minimum at a depth of 5 mm and remaining constant at depth below this (Figures 5-6 (C), (D), (E)). Values of Ω_a at depths of >15 mm were almost constant at a value of ~3.0 during the entire nighttime (Figure 5-6 (F)).

Daytime A_T and C_T values within the water column decreased with time, whereas Ω_a and pH values increased. In addition, Ω_a and pH values within pore waters were constant at depths of >5 mm, with Ω_a values in pore waters at depths of >15 mm being almost constant at 3.0 throughout the day, also observed at night (Figure 5-7 (F)). In comparison, A_T values within pore waters varied significantly, with A_T values in the water column being lower than values at a depth of 5 mm at all times except for the case of 10:00 (Figure 5-7(C)).

Night

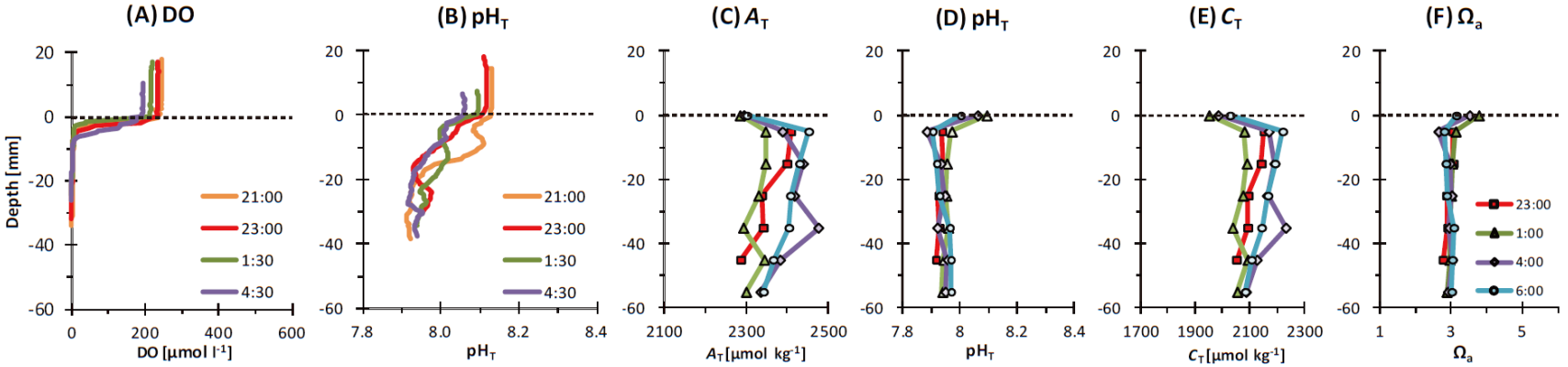

Figure 5-6. (A, B) Results of in situ DO and pH profiling at night measured by microelectrode analysis. (C, D) Results of total alkalinity and pH profiling using pore waters obtained at night. (E, F) C_T and Ω_a profiles calculated using the data shown in C and D.

Day

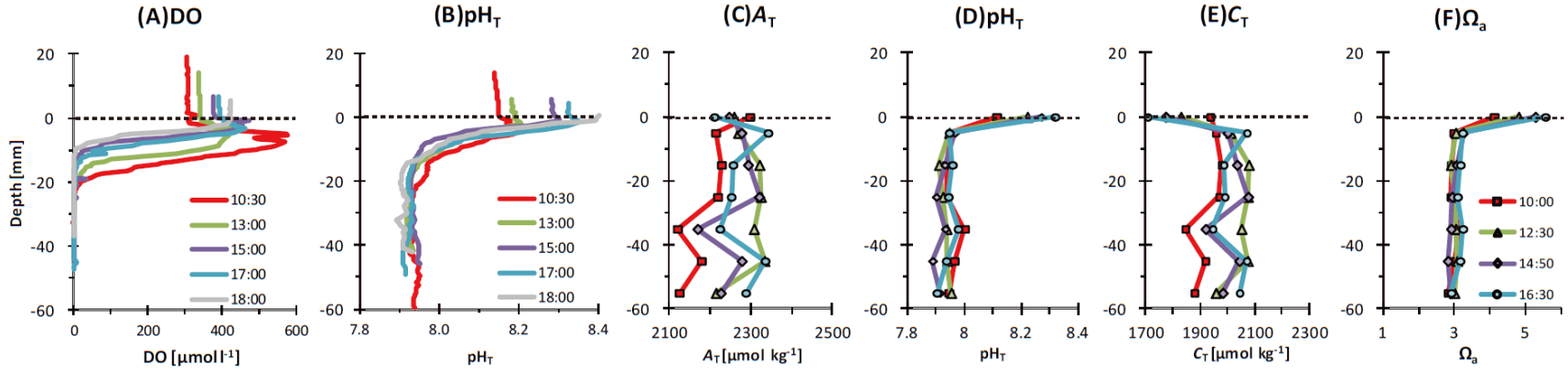

Figure 5-7. (A, B) Results of in situ DO and pH profiling during the day measured by microelectrode analysis. (C, D) Results of total alkalinity and pH profiling using pore waters obtained during the day. (E, F) C_T and Ω_a profiles calculated using the data shown in C and D

5-3-2-3. Nutrient concentration profiles

A series of 10–mm-average pore water profiles of nutrient concentrations (NO_3^-, NO_2^-, NH_4^+, SiO_2 and PO_4^{3-}) are presented in Figures 5-8 and 5-9. Nutrient concentrations in water column were less than those in the sediment except for NO_3^- and SiO_2 at night. Almost all of nutrient concentrations increased with depth. Especially, SiO_2. NO_3^- and NO_2^- values are lower than 1 μmol l^{-1} and 0.5μmol l^{-1}, respectively, except for the case of 20:15. Difference between night and day time were not significant and no common rule for temporal change pattern were seen.

Night

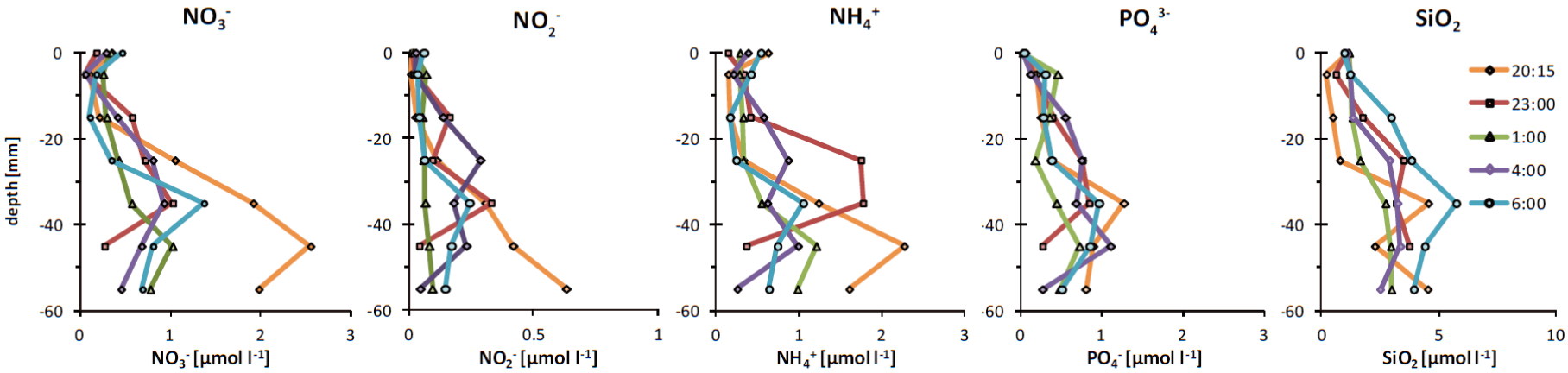

Figure 5-8. Nutrient concentrations (NO_3^-, NO_2^-, NH_4^+, PO_4^- and SiO_2) profiles at night

Day

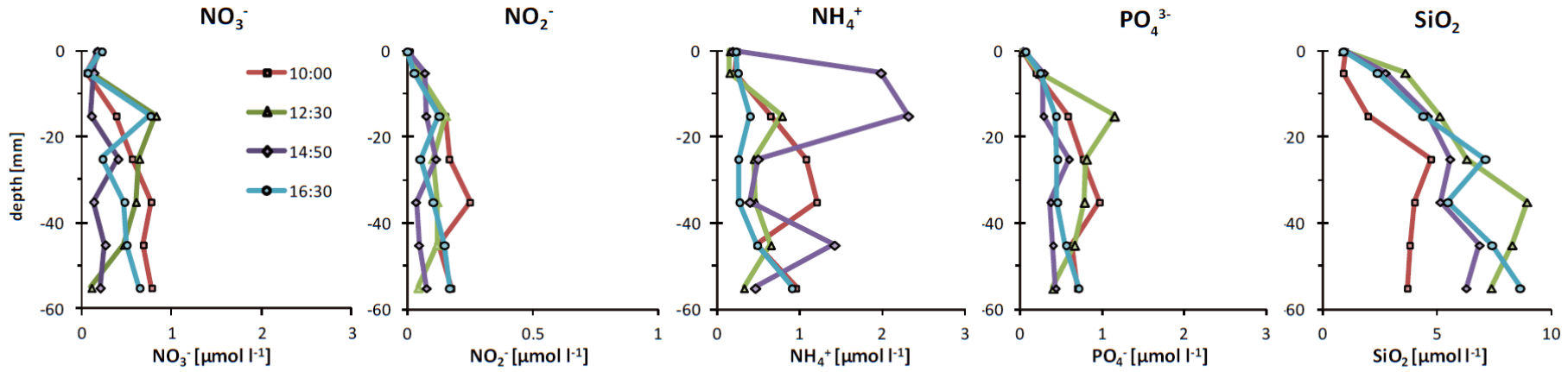

Figure 5-9. Nutrient concentrations (NO_3^-, NO_2^-, NH_4^+, PO_4^- and SiO_2) profiles at day time

5-3-3. eddy covariance

DO fluxes from the high-resolution data for each 20-min interval was undertaken at a frequency of 16 Hz. The eddy flux, as described in Chapter 1-4-3, is defined as $(\overline{U'_z \times C'})$, with $\overline{U_z}$ and $\overline{C}$ values defined using least square linear fits to U_z and C values at a 2-min interval, as determined by calculating a 1-sided cospectrum of $U'_z \times C'$ (Berg et al., 2003). DO concentrations, seawater velocities, and cumulative flux within each burst were carefully examined to identify nonlinear variations that would typically be caused by floating debris temporarily attached to or obstructed the sensors. An example of the raw data, in the form of velocity components and DO concentrations, derived fluxes for each burst, and the final lumped 20-min flux, is shown in Figure 5-10 according to $(\overline{U'_z \times C'})$, with horizontal velocities varying up to 10 cm s^{-1}, and vertical velocities varying up to 2 cm s^{-1}.

Figure 5-10 (C) shows the 2-min calculated cumulative flux for each burst, revealing a clear linear trend that indicates the presence of a strong flux signal within the data and a statistically good representation of all eddy sizes that contribute to the flux. In the case that the R^2 value between time and cumulative O_2 flux values for each time series was higher than 0.5, then the data were used for calculation, whereas low R^2 values indicate data that do not reflect the true flux, primarily because these data included bursts or parts of bursts that contained anomalous data. The 2-min burst eddy flux data were grouped to yield 20-min averaged fluxes and associated standard errors (Figure 5-10 (E)) that were extracted and used in subsequent calculations.

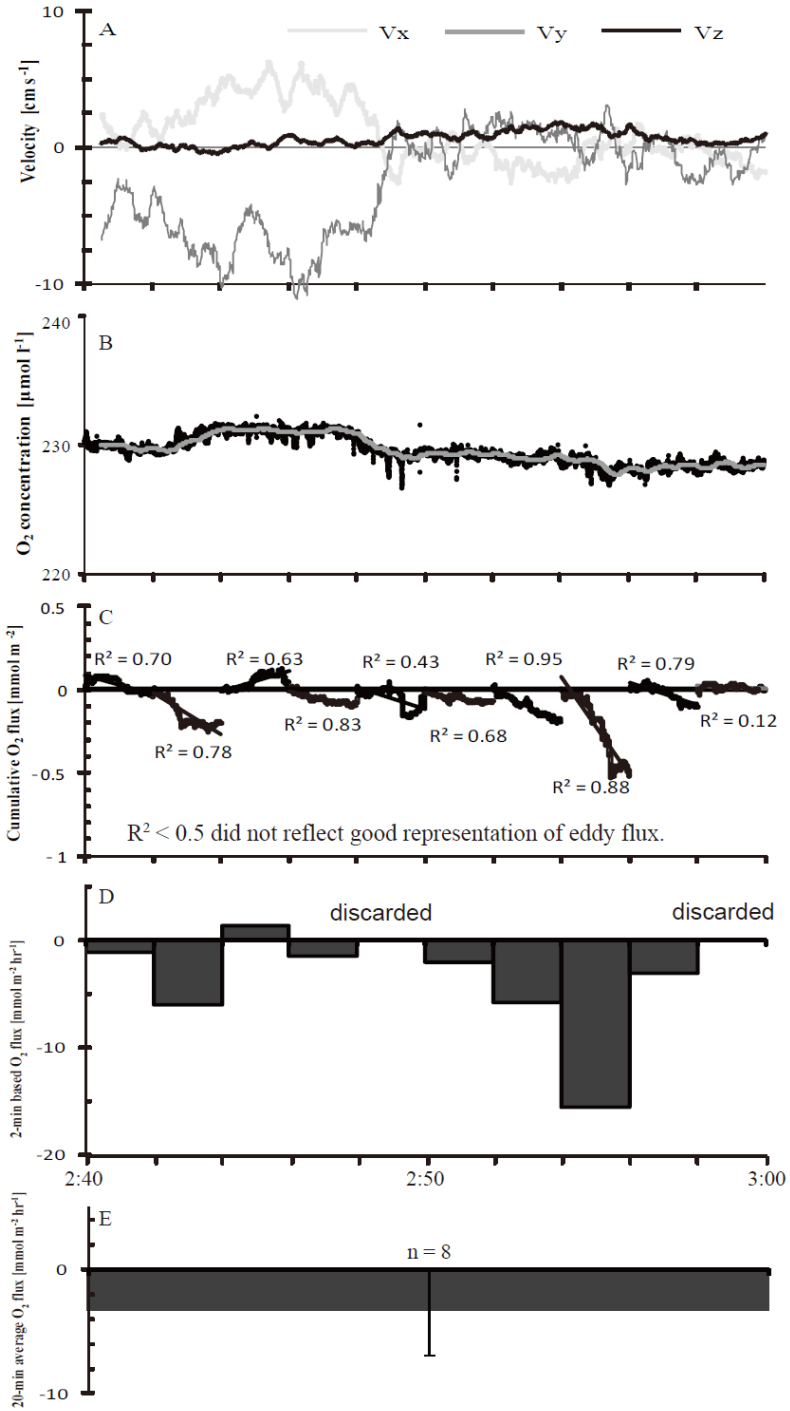

Figure 5-10. Raw eddy covariance data and derived fluxes through one 20-min-long bursts (A) Three mean current velocity (30-s mean) (B) Measured high temporal resolution DO concentration: Noise is not visible in either velocity or DO data. (C) Calculated cumulative DO flux at sediment-water interface for each burst (D) Calculated DO flux for each burst: The negative values represent O_2 uptake. (E) Averaged DO flux over the ten bursts representing 20-minutes mean value: Error bars are standard errors.

Figure 5-11 shows 20-min-averaged time series changes in O_2 flux; positive values indicate flux of O_2 produced from sediments to water column, whereas negative values represent O_2 flux to sediments from the water column. Nighttime (19:00 to 06:00 local time) O_2 uptake had an average rate of 4.95 ± 0.77 (Standard error; SE) mmol m^{-2} hr^{-1} on 4 October, and 5.66 ± 0.94 (SE) mmol m^{-2} hr^{-1} on 5 October. In comparison, the daytime (06:00 to 19:00) was dominated by O_2 production, with an average rate of production of 23.99 ± 3.19 (SE) mmol m^{-2} hr^{-1} on 5 October and 14.44 ± 9.04 (SE) mmol m^{-2} hr^{-1} on 6 October.

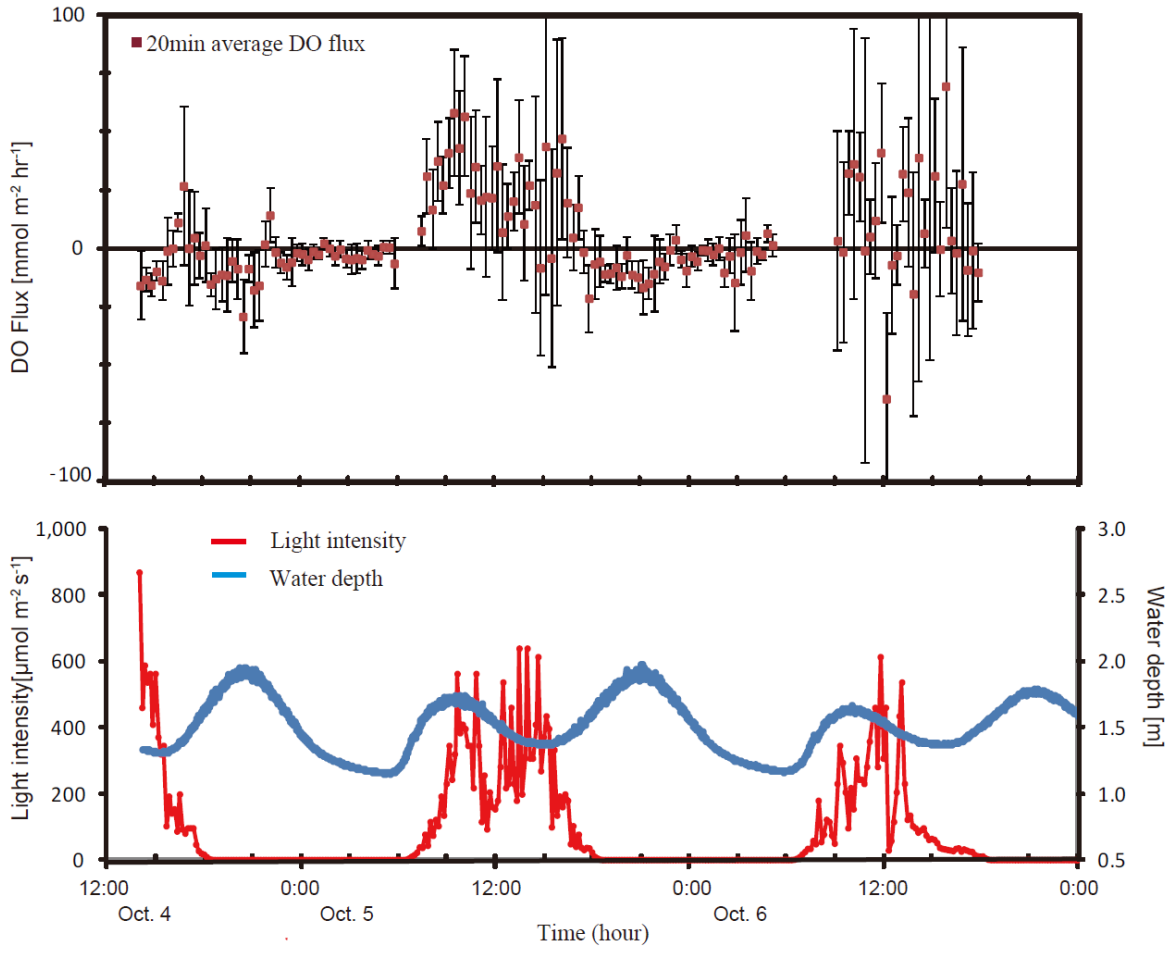

Figure 5-11. Daily changes in twenty minutes average DO flux value at Shiraho reef sand area, water depth, and light intensity from Oct. 4 to Oct. 6

5-4. Discussion

5-4-1. Comparison of pH between microelectrode and pore water sampling

Sediment pore water profiles were measured by both microelectrode and cores. The differences between these two methods should be discussed first. In this chapter, their profiles were examined for comparison since pH_T were the only profiles measured by both microelectrode and cores.

Figures 5-12 and 5-13 show daytime and nighttime pH_T profiles measured by microelectrode and pore water analysis, respectively. The pH of water column and pore water in the sediment deeper than 25mm depth showed no significant difference between the two methods. However, pH measured by pore water analysis at the depth less than 25 mm was slightly lower than that of microelectrode. This difference is considered due to the following reasons. There were many burrows in the upper 10 mm sediment, and micro topography were not uniform. While microelectrode profile reflects just one sticked profile, pore water analysis reflects averages of six cores. Moreover, two pH profiles were not measured strictly at the same time. Also, since pH microelectrode is very sensitive, the values were not stable if something touched it. Discussion in the following sections are described considering the above factors.

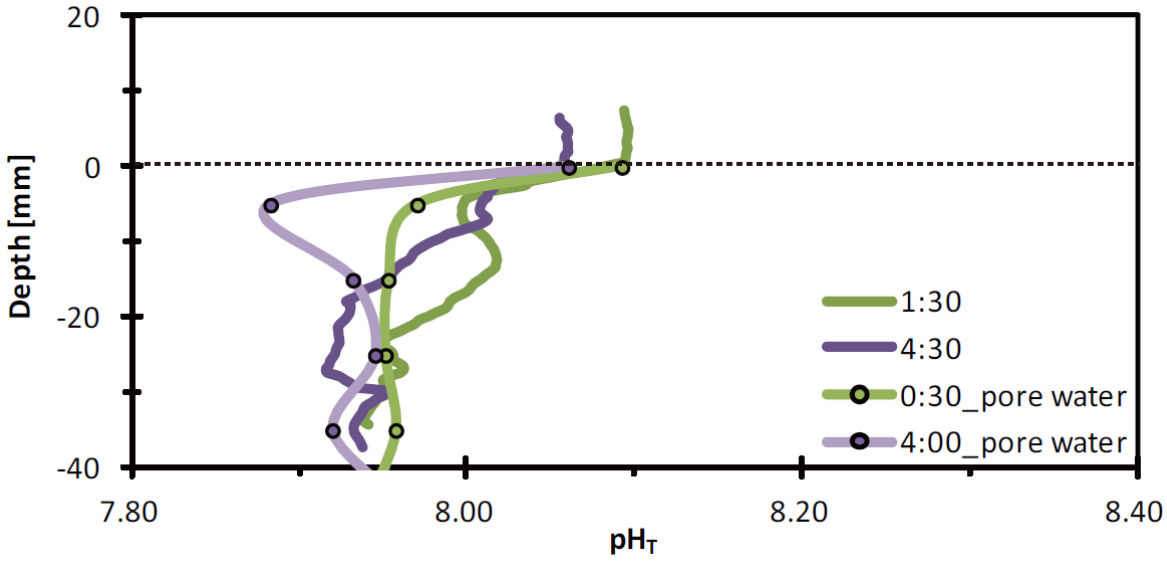

Figure 5-12. pH_T profile measured by microelectrode and pore water at night

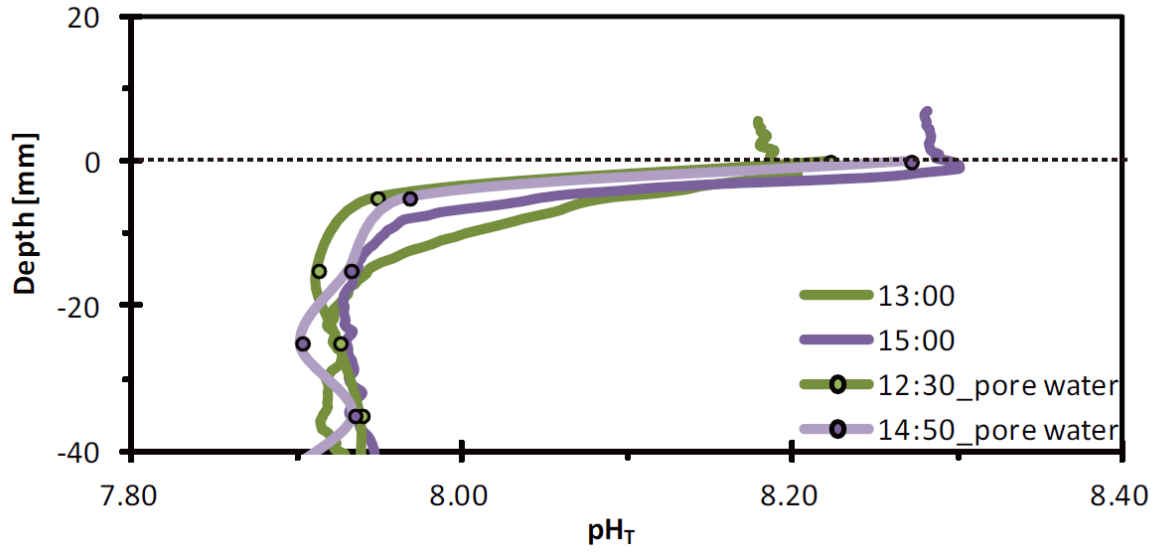

Figure 5-13. pH_T profile measured by microelectrode and pore water at day time

5-4-2. Sediment pore water profile

Figure 5-14 shows a summary of DO and carbonate profiles obtained during the study. The saturation state of aragonite (Ω_a) was converted to foraminifera (Ω_{fora}) values determined by this study (Chapter 3). Using equation (3-4) in Chapter 3, when dissolution rate is equal to zero, Ω_{fora} is defined to be 1.0.

DO and Ω_{fora} values in the water column decreased with time during night as a result of nighttime respiration by organisms (Kayanne et al., 2005, Watanabe et al., 2013), with DO decreases with depth defining a downward convex curve at depths of 0-10 mm. When reactions occur in sediment, the profiles of solutes show decrease or increase with convex curve according to Fick's law. Aerobic respiration is described as follows:

$$CH_2O + O_2 \rightarrow CO_2 + H_2O \quad \text{(aerobic respiration)} \quad (5\text{-}3)$$

Thus, DO decreases with downward convex curve means that pH and Ω_a values also decreased as respiration by some organisms in sediment consumed oxygen and produced CO_2.

Anaerobic organism-related reaction should occur at depths of >10 mm, as O_2 concentrations were exhausted at this depth. These O_2-depleted conditions may cause, denitrification, Mn reduction, Fe reduction, and eventually sulfate reduction. Chen (2002) summarized these reactions as follows:

$$(CH_2O)_{106}(NH_3)_{16}H_3PO_4 + 84.8HNO_3$$

$$\rightarrow 106CO_2 + 148.4H_2O + 42.4N_2 + 16NH_3 + H_3PO_4 \quad \text{(denitrification)} \quad (5\text{-}4)$$

$$(CH_2O)_{106}(NH_3)_{16}H_3PO_4 + 236MnO_2 + 472H^+$$

$$\rightarrow 106CO_2 + 366H_2O + 236Mn^{2+} + 8N_2 + H_3PO_4 \quad \text{(Mn reduction)} \quad (5\text{-}5)$$

$(CH_2O)_{106}(NH_3)_{16}H_3PO_4 + 424FeOOH + 848H^+$

$\rightarrow 106CO_2 + 742H_2O + 424Fe^{2+} + 16NH_3 + H_3PO_4$ (Fe reduction) (5-6)

$(CH_2O)_{106}(NH_3)_{16}H_3PO_4 + 53SO_4^{2-} + 106H^+$

$\rightarrow 106CO_2 + 106H_2O + 53H_2S + 16NH_3 + H_3PO_4$ (sulfate reduction) (5-7)

with all of these processes producing CO_2.

On the other hand, Ω_{fora} values are generally 1.0 at depths of >5 mm, whereas A_T values are unstable. More than 40 % of the sediment samples consisted of foraminifera (Figure 2-3), and the dissolution of calcium carbonate can be described as follows:

$$CaCO_3 + CO_2 + H_2O \rightarrow Ca^{2+} + 2HCO_3^- \quad (5\text{-}8)$$

in a reaction that consumes CO_2. This indicates that if any organic reactions including aerobic respiration occur, inorganic Mg-calcite dissolution would act to keep Ω values constant.

Significant nighttime decreases in DO within the uppermost 10 mm of sediment were coincident with a two-step decrease in pH between depths of 0 and 20 mm (Figure 5-6), as previously observed by Rao et al. (2012), who measured nighttime DO and pH profiles using microelectrodes at Heron Reef, Australia. Although the two study sites are different, the DO values at Heron Reef were depleted in the upper 6 mm of sediment, whereas pH values decreased in the upper 30 mm before reaching a constant value of about 7.5. This indicates that some of the reactions described above (reactions 5-4 to 7) may decrease pH values under anaerobic conditions at depths between 10 and 20 mm. Miyajima et al. (2001) reported that denitrification rate at sandy area in Shiraho reef was 1.7-6.5 μmol m^{-2} h^{-1} between 0-15 cm depths. Although this value was 100-1000 times smaller than DO flux at sediment-water interface measured by this study, denitfirication may be one of the most considerable reactions under anaerobic conditions.

In comparison, daytime conditions led to maximum DO and pH values at depths of 2–9 mm, due to benthic photosynthesis and calcification in sunlit surface sediments that promote O_2 evolution and CO_2 uptake, although the depths of these maxima were variable because of light conditions. These benthic organisms were mainly Bacillariophyta (diatoms) in sediment (Suzumura et al., 2002). Deeper sediments have pore-water O_2 and pH values that decreased as a result of organic matter oxidation. In addition, Mg-calcite would dissolve in deeper sediments even during the daytime, as Ω_{fora} values were generally 1.0 at depths of >5 mm.

Rao et al. (2012) also measured concentrations of nutrient (NO_3^-, NO_2^-, NH_4^+ and SiO_2) in pore-water. These profiles (Figure 5-15) demonstrate similar trend to my observation except for NH_4^+, which is ten times higher at Heron reef than that at Shiraho Reef. This should be because of wastewater and ground water influence to pore water, as Heron reef site was only 20 meter from the shore line.

In Chapter 6, I will focus on profiles at night when drastic and irregular O_2 changes have not been observed between surface sediment, to discuss the mechanism of Mg-calcite dissolution and its future impact by using A_T-C_T diagram.

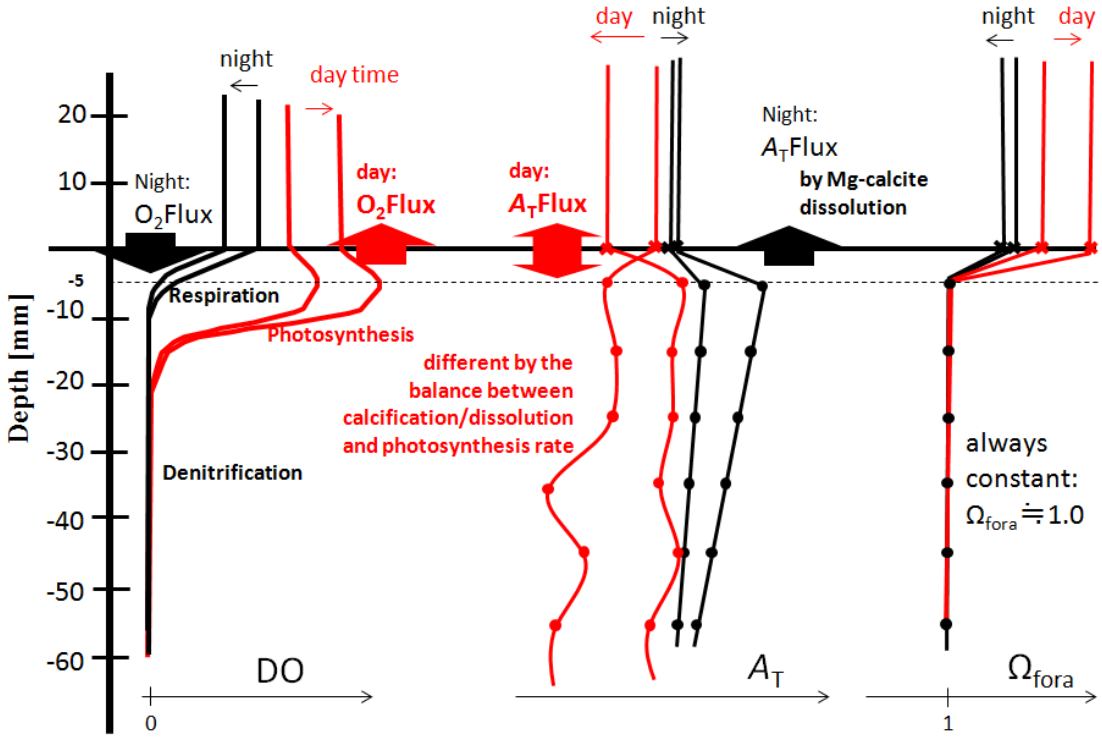

Figure 5-14. A summary of the typical profiles of DO, A_T and Ω_{fora} at night and day time: Black lines show night profiles, and red lines show day time profiles. A_T and Ω_{fora} were measured by pore water

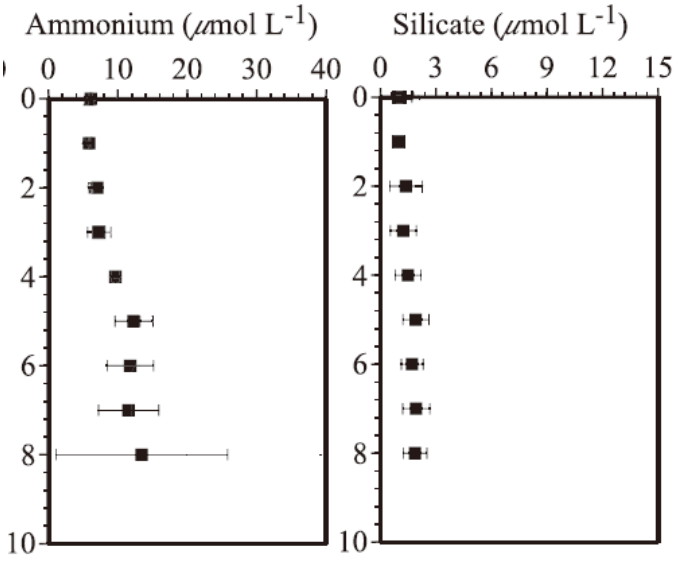

Figure 5-15. Profiles of pore-water solutes in Heron Reef sediments cited from Rao et al. (2012): Symbols represent the mean ± 1 SD of replicate profiles of ammonium and silicate (n = 3).

5-4-3. DO flux estimated from eddy covariance

Daily average DO fluxes measured by EC were 4.95 ± 0.77 and 5.66 ± 0.94 mmol m^{-2} hr^{-1} uptake at night, and 23.99 ± 3.19 and 14.44 ± 9.04 mmol m^{-2} hr^{-1} production during the day. These changes are considered to have been caused by production of O_2 during daytime photosynthesis by microalgae within the uppermost ~10 mm of the sediments, and respiration during the night that consumed O_2. Variations in light intensity as a result of change in cloud cover would explain the observation that the standard deviation of the daytime O_2 flux was 5-10 times larger than that during the nighttime; microelectrode-derived O_2 profiles show the similar variations.

The DO fluxes estimated during this study are 1.5-2 times higher during the night and 5-7 times higher during the day than those estimated by chamber experiment by Nakamura and Nakamori (2009). Previous studies have concluded that because chamber experiments and core incubations cannot duplicate hydrodynamic conditions, DO fluxes measured by these methods are underestimated compared with the fluxes measured using EC, even though weather conditions and hydrodynamic conditions differed among the study sites (Hume et al., 2011, Reimers et al., 2012).

In general, DO flux increases with an increase in horizontal current velocity (Hume et al., 2011, Berg et al., 2007). Figure 5-16 shows the relationship between nighttime horizontal velocities and DO fluxes during flood tide from 19:00 to 21:20 and ebb tide from 21:20 to 6:00 at each day. Unlike previous studies, there are no significant correlation between DO flux and horizontal velocity as determined by analysis of covariance (ANCOVA). In comparison, the average DO uptake during the flood tide was significantly different from that during the ebb tide as determined by *t*–test. While the average DO uptake during the flood tide was 11.3 mmol m^{-2} hr^{-1}, the average uptake during the ebb tide was 3.0 mmol m^{-2} hr^{-1}.

The constant nighttime O_2 gradient means that flood and ebb tides would have different hydrodynamic mechanisms, resulting in different diffusion coefficients.

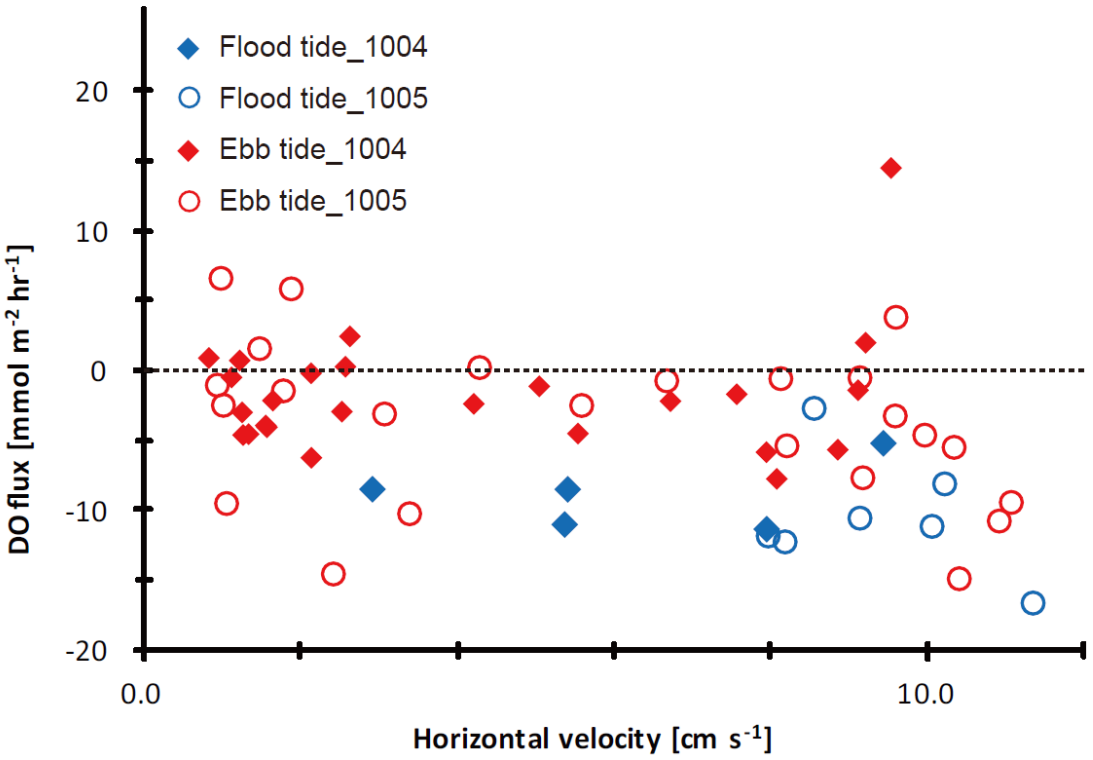

Figure 5-16. Relationship between DO flux and horizontal velocity: Blue symbols indicate flood tide time and red symbols indicate ebb tide time. Solid diamonds were observed on 4 to 5 Oct. at night and open circles were observed on 5 to 6 Oct. at night.

5-4-4. Diffusion coefficient calculated by eddy covariance and DO profile

Nighttime diffusion coefficients is calculated using DO flux observations obtained by eddy covariance estimations and O_2 profiling measured by microelectrode. As described in Chapter 5-4-1, microelectrode analysis does not reflect the average profile of sandy area, but instead yields a specific profile at the observed point. Therefore ideally numerous concurrent profiles should be measured for evaluating the average profile of sandy area. However, since only one profile could be measured at once during this study, diffusion coefficients calculated by average nighttime DO gradients and DO fluxes are discussed.

Table 5-1 summarizes the parameters observed during the night of 4 October, with an average DO flux of 4.60 ± 2.50 mmol m^{-2} hr^{-1} and an average DO gradient at the sediment-water interface of 53.4 ± 19.6 μmol l^{-1} mm^{-1}, yielding a nighttime average diffusion coefficeient at sediment-water interface of 4.9 ± 2.4 × 10^{-4} cm^2 s^{-1}. Li and Gregory (1974) determined molecular diffusion of HCO_3^- as 11.8 × 10^{-6} cm^2 s^{-1}, and Berner (1980) reported that diffusion coefficient (D_T) in shallow water sediments was 30-100 times higher than molecular diffusion (D_s). The diffusion coefficients estimated in this study are conformable with those obtained by previous studies.

As mentioned in Chapter 5-4-3, DO flux was different between at flood tide and ebb tide. Indeed, according to Table 5-1, while diffusion coefficient at flood tide was 9.3 ± 2.7 × 10^{-4} cm^2 s^{-1}, mean diffusion coefficient at ebb tide was 4.2 ± 2.1 × 10^{-4} cm^2 s^{-1} though only a few data was given. Figure 5-17 shows calculated diffusion coefficient on 4 Oct. at night, water depth, and its one minute standard deviation, which indicated the changes in seawater pressure. Diffusion coefficient at day time was not calculated because standard deviation of day time DO flux was large. The value at 21 pm (flood tide) was highest among all four cases, and that at 1:30 am (ebb tide) was lowest among all. Calculated diffusion coefficient seems to

be high when the fluctuation of water depth increases. If fluctuation of water depth increases, pressure in water column changes and diffusion coefficient at sediment-water interface will increase. Precht and Huettel (2004) reported that both wave-induced oscillating flows and horizontal current increase advection of pore water. At Shiraho reef area, diffusion coefficient would be influenced not only by the current but also by some physical process such as pressure change in water column which are different between flood tide and ebb tide. However, as there are only four obtained data, further observation is necessary.

These diffusion coefficient values was combined with A_T gradients to yield A_T flux estimates (Table 5-1). All A_T fluxes estimated from DO profiles and DO fluxes were based on ebb tide time because data in flood tide were not observed. Estimated A_T fluxes were 1.07 mmol m^{-2} hr^{-1} at 01:00 4 October, 1.62 mmol m^{-2} hr^{-1} at 04:00, and 2.60 mmol m^{-2} hr^{-1} at 06:00. Here, a simple A_T profile and average values are considered, although in reality the A_T profile at sediment-water interface may be complex and the precise A_T flux could be significantly different. However, as discussed in Chapter 5-4-1, the pore water A_T values represent average values for the A_T profile across the sandy area, suggesting that those values represented the typical A_T flux at sand area.

Table 5-1. Observed and calculated parameters on 4 Oct. at night: Values are shown as average and standard error (SE).

4 Oct. Night	DO Flux [mmol m^{-2} hr^{-1}]	DO slope [μmol kg^{-1} mm^{-1}]	Diffusion coefficient [10^{-4} cm^2 s^{-1}]	A_T slope [μmol kg^{-1} mm^{-1}]	Calculated A_T Flux [mmol m^{-2} hr^{-1}]
21:00	−11.5±3.4	70.1	9.3±2.7	---	---
23:30	−5.2±4.2	47.8	6.2±4.9	---	---
1:00	---	---	2.0−4.9(assumued)	12.4	0.44−1.07
1:30	−2.4±1.1	67.6	2.0±0.9	---	---
4:00	---	---	4.4−4.9(assumed)	18.8	1.45−1.62
4:30	−2.2±1.0	28.1	4.4±2.0	---	---
6:00	---	---	4.4−4.9(assumed)	30.2	2.33−2.60
average	−4.60±2.50	53.4±19.6	4.9±2.4	---	---

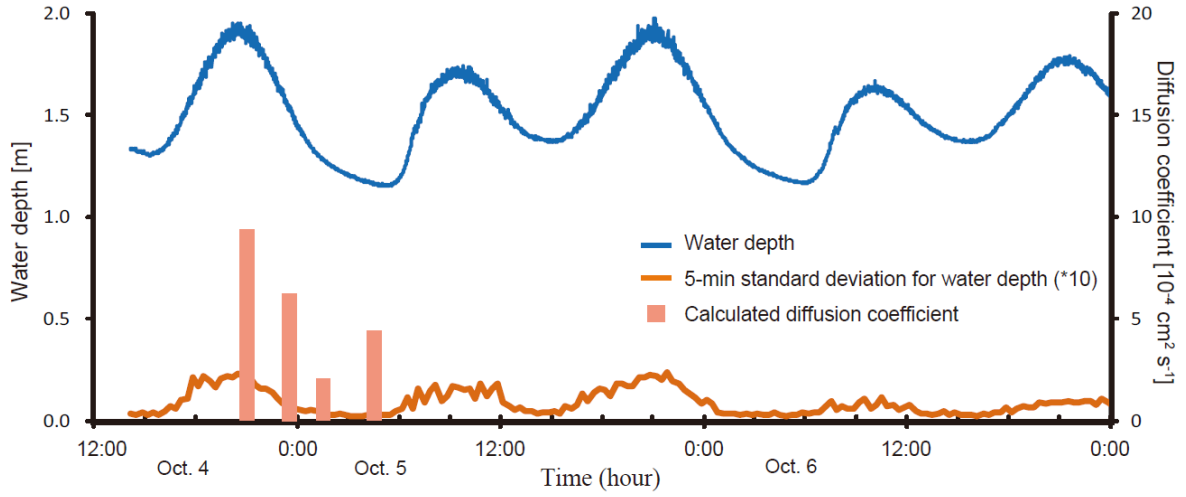

Figure 5-17. Relationship between water depth, its 5-min standard deviation for water depth, and diffusion coefficient calculated by EC and DO slope at sediment-water interface: The values of standard deviation lines are amplified tenfold for easiness to see.

Chapter 6.

General discussion

6-1. Comparison of A_T flux estimated by flow-controlled chamber and EC and A_T profile in sediment

Figure 6-1 (A) shows the nighttime A_T flux plotted against Ω_{fora} in water column determined by flow-controlled chamber experiment and estimated based on the relationship between EC and A_T gradient at sediment-water interface. A_T flux calculated by diffusion coefficient and A_T profile in sediment was plotted in red symbols, while dissolution rates determined by the flow-controlled chamber experiment were converted to A_T flux. According to both estimation, A_T flux could occur even when Ω_{fora} in water column was higher than 1.0 because A_T in the pore water was higher than that in the water column, which produced the upward A_T flux.

On the other hand, flow-controlled chamber experiment showed that A_T flux did not change with decreasing Ω_{fora} under CO_2 added condition. Figure 6-1 (B) shows the relationship between bulk sediment dissolution rate and Ω_{fora} determined by laboratory experiment in this study (Chapter 3), which indicates that A_T flux increases with decreasing $\Omega_{fora.}$ On the other hand, this relationship was not observed in the flow-controlled chamber experiment, suggesting that effect of Ω_{fora} decrease in water column did not affect the A_T flux at the sand area although dissolution rate of individual Mg-calcite mineral increases as Ω_{fora} decreases in seawater.

The fact that the CO_2 increase in the water column did not affect the A_T flux in the chamber experiment would be related to the imperfect representation of real condition inside the

chamber due to its methodological weakness because pore water processes in sediment were not considered at all in chamber experiment. Indeed, results of chamber experiment especially under CO_2 added condition may not represent what will happen in the actual environment in the future, primarily because only seawater in water column was changed in short-time experiment but the pore water in sediment would not be changed.

I reveal that A_T flux did not increase if only Ω_{fora} in water column decreased. It is essential to understand not only the water column chemistry but also the profiles of the pore water chemistry (carbonate and DO) to accurately predict the A_T flux.

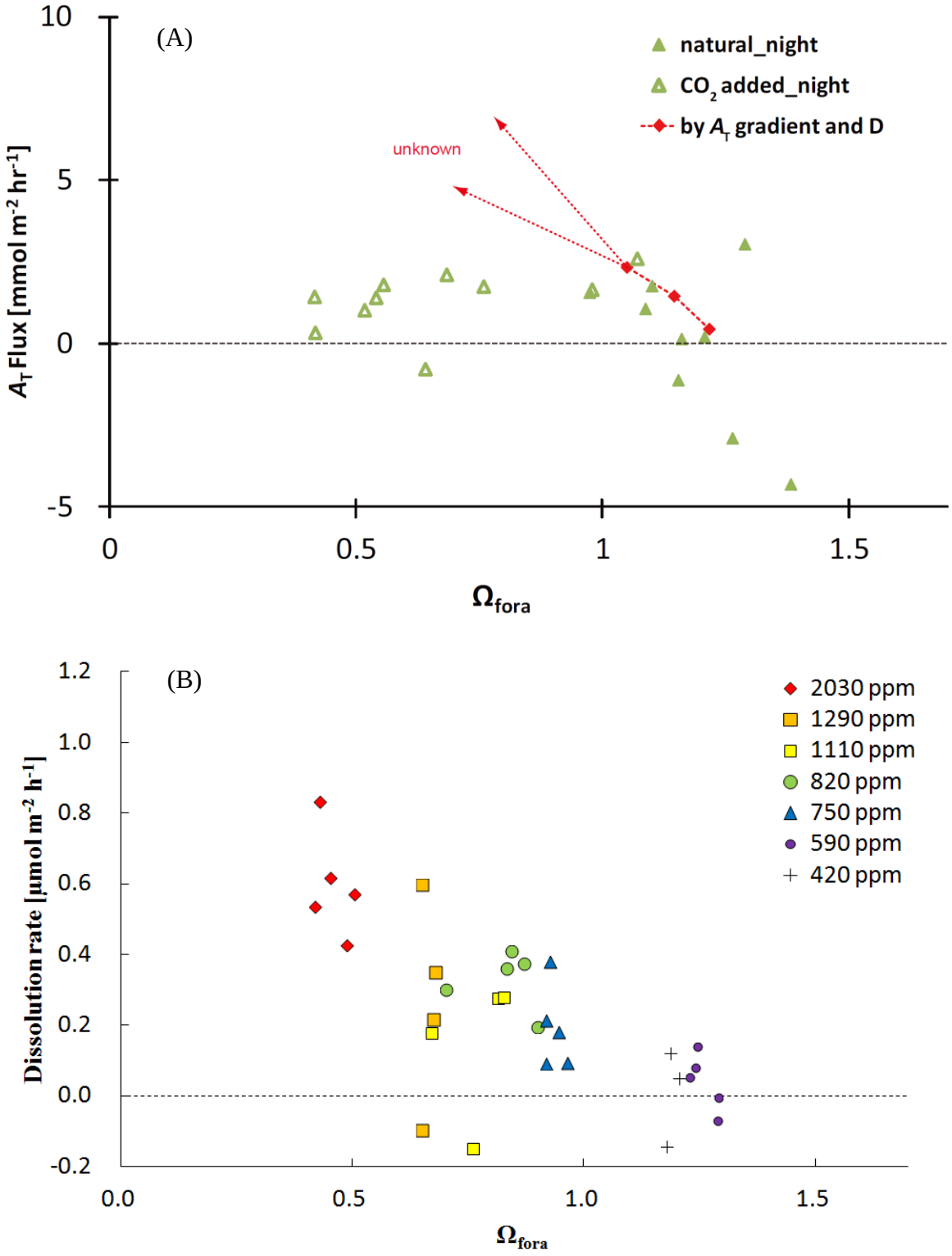

Figure 6-1. (A) The relationship between average A_T flux Ω_{fora} at night: triangle symbols indicate flow-controlled chamber, and red symbols indicate values calculated by A_T profiles and diffusion coefficient measured by EC. (B) The relationship between average dissolution rate and Ω_{fora} (bulk) measured by laboratory experiment in this study.

6-2. Mechanism of Mg-calcite dissolution in coral sand area

Figure 6-2 summarizes typical nighttime DO, A_T, and Ω_{fora} profiles within top 30 mm of the sand. DO profiles within sediments are based on microelectrode observation; other parameters were based on pore water analysis. The sediments can be subdivided into three zones based on DO and Ω_{fora} profiles, with zone I having DO values of >0 and Ω_{fora} values of >1, zone II having DO > 0 and Ω_{fora} = 1, and zone III having DO = 0 and Ω_{fora} = 1. At depths greater than "x" mm (i.e. boundary between layer I and layer II), Ω_{fora} is assumed to be equal to 1.0.

Although the hydrodynamics within the sediment are unknown, diffusion coefficients within the sediment are assumed to be constant with depth. Under this assumption, when reactions such as respiration or carbonate dissolution occur, the profiles of solutes show decrease or increase with downward convex curve according to Fick's law. Thus, the downward convex decrease in DO observed in zone I suggests that C_T should also increase with a downward convex curve, whereas A_T values are expected to increase linearly, primarily as no Mg-calcite dissolution is expected to have occurred. In comparison, zone II, between "x" mm and 10 mm depth, should have downward convex change in both A_T and C_T as a result of respiration and Mg-calcite dissolution. Here, the peak values of A_T and C_T are assumed to occur at a depth of 5 mm, though only average values between 0 to 10 mm were observed. In depths of >10 mm within zone III, A_T and C_T values decrease linearly or with downward convex curve; linear decreases indicate that no reactions occurred between 10 and 30 mm depth, and some reactions occurred at deeper than 30 mm, with gradients at depths >10 mm caused by diffusion alone. In comparison, downward convex curves suggest that both denitrification and Mg-calcite dissolution occurred, keeping Ω_{fora} values at 1.0. In addition, a Ω_{fora} isograms within A_T-C_T diagram plots between dissolution and denitrification vectors

(Figure 6-3), indicating that Ω_{fora} values could remain at a constant value of 1.0 as a result of the combined effects of both reactions.

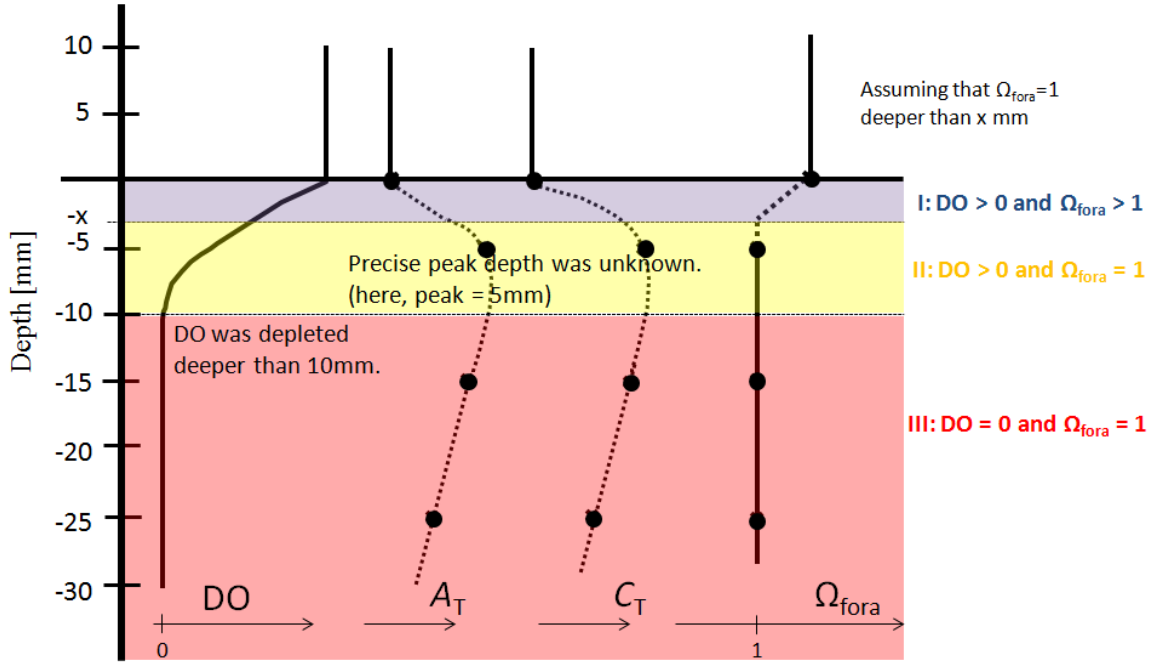

Figure 6-2. A summary of typical profiles of DO, A_T, C_T and Ω_{fora} at night: Solid lines are based on microelectrode observation and pore water analysis, and dotted lines are considered based on carbonate parameters measured by pore water analysis, which are shown by solid circle symbol.

6-3. A_T flux at sediment-water interface in A_T-C_T diagram

Previous studies evaluated Mg-calcite dissolution as a reaction between water column and the sediment surface (Andersson et al., 2003; Morse et al., 2006). However, the data presented here indicate that A_T increase within the water column were caused by A_T out flux from the sediments dues to A_T gradient at a depth of 0-5 mm. In addition, Ω_{fora} values in sediments at depths of >5mm are constant, at a value of 1.0. In this section, A_T flux will be discussed by using water column-sediment pore water A_T, C_T, Ω_{fora} and DO profiles and A_T-C_T diagram considering above.

Figure 6-3 shows the pore water carbonate chemistry (A_T and C_T) in both sediment and the water column; black dashed lines are Ω_{fora} contours determined by this study (Chapter 3) and dashed color vectors indicate the changes in A_T and C_T caused by chemical reactions (defined by Chen, 2002, Table 6-1). Water column A_T and C_T values decreased during the daytime as a result of net photosynthesis and calcification with the proportion of about five to one, whereas they increased during the nighttime as a result of net dissolution and respiration with the proportion of about seven to one (Figure 5-5); the rates of these increases and decreases can be calculated by the sum of each vector (Watanabe et al., 2006). In comparison, sediment hosted pore waters almost always have Ω_{fora} values of 1.0 although A_T and C_T values in sediment were not constant due to respiration and Mg-calcite dissolution.

Figure 6-4 shows the relationship between A_T and C_T values within both the water column and pore waters in sediments at night. Each vector indicates changes in A_T and C_T with depth based on the profiles shown in Figure 6-2; these figures show that C_T increased with respiration and Mg-calcite dissolved within zone II, leading to an increase in A_T. This reaction causes a difference between A_T values within the water column and the pore water within the sediments, causing A_T flux at the sediment-water interface.

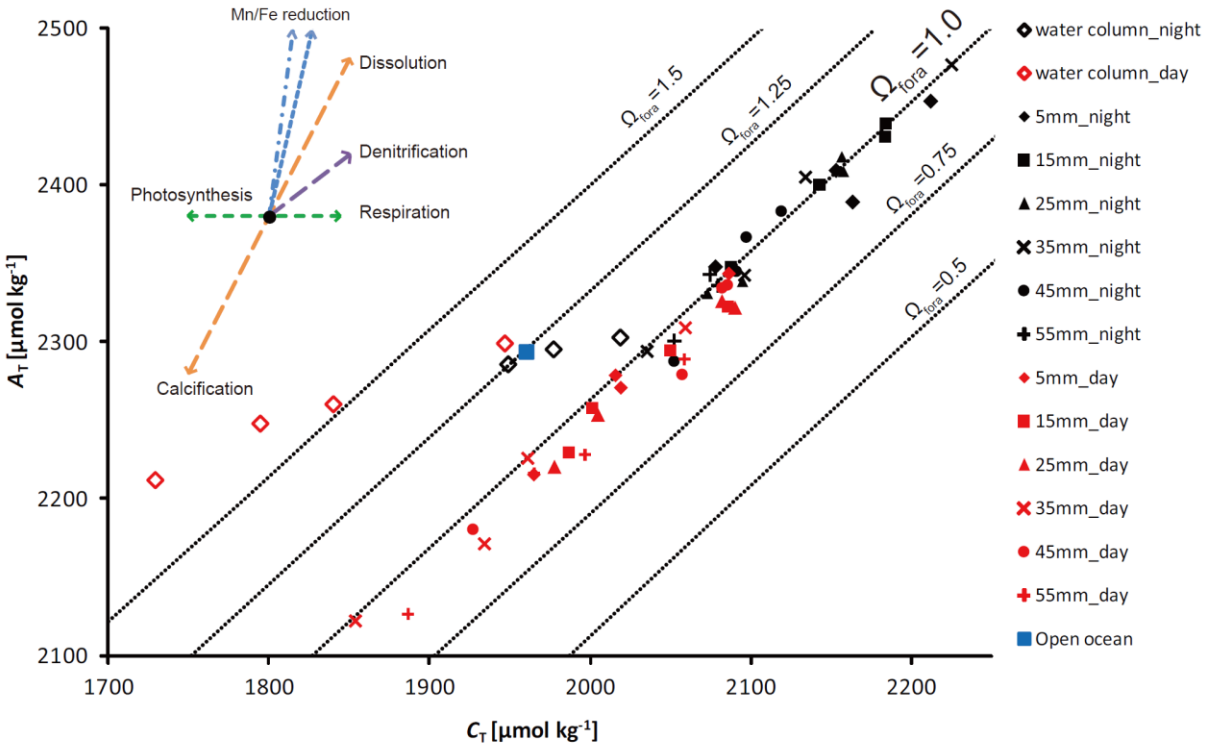

Figure 6-3. A_T-C_T diagram: Black dashed lines indicate Ω_{fora}. Black symbols indicate night and red indicate day time values. Open diamonds show water column A_T and C_T, solids show pore water values in the sediment. Blue solid square indicates typical open ocean vlue at Shiraho in summer. Several color vectors indicate each chemical reaction shown in Table 6-1.

Table 6-1. The relationship between metabolisms and A_T, C_T changes cited from Chen (2002)

	Metabolism	Reaction	ΔTA	ΔDIC	ΔTA/ΔDIC**
Production					
	Photosynthesis* (using NO_3^-)	$106CO_2 + 122H_2O + 16HNO_3 + H_3PO_4 <-> (CH_2O)_{106}(NH_3)_{16}H_3PO_4 + 138O_2$	17	-106	-0.16
	Photosynthesis* (using NH_4^+)	$106CO_2 + 106H_2O + 16\,NH_3 + H_3PO_4 <-> (CH_2O)_{106}(NH_3)_{16}H_3PO_4 + 106O_2$	-15	-106	0.14
	Calcification	$Ca_2^+ + 2HCO_3^- <-> CaCO_3 + H_2O + CO_2$	-2	-1	2
	NH_3 oxidation	$5NH_3 + 3HNO_3 -> 4N_2 + 9H_2O$	6***	---	
Decomposition/dissolution					
	Aerobic respiration (releasing NH_4^+)	$(CH_2O)_{106}(NH_3)_{16}H_3PO_4 + 106O_2 <-> 106CO_2 + 106H_2O + 16NH_3 + H_3PO_4$	15	106	0.14
	Dissolution of $CaCO_3$	$CaCO_3 + H_2O + CO_2 <-> Ca_2^+ + 2HCO_3^-$	2	1	2
	Denitrification	$(CH_2O)_{106}(NH_3)_{16}H_3PO_4 + 84.8HNO_3 <-> 106CO_2 + 148.4H_2O + 42.4N_2 + 16NH_3 + H_3PO_4$	83.8	106	0.79
	Manganese reduction	$(CH_2O)_{106}(NH_3)_{16}H_3PO_4 + 236MnO_2 + 472H^+ <-> 106CO_2 + 366H_2O + 236Mn^{2+} + 8N_2 + H_3PO_4$	471	106	4.4
	Iron reduction	$(CH_2O)_{106}(NH_3)_{16}H_3PO_4 + 424FeOOH + 848H^+ <-> 106CO_2 + 742H_2O + 424Fe^{2+} + 16NH_3 + H_3PO_4$	847	106	8.0
	Sulfate reduction	$(CH_2O)_{106}(NH_3)_{16}H_3PO_4 + 53SO_4^{2-} + 106H^+ <-> 106CO_2 + 106H_2O + 53H_2S + 16NH_3 + H_3PO_4$	105	106	0.99
	Methanogenesis	$CH_4 + SO_4^{2-} <-> HCO_3^- + HS^- + H_2O$	1	106	0.01

In this table, TA means A_T, and DIC means C_T.

* Redfield ratio is assumed for the organic matter production/decomposition

** Which is equivalent to the slope on the A_T- C_T diagram

*** When each mole of NH_3 is oxidized

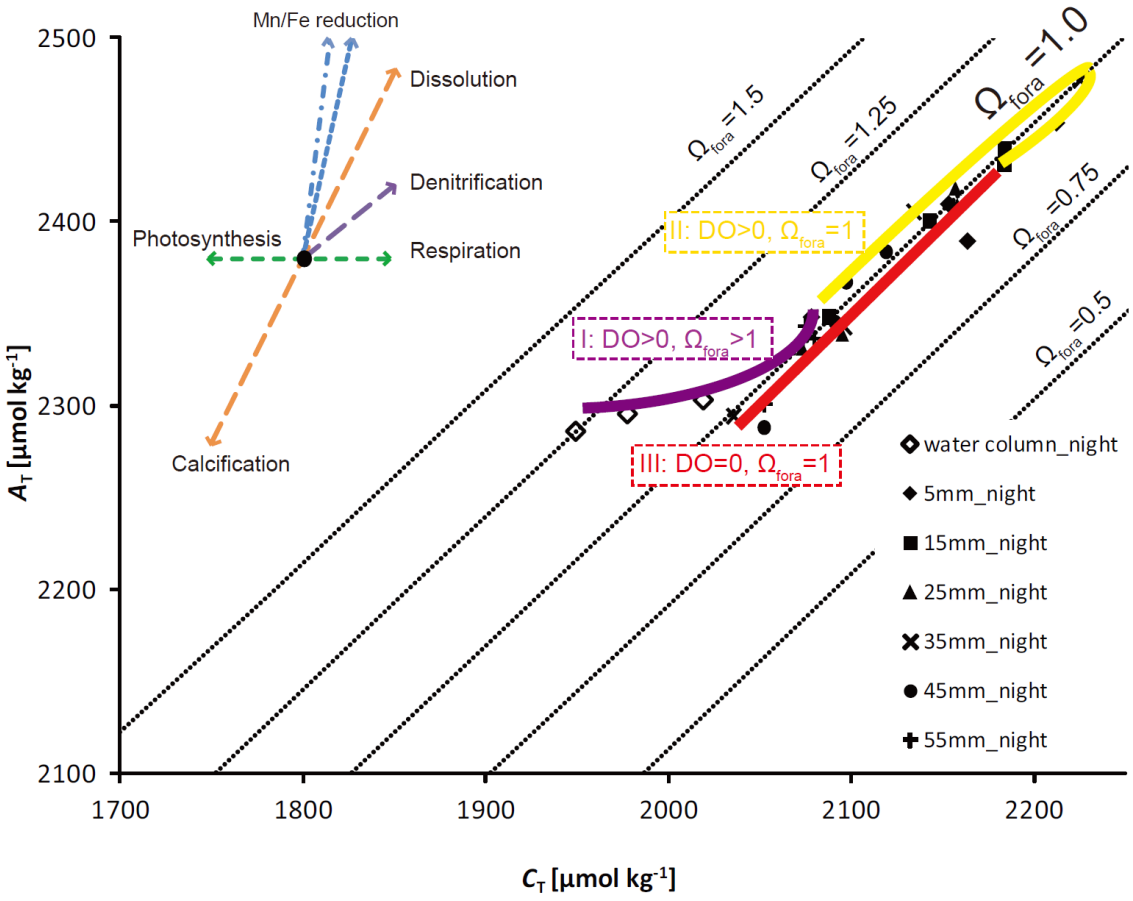

Figure 6-4. A summary of A_T and C_T in water column and in sediment at night: Three color lines (purple, yellow, and red) indicate changes in A_T and C_T according to profiles in Figure 6-2.

6-4. Future impact of ocean acidification on Mg-calcite dissolution

6-4-1. Qualitative assessment for ocean acidification

The burning of fossil fuels and future uptake of CO_2 by the oceans are predicted to reduce Ω_a in water column to 2.0 ~ 3.0 by 2100 (Kleypas et al., 2006). Previous studies evaluated Mg-calcite dissolution by using 1) non-biogenic Mg-calcite threshold and 2) relationship between dissolution rate and saturation state in water column (Andersson et al., 2003, 2009, Morse et al., 2006). However, this study shows that the Ω_a dissolution threshold of biogenic Mg-calcite in taxa such as coralline algae and foraminifera is 3.0 to 3.2 based on laboratory experiment (Chapter 3-3), and upward A_T flux is caused by both organic reaction such as aerobic respiration and inorganic Mg-calcite dissolution (Chapter 5-4-2). The result of this study suggests that A_T flux at sediment-water interface should be evaluated by diffusion coefficient of A_T and A_T gradient at sediment-water interface (Chapter 6-1). In this chapter, future A_T increase in water column at coral reef community caused by Mg-calcite dissolution in sediment is estimated based on A_T profile and A_T-C_T diagram.

Figure 6-5 shows the predicted A_T profile accompanying with seawater pCO_2 increase; this shows that if Ω_{fora} values within the water column become < 1.0 (under-saturated) and if DO profile within the sediment does not change, zone I would disappear, leading to an increase in the expansion of zone II to the sediment surface and Mg-calcite dissolution would occur all over through the sediment. In turn, this would lead to a steepening of A_T gradient, causing an increase in upward A_T flux at sediment-water interface.

Figure 6-6 shows A_T-C_T diagram that illustrates the future impact of increasing A_T flux. There were few occasions during nighttime spring tides when Ω_{fora} values in the water column were < 1.0 under CO_2 = 400 ppm condition (Figure 6-6: yellow ellipse area). This indicates that only a minor A_T flux would be observed. However, pCO_2 increase in seawater without a

change in the rate of biological photosynthesis and/or calcification causes the range of A_T and C_T values to move parallel to the change in C_T, as A_T values are not changed by increases in anthropogenic CO_2. This causes a shift from the yellow to red ellipses area (Figure 6-6). Once Ω_{fora} values within the water column become < 1.0, A_T flux at the sediment-water interface will increase, primarily as the A_T gradient at depths of 0-5 mm will also increase. This indicates that as Ω_{fora} values within the water column decrease, Mg-calcite within the sediment will more readily dissolve, suggesting in turn that A_T flux would also increase drastically, as all of the Mg-calcite within the sediment would dissolve.

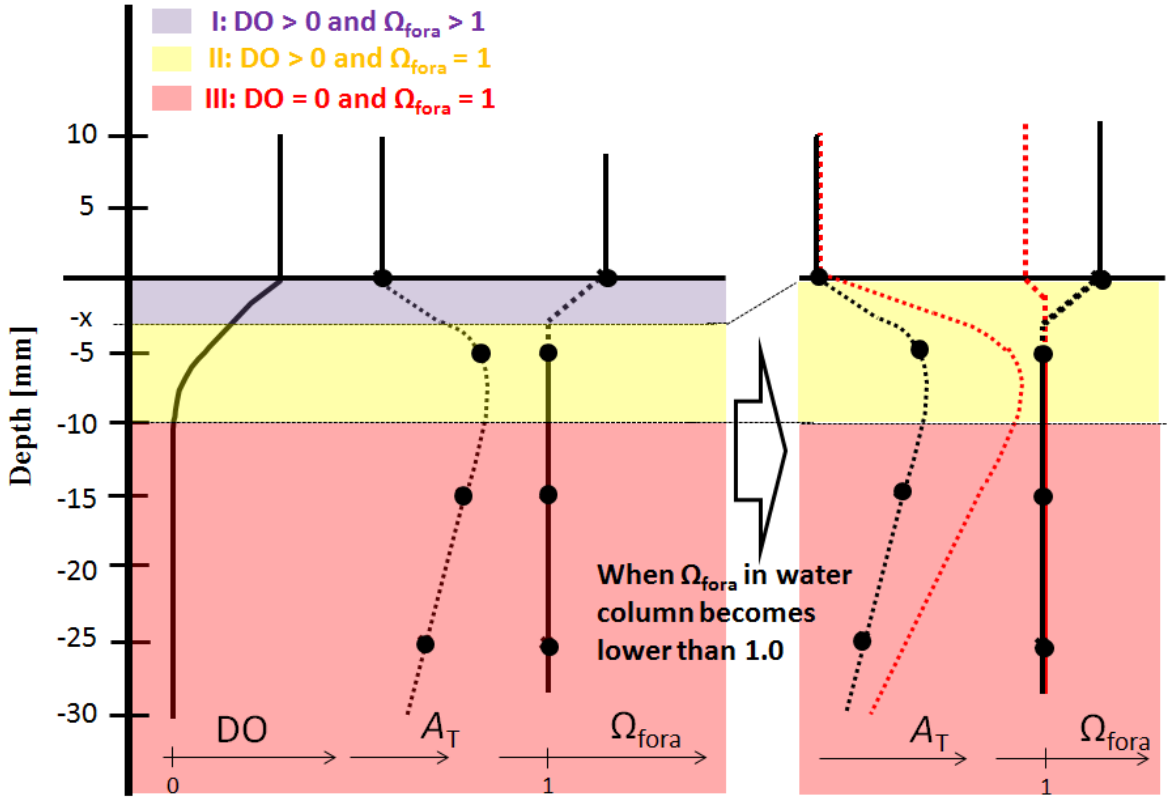

Figure 6-5. Estimated A_T and Ω_{fora} profiles when pCO_2 increases by ocean acidification and Ω_{fora} in water column decreases below 1.0: Solid black lines are based on microelectrode observation and pore water analysis, and dotted black lines are considered based on carbonate parameters measured by pore water analysis, which are shown by solid circle symbol. Red dotted lines are estimated profiles when Ω_{fora} in water column becomes lower than 1.0.

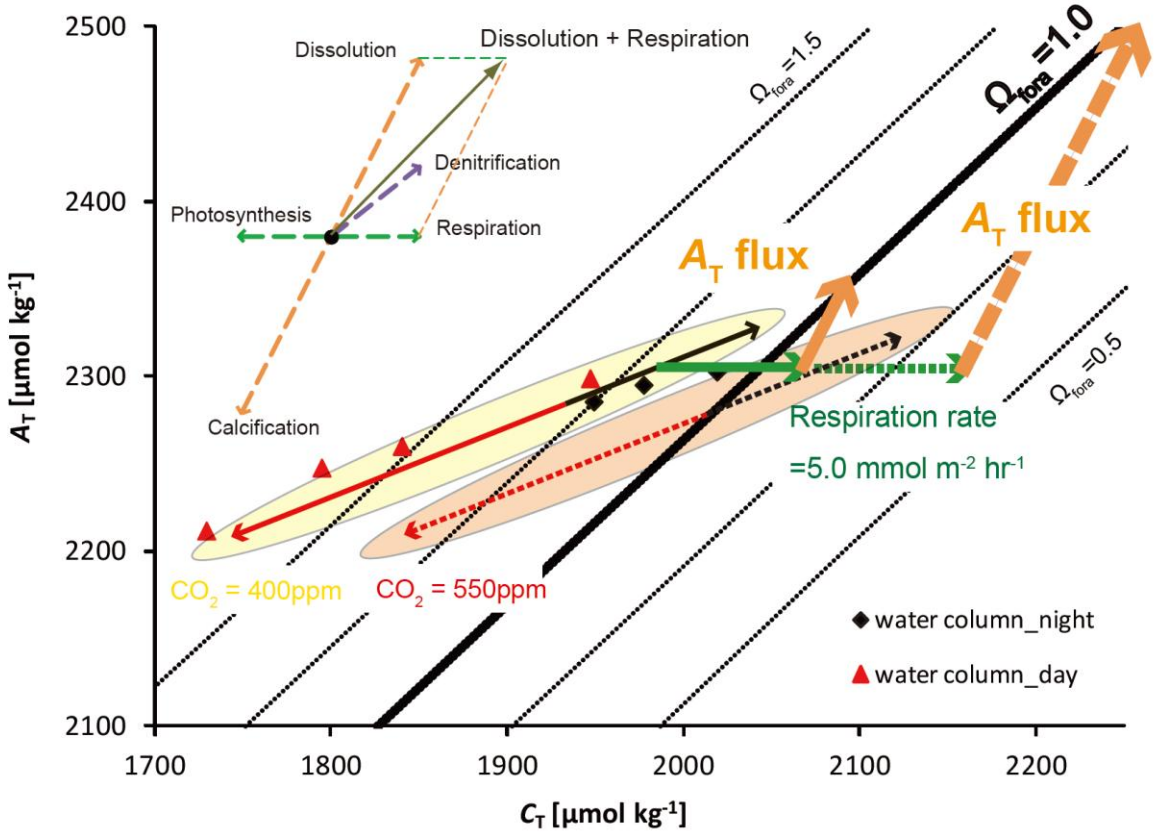

Figure 6-6. Future impact of A_T flux increase based on A_T-C_T diagram: Red and black vectors indicate A_T and C_T changes in water column during day time and nighttime, respectively. Oblique lines are isograms of Ω_{fora} with Ω_{fora} = 1 shown by a thick solid line. Under present pCO_2 concentration of 400 ppm, the water column chemistry changes by the metabolism of the coral reef community in Shiraho reef within the yellow ellipse area. In sediment, respiration shown by a green vector is compensated by dissolution shown by an orange vector to reach the constant Ω_{fora} of 1.0 shown by a thick solid line. When pCO_2 in seawater increases up to 550 ppm and the metabolism of the coral reef community is not changed, water column chemistry in 550 ppm will be shifted to red ellipse area, and estimated A_T flux will be shown by dotted orange vector under the assumption that respiration rate is constant (i.e. dotted green vector is equal to solid green vector).

6-4-2. Buffering capacity against ocean acidification

Previous section (6-4-1) shows the qualitative evaluation for Mg-calcite dissolution against ocean acidification. Here, A_T-C_T diagram, by which metabolism rate can be shown graphically, is used to quantitatively predict increase in upward A_T flux from carbonate dissolution in sediments by the ocean acidification, which would act as a buffer against it.

In A_T-C_T diagram, the water column chemistry changes by the metabolism of the coral reef community in Shiraho reef is shown by yellow ellipse area in Figure 6-6. If chemical reaction within upper 10 mm zone is assumed to be equal to the observed flux at sediment-water interface, solid green vector and solid orange vector in Figure 6-6 indicate the O_2 uptake and upward A_T flux at nighttime median case. When pCO_2 in seawater increases up to 550 ppm and metabolism of the Shiraho reef community is not changed, water column chemistry in 550 ppm will be shifted to red ellipse area in Figure 6-6. If the respiration rate in sediment is constant, upward A_T flux will be shown by dotted orange vector. This estimated A_T flux is at least higher than respiration rate because the equivalent respiration and dissolution corresponds to isograms of Ω_{fora} (oblique black line in Figure 6-6). Thus, at least dissolution rate of 5.0 mmol m^{-2} hr^{-1} would occur since average nighttime O_2 uptake measured in this study was about 5.0 mmol m^{-2} hr^{-1},

Table 6-2 lists the net dissolution rate at sand area or whole of coral reef community and Ω_a in water column. When Ω_a in water column decreased from 3.1 to 1.0, net carbonate dissolution was observed in all studies. Dissolution rate measured by A_T difference in water column had wide ranges among different studies because it is difficult to evaluate how the ocean acidification in water column affects to process in sediment. From this study, A_T flux at sediment-water interface is shown by the relationship between aerobic respiration and Mg-calcite dissolution, and minimum estimation would be obtained if respiration rate in sediment

is constant. At least 5.0 mmol m^{-2} hr^{-1} Mg-calcite dissolution estimated in this study is larger than previous studies, suggesting that they would underestimate the effect of Mg-calcite dissolution due to ignorance of processes in sediment.

Kayanne et al. (2005) estimated net community calcification rate to be 70 to 127 mmol m^{-2} day^{-1} for Shiraho reef. At least 60 mmol m^{-2} day^{-1} Mg-calcite dissolution were estimated under $\Omega_{fora} < 1$ condition in water column in this study. This value consists of 47-86 % of net community calcification rate. Because the sandy regions are about three times larger than the coral habitats at Shiraho reef, Mg-calcite dissolution in these sands would decline net ecosystem calcification significantly. Moreover, most calcifers except foraminifera show negative effect of calcification for ocean acidification (Chapter 1-2-1), which will also promote the decrease of net ecosystem calcification and change the component of sediment. On the other hand, Mg-calcite dissolution increases A_T in water column, indicating the buffer effect to ocean acidification. If assumed background water has Ω_a of 2.93 and pCO_2 = 550 ppm, the value of Ω_a will decrease to 2.8 under average conditions of Shiraho reef (5.0 mmol m^{-2} hr^{-1} respiration rate with duration time of 4 hr and water depth of 1.4 m).

The effect of Mg-calcite dissolution with global scale is considered by area of shallow carbonate sand and the estimated dissolution rate. Morse et al. (2006) estimated that sediment area which mainly consisted of Mg-calcite in shallow sediment was 6.9×10^6 km^2. Since estimated minimum dissolution rate at sand area was 5.0 mmol m^{-2} hr^{-1} and it always occurs during only nighttime at everywhere Mg-calcite existed in sediment, 1.5×10^{-3} PgC/yr of CO_2 uptake is obtained by multiplication of 6.9×10^6 km^2 and 5.0 mmol m^{-2} hr^{-1}. On the other hand, the world ocean takes up about 2.0 $\pm$ 0.6 PgC/yr of CO_2 emitted by anthropogenic combustion of fossil fuels (Takahashi et al., 2002). Although this 1.5×10^{-3} PgC/yr of CO_2

uptake is still minimum, the effect of Mg-calcite dissolution would have an influence especially to the carbon cycle in each community rather than whole of the global scale.

Table 6-2. Carbonate dissolution rates reported from carbonate environments and mesocosms

Reference	Location	Dissolution rate [mmol m^{-2} h^{-1}]	Ω_a	Benthic condition
Andersson et al. (2007)	Bahama	0.2 to 0.8	1.2 to 1.9	carbonate sediment (20 to 25 m depth)
Andersson et al. (2009)	Hawaii mesocosm	2.2 to 3.6	1.0 to 2.0	20 to 30% coral cover
Boucher et al. (1998)	Moorea	0.7	—	31% coral cover
Leclercq et al. (2002)	Monaco mesocosm	0.8	Water column: 2.7 to 5.2 Pore water:1.9	sand community
Suzuki et al. (1995)	Ishigaki	3	1.7 to 3.1	19% coral cover
Yates and Halley (2006)	Hawaii	1.4	1.8 to 2.6	patch reef 22%
		1	1.5 to 2.6	patch reef 10%
		1.1	2.0 to 2.5	coral rubble
		0.3	2.1 to 2.6	sand bottom

Chapter 7.

Summary and future studies

7-1. Summary

Previous studies considered A_T increase in water column as a dissolution reaction between water column and surface of the sediment, which ignored the process within sediment. However, flux at sediment-water interface must be calculated based on diffusion coefficient and concentration gradient at sediment-water interface. Further, pore water in the sediment has more CO_2 than that in water column because of respiration and probably denitirification, which influences A_T slope.

In this study, first, exact threshold of biogenic Mg-calcite dissolution was determined by laboratory experiment. Then, two different field observations, flow-controlled chamber experiment, and the estimation of diffusion coefficient measured by EC and A_T slope were conducted in order to calculate A_T flux at sediment-water interface under natural flow condition. This is the first study to determine A_T flux based on diffusion coefficient and A_T slope, which were measured by *in-situ* field observation.

According to laboratory experiment, dissolution of bulk carbonate sediments occurs at Ω_a values of 3.7 to 3.8. Mg-calcite derived from foraminifera and coralline algae dissolves at Ω_a values between 3.0 and 3.2. The solubilities of foraminiferans and coralline algae obtained by this study agree wtih Plummer and Mackenzie (1974) solubility.

Chamber experiment which can control flow rate were designed and conducted in order to understand relationship between A_T flux and Ω_a in water column. Data showed that there were

no significant differences in dissolution/calcification rate between high-flow and low-flow. While dissolution rate increases as Ω_a decreased in laboratory experiment, dissolution rate measured by flow-controlled chamber did not change. It would mean that carbonate profiles in sediment was not affected by high pCO_2 in water column because of short time experiment or a little amount of water column in chamber.

O_2 and carbonate profiles were measured by microelectrode and pore water analysis. Between 0 and 10 mm depth, micro organism respiration would consume oxygen and produce CO_2, and pH decreased at night. On the contrary, O_2 increased by the photosynthesis during day time. Deeper than at least 10 mm, O_2 was depleted even during the day time. On the other hand, Ω_{fora} was always constant at the value of 1.0. Both organic reaction such as respiration and inorganic Mg-calcite dissolution is considered to have occurred and keep Ω_{fora} constant in the sediment.

All data were conbined, A_T flux from sediment to water column occurred by the A_T gradient within the sediment caused by organic CO_2 production such as respiration or denitrification. Therefore, even when Ω_{fora} in water column was higher than 1.0, A_T flux at sediment-water interface could be observed. Moreover, once seawater in water column is over the threshold of Mg-calcite dissolution, estimated A_T flux could increase drastically.

7-2. Future studies

Table 7-1 shows problems about Mg-calcite dissolution among laboratory experiment, flow-controlled chamber, and EC + A_T profile in this study. While threshold of carbonate mineral dissolution and gross dissolution rate of each minerals at several pCO_2 level can be measured by laboratory experiment, it is hard to apply it to field observation directly because physical condition such as flow rate and biological condition in the sediment were not considered by laboratory experiment. By flow-controlled chamber, A_T flux at several pCO_2 level can be calculated but processes in sediment were not considered at all. On the other hand, though processses in sediment can be considered by EC + A_T profile, pCO_2 conditions can not be manipulated. All the medthodology have pros and cons.

In order to estimate the effect of Mg-calcite dissolution on ocean acidification, model study is a powerful tool. However, mechanism of Mg-calcite dissolution has to be revealed before establishing the model. In this study, both laboratory experiment, field experiment and field observation were conducted. In laboratoy experiment, threshold of Mg-calcite dissolution that would occur in actual environment was determined, and it was applied to the field observation result using Ω_{fora} . From this study, it comes out that A_T increase in water column is caused by the process in sediment, and it is the key for evaluating future impact on buffering effect on ocean acidification.

It is important to estimate A_T flux at sand area in coral reefs more precisely because coral reef community has long been known to alter their own seawater chemistry, through processes of photosynthesis, respiration, calcification, and dissolution. In this study, while A_T flux at night was discussed, DO and A_T fluxes during day time were not discussed particularly because photosynthesis and calcification caused by organisms in surface of the sediment is complex and variable by light intensity. Micro organisms and calcifers living in sediment

should be identified and its response to light, temperature, and pCO_2 increase should be clarified.

The first and important task for estimating precise A_T flux is to determine A_T profile in sediment more precisely. In this study, carbonate parameters such as A_T and C_T were measured by pore water sampling with 10 mm interval because their profiles can not be measured by microelectrode technically. Thus, for example, ex-situ observation of A_T profile by using a pH planar optode, by which pH distribution can be observed, would be necessary.

Next, diffusion coefficient in sediment should be measured. In this study, diffusion coefficient observed at sediment-water interface was adopted in sediment, and A_T flux was discussed. However, diffusion coefficient in sediment would decrease with depth because the effect of wave and current becomes weaker with depth.

If those data are obtained, carbonate profiles and A_T flux at sediment-water interface would be predicted by giving the carbonate values in water column and sediment characteristics. It would enable us to evaluate quantitative feedback by Mg-calcite dissolution in sand area in coral reefs, and to estimate future impact more precisely, and carbonate cycle in coral reef community would be understood more exactly.

Furthermore, A_T increase in water column is not understood by diffusion coefficient and profile in sediment (i.e. diagenetic model) in previous studies. They evaluated A_T increase in water column including deep sea and coastal area as the relationship between water column and surface of the sediment. Although biological and hydrodynamic conditions of coral reefs are different from those of other areas, results from this study could be applied to those areas because mechanism of flux is similar. Thus, the effect of carbonate dissolution should be evaluated more quantitatively to further understanding of global carbonate cycle.

Table 7-1. Gaps about Mg-calcite dissolution from this study (Laboratory experiment vs Flow-controlled chamber vs EC + A_T profile)

	My laboratory experiment	Flow-controlled chamber	EC + profile
current and wave	×	△	○
process in sediment	×	×	○
pCO_2 control	○	○	×
seawater in water column	○	○	○
seawater in sediment		×	○
merit	Gross dissolution rate on each particle can be measured	Net dissolution rate can be measured at several pCO_2 level	A_T flux under natural condition can be measured.
demerit	Physical and biological condition can not be reproduced, and the data should be applied to field.	Only seawater in water column can be measured. Processes in sediment are not considered	Calculated A_T flux is indirect. CO_2 condition can not be manipulated.

Acknowledgements

I am deeply indebted to Professor Hajime Kayanne, Department of Earth and Planetary Science, University of Tokyo. Without his a lot of valuable suggestions and continuous encoragement, this study would not be finished.

I am very grateful for Dr. T. Kuwae, Dr. M. Tanaka and Dr. T. Tokoro, Port and Airport Research Institute, for their valuable suggestions on theoretical component of this study, field measurements and laboratory analysis.

I really appreciate Professor R. Tada for their many valuable suggestions and advices on this study. I also appreciate Prfessor H. Kawahata, Professor E. Tajika, and Dr. Y. Sekine for their valuable commnents and advices on this study.

I thank Professor K. Nadaoka, Tokyo Institute of Technology, Dr. A. Watanabe, Dr. T. Nakamura and their laboratory members. They suggested many valuable advices and supported for field survey in Ishigaki Island.

I am very grateful for Dr. K. Nozaki, Dr. A. Negishi, and Dr. K. Kato, National Institute of Advanced Industrial Science and Technology, for their kind helps on my study, laboratory analysis, and field observations.

I am grateful for Mr. H. Kimoto, Mr. K. Kinoshita, and Mr. M. Tsuda, Kimoto Electric Co. Ltd, Mr. T. Kaku and Mr. S. Kaku, Kanto-Rika Co. Ltd, Mr. J. Kaneko, JFE Advantech Co. Ltd, and Ms. S. Miyamoto, PTT Co. Ltd for technical development and support for laboratory and field experiments.

I appreciate all the members of Professor Kayanne's laboratory for their helps on my study and daily works, especially Dr. S. Harii, Dr. T. Hosono, Dr. N. Nakamura, Dr. C. Hongo, and

Mr. M. Terai for their valuable comments, Ms. S. Inoue, Mr. K. Shimizu, Mr. G. Hosoi, Ms. Y. Aiba, Mr. K. Aoki, Mr. T. Suzuki, Ms. T. Tanaya and Ms. A. Nagoshi for supporting field survey and daily works, Ms. N. Igarashi and Ms. N. Fujita for their assistances in daily works; I thank all of other members and graduates in the laboratory.

I am indebted to Mr. M. Taira and his familiy, Mr. E. Shimabukuro and his family for their supports in Ishigaki Island survey. Finally, I appreciate my parents, brother, family, and best friends for all of their heartwarming supports and encouragement.

References

Alongi, D. M., J. Pfitzner, and L. A. Trott (2006), Deposition and cycling of carbon and nitrogen in carbonate mud of the lagoons of Arlington and Sudbury Reefs, Great Barrier Reef, *Coral Reefs, 25*, 123–143, doi:10.1007/s00338-005-0069-2.

Andersson, A. J., F. T. Mackenzie, and L. M. Ver (2003), Solution of shallow-water carbonates: an insignificant buffer against rising atmospheric CO_2, *Geology,* 31, 513–516.

Andersson, A. J., N. R. Bates, and F. T. Mackenzie (2007), Dissolution of carbonate sediments under rising pCO_2 and ocean acidification: observations from Devil's Hole, Bermuda, *Aquat. Geochem.,* 13, 237–264.

Andersson, A. J., I. B. Kuffner, F. T. Mackenzie, P. L. Jokiel, K. S. Rodgers, and A. A. Tan (2009), Net Loss of $CaCO_3$ from a subtropical calcifying community due to seawater acidification: mesocosm-scale experimental evidence, *Biogeosciences,* 6, 1811–1823.

Andersson, A. J., and F. T. Mackenzie (2012), Revisiting four scientific debates in ocean acidification research, *Biogeosciences,* 9, 893–905.

Andersson, A. J., and D. Gledhill (2013), Ocean Acidification and Coral Reefs: Effects on Breakdown, Dissolution, and Net Ecosystem Calcification, *Annu. Rev. Mar. Sci.,* 5, 321–48.

Baldocchi, D., E. Falge, L. H. Gu et al. (2001), FLUXNET: a new tool to study the temporal and spatial variability of ecosystemscale carbon dioxide, water vapor, and energy flux densities, *Bulletin of the American Meteorological Society, 82,* 2415–2434.

Bentov, S. and J. Erez (2006), Impact of biomineralization processes on the Mg content of foraminiferal shells, *Geochemistry Geophysics Geosystems,* 7, Number 1 Q01P08, doi:10.1029/2005GC001015 ISSN: 1525-2027

Berg, P., H. Røy, F. Janssen, V. Meyer, B. B. Jørgensen, M. Huettel, and D. de Beer (2003), Oxygen uptake by aquatic sediments measured with a novel non-invasive eddy-correlation technique, *Mar. Ecol. Prog. Ser., 261,* 75–83, doi:10.3354/meps261075.

Berg, P., H. Røy, and P. Wiberg (2007), Eddy correlation flux measurements: The sediment surface area that contributes to the flux, *Limnol. Oceanogr., 52,* 1672–1684, doi:10.4319/lo.2007.52.4.1672.

Berg, P., and M. Huettel (2008), Monitoring the seafloor using the noninvasive eddy correlation technique: Integrated benthic exchange dynamics, *Oceanography, 21,* 164–167, doi:10.5670/oceanog.2008.13.

Berg, P., R. N. Glud, A. Hume, H. Stahl, K. Oguri, V. Meyer, and H. Kitazato (2009), Eddy correlation measurements of oxygen uptake in deep ocean sediments, *Limnol. Oceanogr. Methods, 7,* 576–584, doi:10.4319/lom.2009.7.576.

Berner, R. A. (1980), Early diagenesis. A theoretical approach. Princeton University Press, Princeton, NJ.

Bischoff, W.D., F. T. Mackenzie, F.C. Bishop (1987), Stabilities of synthetic Mg-calcites in aqueous solution: comparison with biogenic materials, *Geochim. Cosmochim. Acta 51,* 1413–1423.

Bischoff, W.D., M. A. Bertram, F. T. Mackenzie, and F. C. Bishop (1993), Diagenetic stabilization pathways of Mg-calcites, *Carb. Evap, 8,* 82–89.

Blackmon, P. D., and R. Todd (1959), Mineralogy of some foraminifera as related to their classification and ecology, *Jour. Paleontology*, 33, 1-15.

Borowitzka, M.A. (1982), Mechanisms in algal calciflcation, *Progress in Phycological Research,* 1, 137-177

Boucher, G., J. Clavier, C. Hily, and J.-P. Gattuso (1998), Contribution of soft-bottoms to the community metabolism (primary production and calcification) of a barrier reef flat (Moorea, French Polynesia), *J. Exp. Mar. Biol. Ecol., 225*, 269–283.

Boudreau B. P. (1997), Diagenetic models and their implementation. Springer-Verlag, Heidelberg

Brand, A., D. F. McGinnis, B. Wehrli, and A. Wüest (2008), Intermittent oxygen flux from the interior into the bottom boundary of lakes as observed by eddy correlation, *Limnol. Oceanogr., 53*, 1997–2006, doi:10.4319/lo.2008.53.5.1997.

Brunauer, S., Emmett, P. H. and E. Teller (1938), Adsorption of Gases in Multimolecular Layers, *Journal of American chemistry society., 60,* 309–319, doi:10.1021/ja01269a023.

Burba, G. G., and D. J. Anderson (2010), A Brief Practical Guide to Eddy Covariance Flux Measurements: Principles and Workflow Examples for Scientific and Industrial Applications. *LI-COR Biosciences,* Lincoln, USA, 211 pp.

Burdige, D. J., R. C. Zimmerman, and X. Hu (2008), Rates of carbonate dissolution in permeable sediments estimated from pore-water profiles: The role of sea grasses, *Limnol. Oceanogr., 53(2)*, 549–565.

Busenberg, E., L. N. Plummer (1989), Thermodynamics of magnesian calcite solid-solutions at 25 °C and 1 atm pressure. *Geochim. Cosmochim. Acta, 53*, 1189–1208.

Caldeira, K. and M. E. Wickett (2003), Anthropogenic carbon and ocean pH, *Nature, 425*, 365–365.

Chen, C-T. A (2002), Shelf-vs. dissolution-generated alkalinity above the chemical lysocline, *Deep-Sea Research II*, 49, 5365–5375.

Comeau, S., P. J. Edmunds, N. B. Spindel, and R. C. Carpenter (2013), The responses of eight coral reef calcifiers to increasing partial pressure of CO_2 do not exhibit a tipping point, *Limnol. Oceanogr., 58(1)*, 2013, 388–398. doi:10.4319/lo.2013.58.1.0388

Cyronak, T., I. R. Santos, A. McMahon, and B. D. Eyre (2013), Carbon cycling hysteresis in permeable carbonate sands over a diel cycle: Implications for ocean acidification, *Limnol. Oceanogr., 58(1)*, 131–143. doi:10.4319/lo.2013.58.1.0131

Dickson, A. G. and F. J. Millero (1987), A comparison of the equilibrium-constants for the dissociation of carbonic-acid in seawater media. *Deep-Sea Res, 34*, 1733–1743

Dickson, A. G. (2010), The carbon dioxide system in seawater: equilibrium chemistry and measurements, in: Guide to Best Practices in Ocean Acidification Reseach and Data Reporting, edited by: Riebesell, U., Fabry, V. J., Hansson, L., and Gattuso, J.-P., Luxembourg, *Office for Official Publications of the European Communities*, 17–40.

DOE (1994), Handbook of Methods for the Analysis of the Various Parameters of the Carbon Dioxide System in Sea Water, v. 2, edites by: Dickson, A. G. and Goyet, C., ORNL/CDIAC-74.

Doney, S., W. M. Balch, V. J. Fabry, and R. A. Feely (2009), Ocean Acidification A Critical Emerging Problem for the Ocean Sciences, *Oceanography*, 22, 16-25.

Friedman, G. M (1959), Identification of carbonate minerals by staining methods, *Journal of Sedimentary Petrology*, 29, 87-97.

Fujita, K., M. Hikami, A. Suzuki, A. Kuroyanagi, K. Sakai, H. Kawahata, and Y. Nojiri (2011), Effects of ocean acidification on calcification of symbiont‐bearing reef foraminifers, *Biogeosciences, 8,* 2089‐2098, doi:10.5194/bg-8-2089-2011.

Gattuso, J.-P. and L. Hansson (2011), L.: Ocean acidification, Oxford University Press, 311pp.

Gehlen, M., F. C. Bassinot, L. Chou, and D. McCorkle (2005), Reassessing the dissolution of marine carbonates: II. Reaction kinetics, *Deep-Sea Research I, 52*, 1461–1476.

Glud. R. N., B.D. Eyre, and N. Patten (2008), Biogeochemical responses to mass coral spawning at the Great Barrier Reef: Effects on respiration and primary production, *Limnol. Oceanogr.*, 53(3), 1014–1024

Glud, R. N., P. Berg, A. Hume, P. Batty, and M. E. Blicher (2010), Benthic O_2 exchange rates across hard-bottom substrates quantified by eddy correlation in a sub-Arctic fjord system, *Mar. Ecol. Prog. Ser., 417*, 1–12, doi:10.3354/meps08795.

Goldsmith, J. R, D. L. Graf and Joensuu (1955), The occurrence of magnesium calcite in nature, *Geochim. Cosmochim. Acta*, 7, 212-230.

Goldsmith, J. R. and D. L. Graf (1958), Relation between lattice constants and composition of the Ca-Mg carbonates, *Am. Mineral, 43*, 84-101.

Hales, B. and S. Emerson (1997), Evidence in support of first-order dissolution kinetics of calcite in seawater, *Earth and Planetary Science Letters, 148*, 317-327.

Hikami, M., H. Ushie, T. Irie, K. Fujita, A. Kuroyanagi et al. (2011), Contrasting calcification responses to ocean acidification between two reef foraminifers harboring different algal symbionts, *Geophysical Research Leters, 38,* L19601, doi:10.1029/2011GL048501

Hoegh-Guldberg O, P. J. Mumby, A. J. Hooten, R. S. Steneck, P. Greenfield et al. (2007), Coral reefs under rapid climate change and ocean acidification. *Science 318*, 1737–1742.

Hu, X., and D. J. BURDIGE (2007), Enriched stable carbon isotopes in the pore waters of carbonate sediments dominated by seagrasses: Evidence for coupled carbonate dissolution and reprecipitation, *Geochim. Cosmochim. Acta, 71,* 129–144.

Huettel, M. and G. Gust (1992), Solute release mechanisms from confined sediment cores in stirred benthic chambers and flume flows. *Mar. Ecol. Prog. Ser.*, 82, 2241–2249.

Hume, A. C., P. Berg, and K. J. McGlathery (2011), Dissolved oxygen fluxes and ecosystem metabolism in an eelgrass (Zostera marina) meadow measured with the eddy correlation technique, *Limnol. Oceanogr., 56,* 86–96, doi:10.4319/lo.2011.56.1.0086.

Kayanne, H, A. Suzuki, and H. Saito (1995), Diurnal Changes in the Partial Pressure of Carbon Dioxide in Coral Reef Water, *Science, 269*, 214-216.

Kayanne, H., H. Hata, S. Kudo, H. Yamano, A. Watanabe et al. (2005), Seasonal and bleaching-induced changes in coral reef metabolism and CO_2 flux, *Global Biogeochem. Cy., 19,* GB3015, doi:10.1029/2004GB002400.

Keir, R. S. (1980), The dissolution kinetics of biogenic calcium carbonates in seawater, *Geochim. Cosmochim. Acta, 44*, 241–252.

Kimoto, H., H. Kayanne, S. Kudo, K. Nozaki, A. Negishi, and K. Kato (2001), A high time-resolution analyzer for total alkalinity of seawater, based on continuous potentiometric measurement, *Anal. Sci., 17,* Supplement, i415– i418.

Kimoto, H., K. Nozaki, S. Kudo, K. Kato, A. Negishi, and H. Kayanne (2002), Achieving High Time-Resolution with a New Flow-through Type Analyzer for Total Inorganic Carbon in Seawater, *Anal. Sci., 18,* 247-253.

Kleypas, J. A., R. W. Buddemeier, D. Archer, J. P. Gattuso, C. Langdon, and B. N. Opdyke (1999), Geochemical consequences of increased atmospheric carbon dioxide on coral reefs, *Science*, 284, 118–120.

Kleypas, J. A., R. A. Feely, V. J. Fabry, C. Langdon, C. L. Sabine, and L. L. Robbins (2006), Impacts of ocean acidification on coral reefs and other marine calcifiers: a guide for future research, report of a workshop held 18-20 April 2005, St. Petersburg, FL, sponsored by NSF, NOAA, and the US Geological Survey.

Kroeker, K. S., R. L. Kordas, R. Crim, I. E. Hendriks, L. Ramajo, G. S. Singh, C. M. Duarte, and J. P. Gattuso (2013), Impacts of ocean acidification on marine organisms: quantifying sensitivities and interaction with warming, *Global Change Biology*, 19, 1884–1896, doi: 10.1111/gcb.12179.

Kuffner, I. B., A. J. Andersson, P. L. Jokiel, K. S. Rodgers, and F. T. Mackenzie (2008), Decreased abundance of crustose coralline algae due to ocean acidification, *Nat. Geosci., 1,* 114–117, doi:10.1038/ngeo100.

Kuroyanagi, A., H. Kawahata, A. Suzuki, K. Fujita, and T. Irie (2009), Impacts of ocean acidification on large benthic foraminifers: Results from laboratory experiments, *Mar. Micropaleontol., 73*, 190–195, doi:10.1016/j.marmicro.2009.09.003.

Kuwae, T., K. Kamio, T. Inoue, E. Miyoshi, and Y. Uchiyama (2006), Oxygen exchange flux between sediment and water in an intertidal sandflat, measured in situ by the eddy-correlation method, *Mar. Ecol. Prog. Ser., 307*, 59–68, doi:10.3354/meps307059.

Lafon, G. M (1990), In Fluid-Mineral Interactions: A Tribute to H. P. Eugster; Spencer, R. J., Chou, I-M., Eds.; Special Publication Series No. 2; The Geochemical Society: San Antonio, TX, p 23.

Leclercq, N., J. –P. Gattuso, and J. Jaubert (2002), Primary production, respiration, and calcification of a coral reef mesocosm under increased CO_2 partial pressure, *Limnol. Oceanogr., 47*, 558–564.

Li, Y-H., and S. Gregory (1974), Diffusion of ions in seawater and in deep-sea sediments, *Geochim. Et Cosmochim. Acta.* 38, 703-714.

Long, M. H., P. Berg, D. Beer, and J. C. Zieman1 (2013), In Situ Coral Reef Oxygen Metabolism: An Eddy Correlation Study, *PlosOne, 8*, e58581

McGinnis, D. F., P. Berg, A. Brand, C. Lorrai, T. J. Edmonds, and A. Wüest (2008), Measurements of eddy correlation oxygen fluxes in shallow freshwaters: Towards routine applications and analysis, *Geophys. Res. Lett., 35*, L04403, doi:10.1029/2007GL032747.

Mehrbach, C., C. H. Culberson, J. E. Hawley, and R. M. Pytkowicz (1973), Measurement of the apparent dissociation constants of carbonic acid in seawater at atmospheric pressure, *Limnol. Oceanogr., 18*, 897–907.

Millero, F. J. (2006), Chemical oceanography. CRC/ Taylor and Francis, Boca Raton, FL.

Miyajima, T., M. Suzumura, Y. Umezawa, and I. Koike (2001), Microbiological nitrogen transformation in carbonate sediments of a coral-reef lagoon and associated seagrass beds, *Mar Ecol Prog Ser*, 217, 273-286.

Morse, J. W. and F. T. Mackenzie (1990), Geochemistry of sedimentary carbonates, Elseiver Science Publishing Co., 707p.

Morse, J. W., A. J. Andersson, and F. T. Mackenzie (2006), Initial responses of carbonate-rich shelf sediments to rising atmospheric pCO_2 and ocean acidification: role of high Mg-calcites, *Geochim. Cosmochim. Acta, 70*, 5814–5830.

Morse, J. W., R. S. Arvidson, and A. Luttge (2007), Calcium Carbonate Formation and Dissolution, *Chem. Rev, 107*, 342-381.

Mucci, A., and J. W. Morse (1984), The solubility of calcite in seawater of various magnesium concentrations, It = 0.697 m at 25 °C and one atmosphere total pressure, *Geochim. Cosmochim. Acta, 48*, 815–822.

Nakamura T., and H. Yamasaki (2006), Morphological changes of pocilloporid corals exposed to water flow, *Proc 10th Int Coral Reef Symp 875*, 872–875.

Nakamura, T., and T. Nakamori (2009), Estimation of photosynthesis and calcification rates at a fringing reef by accounting for diurnal variations and the zonation of coral reef communities on reef flat and slope: a case study for the Shiraho reef, Ishigaki Island, southwest Japan, *Coral Reefs, 28*, 229–250.

Nakamura, T., K. Nadaoka, and A. Watanabe (2013), A coral polyp model of photosynthesis, respiration and calcification incorporating a transcellular ion transport mechanism, *Coral Reefs*, in press, DOI:10.1007/s00338-013-1032-2.

Plummer, L.N., and F. T. Mackenzie (1974), Predicting mineral solubility from rate data: application to the dissolution of Mg-calcites, *Am. J. Sci. 274*, 61–83.

Precht. E., and M. Huettel (2004), Rapid wave-driven advective pore water exchange in a permeable coastal sediment, *Journal of Sea Research, 51*, 93– 107.

Reimers, C. E., H. T. Özkan-Haller, P. Berg, A. Devol, K. McCann-Grosvenor, and R. D. Sanders (2012), Benthic oxygen consumption rates during hypoxic conditions on the Oregon continental shelf: Evaluation of the eddy correlation method, *Journal of Geophysical Research*, 117, C02021, doi:10.1029/2011JC007564

Reynolds, O (1895), On the dynamical theory of incompressible viscous fluids and the determination of the criterion. *Phil Trans R Soc Lond A Math Phys Sci, 186*, 123–164

Ries, J. B., A. L. Cohen and D. C. McCorkle (2009), Marine calcifiers exhibit mixed responses to CO_2-induced ocean acidification, *Geology*, 37, 1131-1134. doi: 10.1130/G30210A.1

Rao, A. M., F. L. Polerecky, D. Ionescu, J. R. F. Meysman, and Dirk de Beer (2012), The influence of pore-water advection, benthic photosynthesis, and respiration on calcium carbonate dynamics in reef sands, *Limnol. Oceanogr., 57*, 809–825.

Sabine, C. L., R. A. Feely, N. Gruber, R. M. Key, K. Lee et al. (2004), The oceanic sink for anthropogenic CO_2, *Science, 305*, 367–371.

Saito, H., N. Tamura., H. Kitano., A. Mito., C. Takahashi., A. Suzuki., and H. Kayanne (1995), A compact seawater pCO_2 measurement system with membrane equilibrator and nondispersive infrared gas analyzer, *Deep Sea Res., Part I., 42*, 2025–2033.

Sarmiento, J. L., and N. Gruber (2006), Ocean biogeochemical dynamics, *Princeton University Press*, 503pp.

Shaw, W. J., and J. H. Trowbridge (2001), The direct evaluation of nearbottom turbulent fluxes in the presence of energetic wave motions, *J. Atmos. Oceanic Technol., 18*, 1540–1557, doi:10.1175/1520-0426(2001) 018<1540:TDEONB>2.0.CO;2.

Silverman J, B. Lazar, L. Cao, K. Caldeira, and J. Erez (2009), Coral reefs may start dissolving when atmospheric CO_2 doubles, *Geophys. Res. Lett.*, 36, L05606

Stanley, S. M. (2008), Effects of Global Seawater Chemistry on Biomineralization: Past, Present, and Future, *Chem. Rev.*, 108, 4483–4498.

Suzuki, A., T. Nakamori, and H. Kayanne (1995), The mechanism of production enhancement in coral reef carbonate system: model and empirical results, *Sediment Geol.*, 99, 259–280.

Suzumura, M., T. Miyajima, H. Hata, Y. Umezawa, H. Kayanne, and I. Koike (2002), Cycling of phosphorus maintains the production of microphytobenthic communities in carbonate sediments of a coral reef, *Limnol. Oceanogr.*, 47(3), 771–781.

Takahashi, T., S. C. Sutherland, C. Sweeney, A. Poisson, N. Metzl, B. Tilbrook, N. Bates, R. Wanninkhof, R. A. Feely, C. Sabine, J. Olafsson, and Y. Nojiri (2002), Global sea-air CO_2 flux based on climatological surface ocean pCO_2, and seasonal biological and temperature effects, *Deep Sea Res., 49*, 1601-1622.

Thorstenson, D.C., and L. N. Plummer (1977), Equilibrium criteria for two component solids reacting with fixed composition in an aqueous phase-example: the magnesian calcites, *Am. J. Sci., 277*, 1203–1233.

Uthicke, S., P. Momigliano, and K. E. Fabricius (2013), High risk of extinction of benthic foraminifera in this century due to ocean acidification, *Nature Scientific Reports, 3*, 1769, doi:10.1038/srep01769

Verma, S. B., D. D. Baldocchi, D. E. Anderson, D. R. Matt, and R. E. Clement (1986), Eddy fluxes of CO_2 water vapor, and sensible heat over a deciduous forest. *Bound.-Layer Meteor., 36,* 71–91.

Vermetten, A. W., M. L. Ganzeveld, A. Jeuken, P. Hofschreuder, and G. M. J. Mohren (1994), CO_2 uptake by a stand of Douglas fir: Flux measurements compared with model calculations. *Agric. For. Meteor., 72,* 57–80.

Veron JEN (1995), Corals in space and time: The biogeography and evolution of the scleractinia. Cornell University Press, Ithaca, NY

Vogel, N. and S. Uthicke (2012), Calcification and photobiology in symbiont-bearing benthic foraminifera and responses to a high CO_2 environment. *J. Exp. Mar. Biol. Ecol. 424,* 15–24.

Walter, L. M. and J. W. Morse (1984), Mg-calcite stabilities: a re-evaluation, *Geochim. Cosmochim. Acta 48,* 1059–1069.

Watanabe, A., H. Kayanne, K. Nozaki, K. Kato, A. Negishi, S. Kudo, H. Kimoto, M. Tsuda, and A. G. Dickson (2004), A rapid precise potentiometric determination of total alkalinity in seawater by a newly developed flow-through analyzer designed for coastal regions, *Mar. Chem., 85*, 75– 87.

Watanabe, A., H. Kayanne, H. Hata, S. Kudo, K. Nozaki, K. Kato, A. Negishi, Y. Ikeda, and H. Yamano (2006), Analysis of the seawater CO_2 system in the barrier reef–lagoon system of Palau using total alkalinity-dissolved inorganic carbon diagrams, *Limnol. Oceanogr., 51(4),*1614–1628.

Watanabe, A., T. Yamamoto, K. Nadaoka, Y. Maeda, T. Miyajima, Y. Tanaka, and A. C. Blanco (2013), Spatiotemporal variations in CO_2 flux in a fringing reef simulated using a novel carbonate system dynamics model, *Coral Reefs 32*, 239–254.

Wofsy, S. C., M. L. Goulden, J. W. Munger, S. M. Fan, P. S. Bakwin, B. C. Daube, S. L. Bassow, and F. A. Bazzaz (1993), Net exchange of CO_2 in a mid-latitude forest, *Science, 260,* 1314–1317.

Yates, K. K., and R. B. Halley (2003), Measuring coral reef community metabolism using new benthic chamber technology, *Coral Reefs, 22*, 247–255.

Yates, K. K. and R. B. Halley (2006), CO_3^{2-} concentration and pCO_2 thresholds for calcification and dissolution on the Molokai reef flat, Hawaii, *Biogeosciences, 3*, 357–369, http://www.biogeosciences.net/3/357/2006/.

Zeebe, R. E. and D. Wolf-Gladrow (2003), CO_2 in seawater: equilibrium, kinetics, isotopes, Elseiver Science.

Appendix

Result of laboratory experiment and chamber experiment

Supplementary Table 1. Temperature, calculated salinity, total alkalinity (A_T), total dissolved inorganic carbon (C_T), and water volume: calculated fugacity of CO_2 ($f(CO_2)$) and aragonite saturation state (Ω_a) at experiment temperature, salinity, A_T and C_T; and net dissolution rate between each experimental time interval.

Sampling time(hh:mm)	Temperature (℃)	Salinity (Calculated)	A_T (μ mol kg^{-1})	nA_T (μ mol kg^{-1})	C_T (μ mol kg^{-1})	$f(CO_2)$ (μ atam)	Ω_a	Water Volume (kg)	Average Dissolution Rate (μ mol m^{-2} h^{-1})
Bulk sediment	**Run#1**	pCO_2=2030ppm	Sample weight:12.68g						
0:00	26.6	34.55	2460	2459	2387	1703	1.36	3757	
1:00	26.1	34.56	2463	2461	2391	1694	1.34	3600	
1:15	26.0	34.57	2467	2465	2409	1856	1.24	3444	0.831
2:15	25.9	34.58	2471	2468	2389	1573	1.43	3288	
2:30	25.9	34.58	2469	2465	2406	1792	1.28	3236	0.618
3:30	26.0	34.60	2477	2472	2414	1806	1.28	3080	
3:45	26.0	34.60	2474	2469	2417	1878	1.24	3028	0.535
5:00	26.0	34.62	2480	2474	2391	1518	1.49	2871	
5:15	26.0	34.62	2482	2475	2398	1579	1.44	2819	0.426
6:30	26.3	34.64	2488	2480	2389	1447	1.58	2663	
6:45	26.3	34.64	2489	2480	2406	1612	1.44	2611	0.570
Bulk sediment	**Run#2**	pCO_2=1290ppm	Sample weight:15.72g						
0:00	28.8	34.44	2386	2392	2268	1318	1.73	4395	
1:05	27.7	34.45	2389	2395	2251	1093	1.94	4239	
1:20	27.4	34.45	2388	2394	2250	1080	1.93	4082	
1:35	27.1	34.46	2390	2395	2246	1034	1.98	3926	0.598
2:50	26.6	34.48	2395	2398	2243	973	2.04	3770	
3:05	26.5	34.49	2395	2398	2245	980	2.03	3614	0.351
4:20	26.5	34.51	2400	2401	2247	964	2.06	3457	
4:35	26.5	34.52	2399	2400	2246	963	2.06	3301	
4:50	26.4	34.52	2400	2401	2249	973	2.04	3145	
5:05	26.4	34.53	2399	2399	2260	1046	1.92	2989	0.217
5:50	26.5	34.54	2400	2399	2260	1044	1.94	2832	
6:05	26.5	34.55	2401	2400	2259	1026	1.96	2676	−0.097
Bulk sediment	**Run#3**	pCO_2=1110ppm	Sample weight:11.33g						
0:00	27.8	34.45	2400	2405	2226	935	2.20	3294	
1:30	26.8	34.49	2407	2410	2250	998	2.02	2981	
1:45	26.7	34.50	2405	2407	2249	1004	2.00	2825	0.180
3:00	26.6	34.53	2405	2405	2221	845	2.28	2669	−0.148
5:00	26.5	34.58	2416	2413	2216	777	2.44	2357	0.278
6:15	26.4	34.61	2421	2415	2216	758	2.48	2200	0.279
Bulk sediment	**Run#4**	pCO_2=820ppm	Sample weight:14.11g						
0:00	27.8	34.55	2374	2372	2146	667	2.77	4098	
2:30	26.8	34.55	2377	2375	2154	661	2.70	3786	
2:45	26.8	34.55	2381	2379	2158	661	2.70	3630	0.196
3:45	26.7	34.56	2379	2377	2165	688	2.62	3473	
4:00	26.7	34.56	2377	2375	2162	688	2.61	3317	0.374
7:05	26.5	34.56	2389	2386	2183	725	2.52	3161	
7:20	26.4	34.56	2387	2385	2185	732	2.49	3005	
7:35	26.2	34.56	2388	2385	2185	724	2.49	2900	0.362
9:00	26.0	34.57	2392	2389	2186	710	2.52	2744	
9:15	26.0	34.57	2393	2390	2184	699	2.55	2588	
9:30	25.8	34.57	2395	2393	2192	714	2.49	2432	
9:45	25.5	34.57	2398	2395	2186	679	2.57	2275	0.409

Supplementary Table 1. (continued)

Sampling time(hh:mm)	Temperature (℃)	Salinity (Calculated)	A_T (μ mol kg^{-1})	nA_T (μ mol kg^{-1})	C_T (μ mol kg^{-1})	$f(CO_2)$ (μ atam)	Ω_a	Water Volume (kg)	Average Dissolution Rate (μ mol m^{-2} h^{-1})
Bulk sediment	**Run#5**	pCO_2=750ppm	Sample weight:10.65g						
0:00	29.4	34.44	2372	2378	2160	767	2.64	3431	
2:15	27.7	34.51	2378	2379	2136	621	2.90	2764	0.096
4:30	29.5	34.56	2383	2381	2160	734	2.76	2296	0.093
6:00	29.8	34.60	2390	2384	2167	751	2.76	2140	
6:30	30.0	34.61	2392	2386	2168	751	2.78	1983	0.380
7:00	30.2	34.63	2394	2387	2163	733	2.85	1827	
7:15	30.2	34.63	2393	2386	2165	741	2.83	1671	0.183
Bulk sediment	**Run#6**	pCO_2=590ppm	Sample weight:13.23g						
0:00	26.8	34.47	2400	2404	2104	466	3.47	3962	
0:45	26.4	34.48	2399	2402	2094	440	3.55	3806	
1:00	26.4	34.48	2400	2404	2088	427	3.62	3754	−0.225
1:45	26.3	34.48	2400	2403	2070	389	3.83	3598	
2:00	26.3	34.48	2399	2403	2063	377	3.90	3545	−0.071
2:45	26.4	34.49	2400	2403	2082	412	3.70	3389	
3:00	26.4	34.49	2400	2403	2083	415	3.68	3337	0.052
3:55	26.4	34.49	2404	2406	2089	422	3.66	3285	
4:00	26.4	34.49	2403	2405	2069	387	3.86	3129	
4:15	26.5	34.49	2405	2408	2076	397	3.81	2973	
4:30	26.5	34.50	2404	2406	2063	376	3.94	2816	
4:45	26.5	34.50	2406	2408	2070	386	3.88	2660	
5:00	26.5	34.50	2406	2408	2072	390	3.85	2577	−0.005
6:45	26.4	34.51	2407	2409	2072	385	3.88	2420	
7:00	26.4	34.51	2407	2409	2075	391	3.84	2368	0.081
7:45	26.3	34.51	2408	2409	2076	390	3.84	2212	
8:00	26.3	34.51	2410	2411	2073	383	3.89	2160	0.138
Bulk sediment	**Run#7**	pCO_2=420ppm	Sample weight:10.25g						
0:00	26.4	34.50	2394	2395	2095	452	3.48	2998	
1:00	25.7	34.51	2394	2395	2094	436	3.48	2842	
1:15	25.7	34.51	2393	2394	2082	415	3.59	2790	−0.141
3:32	25.7	34.52	2390	2391	2084	423	3.54	2603	
3:50	25.7	34.52	2389	2389	2064	389	3.73	2446	
4:05	25.8	34.52	2390	2390	2072	402	3.66	2290	
4:20	25.8	34.52	2389	2390	2078	416	3.60	2134	
4:35	25.8	34.52	2391	2391	2083	423	3.55	1957	0.052
6:24	25.8	34.53	2392	2392	2081	416	3.59	1790	
6:40	25.8	34.53	2393	2393	2091	434	3.50	1634	
6:55	25.8	34.53	2393	2393	2076	405	3.66	1446	
7:13	25.8	34.53	2393	2393	2092	435	3.49	1290	0.122

Supplementary Table 1. (continued)

Sampling time(hh:mm)	Temperature (℃)	Salinity (Calculated)	A_T (μ mol kg^{-1})	nA_T (μ mol kg^{-1})	C_T (μ mol kg^{-1})	$f(CO_2)$ (μ atam)	Ω_a	Water Volume (kg)	Average Dissolution Rate (μ mol m^{-2} h^{-1})
Coralline algae	**Run#1**	pCO_2=2000ppm	Sample weight:12.55g						
0:00	26.3	34.31	2412	2427	2375	2115	1.07	3721	
1:00	26.0	34.32	2423	2437	2393	2206	1.03	3564	
1:15	26.0	34.32	2423	2437	2394	2227	1.02	3512	0.884
2:00	26.1	34.34	2429	2442	2379	1932	1.17	3356	
2:15	26.1	34.34	2430	2444	2404	2287	1.01	3304	
2:20	26.1	34.34	2428	2442	2407	2361	0.98	3200	0.329
3:45	26.2	34.36	2448	2460	2414	2191	1.07	3044	
4:00	26.2	34.36	2448	2460	2415	2203	1.06	2992	0.617
5:00	26.2	34.37	2457	2468	2424	2207	1.07	2835	
5:15	26.2	34.37	2457	2468	2420	2155	1.09	2783	0.361
6:30	26.2	34.39	2471	2481	2434	2159	1.10	2627	
6:45	26.2	34.39	2472	2481	2434	2159	1.10	2575	0.445
8:00	26.3	34.41	2487	2496	2447	2129	1.13	2419	
8:15	26.3	34.41	2487	2495	2447	2145	1.12	2367	0.456
9:00	26.3	34.42	2498	2505	2454	2102	1.15	2210	
9:15	26.3	34.43	2499	2507	2457	2124	1.14	2158	0.449
Coralline algae	**Run#2**	pCO_2=1070ppm	Sample weight:12.33g						
0:00	26.6	33.98	2331	2368	2192	1014	1.87	3651	
2:05	26.0	34.03	2341	2375	2228	1182	1.63	3286	
2:20	26.0	34.03	2341	2375	2211	1058	1.78	3234	0.201
3:18	26.0	34.06	2345	2378	2234	1196	1.62	3114	
3:30	26.0	34.06	2346	2379	2234	1194	1.63	3052	0.152
4:05	26.0	34.07	2351	2382	2221	1067	1.79	2896	
4:20	26.0	34.08	2352	2383	2235	1159	1.67	2843	0.320
5:35	26.0	34.11	2359	2388	2242	1164	1.68	2687	
5:50	26.0	34.11	2359	2388	2240	1155	1.69	2635	0.190
6:35	25.9	34.13	2363	2391	2245	1154	1.69	2479	
6:50	25.9	34.13	2364	2392	2248	1168	1.67	2427	0.159
7:45	26.0	34.16	2371	2397	2249	1133	1.73	2271	
8:00	26.0	34.16	2373	2398	2253	1158	1.70	2218	0.250
Coralline algae	**Run#3**	pCO_2=830ppm	Sample weight:10.86g						
0:00	26.5	34.51	2394	2395	2222	877	2.20	3242	
1:40	26.0	34.52	2397	2398	2181	671	2.63	3086	
1:55	25.9	34.52	2398	2399	2172	639	2.72	3033	0.305
3:57	25.6	34.52	2403	2404	2179	637	2.71	2846	
4:15	25.6	34.52	2405	2406	2170	604	2.82	2794	0.171
5:06	25.5	34.53	2406	2407	2190	665	2.62	2648	
5:20	25.5	34.53	2407	2407	2192	669	2.62	2492	0.110
5:35	25.6	34.53	2410	2410	2187	645	2.70	2336	
5:50	25.6	34.53	2413	2413	2202	691	2.57	2185	0.488
Coralline algae	**Run#4**	pCO_2=570ppm	Sample weight:12.55g						
0:00	26.2	34.33	2369	2382	2107	522	3.08	2677	
1:00	26.2	34.34	2371	2384	2131	585	2.86	2521	0.019
1:15	26.2	34.34	2369	2382	2129	584	2.86	2469	
2:45	26.2	34.34	2375	2388	2133	578	2.89	2313	0.126
3:00	26.2	34.34	2375	2387	2132	577	2.89	2261	
4:15	26.3	34.35	2376	2389	2138	594	2.85	2105	0.044
4:30	26.3	34.35	2377	2390	2137	588	2.87	2053	
5:45	26.3	34.35	2379	2392	2137	583	2.90	1896	0.065
6:00	26.3	34.35	2380	2392	2139	588	2.88	1844	
7:00	26.3	34.36	2382	2394	2143	594	2.86	1688	0.045

Supplementary Table 1. (continued)

Sampling time(hh:mm)	Temperature (℃)	Salinity (Calculated)	A_T (μ mol kg^{-1})	nA_T (μ mol kg^{-1})	C_T (μ mol kg^{-1})	$f(CO_2)$ (μ atam)	Ω_a	Water Volume (kg)	Average Dissolution Rate (μ mol m^{-2} h^{-1})
Foraminifera	**Run#1**	pCO_2=2210ppm	Sample weight:11.64g						
0:00	29.2	34.52	2424	2425	2375	2109	1.23	3482	
1:15	26.6	34.54	2432	2431	2393	2127	1.10	3326	
1:30	26.6	34.54	2434	2433	2400	2208	1.07	3269	1.363
2:15	26.4	34.55	2438	2436	2388	1968	1.17	3112	
2:30	26.3	34.56	2438	2436	2413	2337	1.01	3029	0.571
3:55	26.3	34.58	2446	2443	2417	2270	1.04	2873	
4:10	26.3	34.58	2447	2443	2419	2299	1.03	2821	0.559
6:15	26.3	34.61	2459	2453	2428	2247	1.06	2665	
6:30	26.3	34.61	2458	2452	2429	2292	1.04	2613	0.502
7:20	26.3	34.63	2464	2457	2434	2268	1.05	2508	
7:35	26.3	34.63	2463	2456	2437	2342	1.02	2456	0.449
8:10	26.3	34.64	2463	2455	2441	2414	1.00	2352	
8:25	26.3	34.64	2468	2460	2442	2342	1.03	2300	
8:30	26.3	34.65	2465	2457	2442	2380	1.01	2144	0.092
Foraminifera	**Run#2**	pCO_2=1240ppm	Sample weight:10.23g						
0:00	27.5	34.51	2436	2437	2262	925	2.26	2889	
0:45	26.6	34.53	2437	2437	2273	947	2.15	2733	
1:00	26.6	34.53	2438	2438	2281	988	2.08	2681	0.076
2:00	26.2	34.55	2442	2440	2285	977	2.08	2524	
2:15	26.2	34.55	2442	2440	2287	993	2.05	2472	0.294
3:30	26.2	34.58	2447	2443	2288	970	2.10	2316	
3:45	26.2	34.59	2447	2443	2291	986	2.07	2264	0.253
4:30	26.1	34.60	2449	2444	2289	958	2.11	2108	
4:45	26.1	34.61	2450	2444	2289	959	2.11	2056	0.091
5:30	26.1	34.63	2455	2448	2278	878	2.27	1899	
5:45	26.1	34.63	2454	2447	2278	880	1.85	1847	0.335
Foraminifera	**Run#3**	pCO_2=570ppm	Sample weight:11.49g						
0:00	26.4	34.08	2326	2356	2086	563	2.86	3387	
0:45	26.0	34.08	2326	2356	2083	546	2.88	3231	
1:00	26.1	34.08	2325	2355	2081	546	2.88	3179	−0.141
3:00	26.3	34.09	2325	2354	2081	552	2.88	3022	
3:15	26.3	34.09	2325	2355	2073	528	2.97	2970	−0.073
4:15	26.3	34.09	2332	2362	2069	500	3.10	2866	
4:30	26.3	34.10	2331	2361	2075	520	3.01	2731	0.687
6:15	26.3	34.10	2334	2364	2094	566	2.85	2575	
6:30	26.3	34.10	2334	2363	2096	570	2.84	2522	0.145
7:45	26.4	34.11	2337	2366	2099	575	2.84	2366	
8:00	26.5	34.11	2336	2365	2102	587	2.80	2210	
8:15	26.5	34.11	2336	2365	2098	576	2.84	2054	0.115
9:30	26.5	34.11	2341	2370	2109	597	2.78	1897	
9:45	26.5	34.11	2342	2371	2106	585	2.83	1845	0.312
Foraminifera	**Run#4**	pCO_2=510ppm	Sample weight:12.47g						
0:00	26.5	34.37	2403	2414	2135	527	3.18	3694	
1:00	26.2	34.37	2399	2409	2136	532	3.11	3537	
1:15	26.1	34.38	2398	2409	2133	524	3.14	3485	−0.861
2:00	26.0	34.38	2401	2411	2139	533	3.09	3329	
2:15	26.0	34.38	2402	2412	2125	496	3.25	3277	−0.157
4:10	26.0	34.38	2400	2410	2138	530	3.11	3121	
4:25	26.0	34.38	2402	2412	2137	525	3.13	3069	−0.028
5:10	26.0	34.39	2401	2411	2129	507	3.20	2912	
5:25	26.0	34.39	2399	2409	2127	506	3.20	2853	−0.194
6:45	26.1	34.39	2406	2415	2133	509	3.21	2697	
7:00	26.1	34.39	2403	2412	2121	484	3.31	2645	0.315
9:00	26.3	34.40	2402	2411	2125	499	3.26	2333	
9:15	26.3	34.40	2402	2411	2123	494	3.29	2281	−0.127

Supplementary Table 1. (continued)

Sampling time(hh:mm)	Temperature (℃)	Salinity (Calculated)	A_T (μ mol kg^{-1})	nA_T (μ mol kg^{-1})	C_T (μ mol kg^{-1})	$f(CO_2)$ (μ atam)	Ω_a	Water Volume (kg)	Average Dissolution Rate (μ mol m^{-2} h^{-1})
Coral Run#1		pCO_2=2100ppm	Sample weight:12.94g						
0:00	26.3	34.50	2436	2437	2390	2017	1.14	3684	
1:00	26.0	34.51	2435	2436	2412	2302	1.00	3528	
1:15	25.9	34.51	2437	2438	2392	1977	1.14	3476	0.001
2:10	25.7	34.52	2442	2442	2412	2207	1.03	3320	
2:25	25.7	34.53	2442	2442	2397	1980	1.14	3268	0.352
3:30	25.5	34.54	2442	2441	2418	2252	1.01	3111	
3:45	25.5	34.54	2442	2441	2421	2293	0.99	3059	−0.069
4:30	25.4	34.55	2447	2446	2396	1871	1.18	2903	
4:45	25.3	34.55	2448	2447	2425	2261	1.00	2747	
5:00	25.3	34.55	2447	2446	2428	2308	0.98	2590	
5:15	25.2	34.55	2450	2448	2425	2220	1.02	2434	0.289
6:30	25.2	34.57	2454	2452	2433	2265	1.00	2278	
6:45	25.2	34.57	2455	2452	2421	2071	1.09	2226	0.220
Coral Run#2		pCO_2=1550ppm	Sample weight:12.72g						
0:00	26.5	34.84	2579	2556	2473	1470	1.68	3773	
1:00	25.9	34.85	2582	2558	2461	1311	1.80	3617	
1:15	25.8	34.85	2581	2557	2486	1549	1.57	3565	0.242
2:30	25.7	34.86	2582	2557	2482	1483	1.62	3408	
2:45	25.7	34.86	2583	2558	2493	1589	1.53	3356	0.000
4:10	25.6	34.87	2583	2557	2495	1604	1.51	3200	
4:25	25.6	34.88	2583	2557	2485	1499	1.59	3148	−0.032
5:40	25.5	34.89	2585	2558	2487	1506	1.59	2992	
5:55	25.5	34.89	2587	2560	2491	1519	1.59	2940	0.115
7:00	25.6	34.90	2583	2556	2488	1526	1.58	2783	
7:15	25.6	34.90	2582	2555	2498	1645	1.48	2731	−0.207
9:10	25.6	34.91	2585	2557	2487	1503	1.60	2523	
9:30	25.6	34.91	2586	2558	2488	1507	1.60	2367	
9:45	25.6	34.92	2586	2558	2504	1662	1.47	2210	0.055
Coral Run#3		pCO_2=1070ppm	Sample weight:12.97g						
0:00	26.4	34.41	2411	2419	2233	853	2.26	3852	
0:50	26.0	34.44	2409	2416	2250	930	2.08	3652	
1:05	25.9	34.44	2412	2419	2249	908	2.12	3600	−0.151
3:50	26.0	34.50	2418	2420	2263	967	2.04	3076	
4:05	26.0	34.51	2419	2421	2265	969	2.04	3024	0.084
5:20	26.1	34.54	2421	2420	2264	959	2.06	2868	
5:35	26.1	34.54	2420	2419	2266	974	2.04	2816	−0.033
6:20	26.0	34.56	2423	2421	2265	952	2.07	2659	
6:35	26.0	34.56	2424	2422	2266	952	2.07	2607	0.124
7:20	26.0	34.58	2425	2421	2268	961	2.06	2453	
7:35	26.0	34.58	2426	2422	2268	953	2.08	2401	0.006

Supplementary Table 2. Salinity, temperature, total alkalinity (A_T), total dissolved inorganic carbon (C_T): calculated pH_T, fugacity of CO_2, and aragonite saturation state (Ω_a): and dissolution rate between each chamber experiment

Time		CO_2 added or natural	Salinity	Temperature[℃]	A_T [μ mol kg^{-1}]	C_T [μ mol kg^{-1}]	pH_T	$f(CO_2)$ [μ atm]	Ω_a	Dissolution Rate [mmol m^{-2} hr^{-1}]
Non-flow-control chamber experiment at night										
2010/9/5 19:32	Start	natural	33.3	30.52	2228.5	1805.0	8.189	250.4	4.86	
2010/9/5 22:51	↓	natural	33.3	30.22	2233.4	1804.4	8.200	243.0	4.91	0.36
2010/9/6 3:10	↓	natural	33.5	28.70	2235.4	1846.1	8.163	274.3	4.44	0.12
2010/9/6 6:08	End	natural	33.7	28.60	2235.9	1953.8	7.988	454.6	3.29	0.04
2010/9/5 19:45	Start	natural	33.3	30.42	2230.9	1804.6	8.194	247.0	4.89	
2010/9/5 22:59	End	natural	33.3	30.12	2236.5	1811.2	8.196	246.8	4.87	0.43
2010/9/5 19:52	Start	natural	33.3	30.42	2229.9	1808.6	8.187	252.6	4.83	
2010/9/5 23:12	End	natural	33.3	30.17	2233.1	1806.0	8.199	244.3	4.89	0.23
2010/9/6 0:01	Start	added	33.7	29.44	2183.2	1868.5	8.041	380.5	3.62	
2010/9/6 3:18	↓	added	33.7	28.99	2188.6	1951.7	7.906	558.3	2.81	0.41
2010/9/6 6:16	End	added	33.7	28.71	2202.4	1994.5	7.849	656.4	2.52	1.16
2010/9/6 0:10	Start	added	33.7	29.44	2181.7	1922.3	7.943	501.2	3.05	
2010/9/6 3:28	↓	added	33.9	28.32	2238.9	1983.8	7.940	519.7	3	4.33
2010/9/6 6:24	End	added	33.8	28.57	2231.8	1952.5	7.983	460.0	3.26	−0.61
2010/9/10 19:47	Start	natural	34.2	29.74	2199.2	1804.7	8.153	273.9	4.45	
2010/9/11 2:02	End	natural	34.2	29.77	2199.3	1821.0	8.128	295.0	4.29	0.00
2010/9/10 19:56	Start	added	34.2	29.72	2202.7	1866.9	8.061	360.2	3.84	
2010/9/11 2:12	End	added	34.1	29.32	2166.0	1894.3	7.964	467.3	3.14	−1.46
2010/9/10 20:04	Start	added	34.2	29.79	2196.8	1880.5	8.030	392.9	3.63	
2010/9/11 2:20	End	added	34.2	29.59	2202.2	1992.3	7.835	678.9	2.54	0.21
2010/9/11 2:42	Start	added	34.3	29.37	2194.8	1888.4	8.018	405.9	3.52	
2010/9/11 5:24	End	added	34.3	29.22	2194.7	1911.1	7.981	451.6	3.28	−0.01
2010/9/11 2:49	Start	added	34.3	29.27	2203.2	1944.4	7.934	517.1	3.03	
2010/9/11 5:31	End	added	34.3	29.17	2201.2	1973.9	7.875	607.7	2.7	−0.19
2010/9/11 2:58	Start	added	34.3	29.14	2198.8	2018.5	7.776	791.7	2.24	
2010/9/11 5:39	End	added	34.3	29.12	2236.1	2067.2	7.747	871.0	2.14	3.47
2010/9/11 3:31	Start	natural	34.1	29.92	2187.9	1856.5	8.055	363.6	3.79	
2010/9/11 6:09	End	natural	34.1	29.77	2189.5	1862.0	8.051	368.9	3.75	0.15
2010/9/11 19:13	Start	added	34.3	30.07	2156.5	1833.9	8.041	372.2	3.67	
2010/9/12 2:24	End	added	34.3	30.02	2173.9	1867.2	8.013	407.7	3.52	0.60
2010/9/11 19:20	Start	added	34.3	30.04	2154.7	1936.7	7.850	635.7	2.6	
2010/9/12 2:33	End	added	34.3	29.99	2190.6	1993.5	7.802	736.2	2.41	1.24
2010/9/12 3:43	Start	added	34.1	29.79	2192.7	1898.9	7.993	435.9	3.4	
2010/9/12 6:17	End	added	34.1	29.69	2196.5	1898.9	8.001	427.3	3.44	0.37
2010/9/12 3:51	Start	added	34.1	29.57	2185.9	2071.0	7.616	1199.1	1.63	
2010/9/12 6:24	End	added	34.1	29.72	2197.7	2071.7	7.641	1129.4	1.74	1.15
2010/9/13 4:41	Start	natural	34.2	30.42	2158.9	1871.0	7.978	446.8	3.33	
2010/9/13 6:41	End	natural	34.2	30.39	2159.7	1874.3	7.974	452.0	3.3	0.10
2010/9/13 4:50	Start	added	34.2	30.12	2157.8	2072.5	7.528	1480.2	1.37	
2010/9/13 6:48	End	added	34.2	30.22	2165.2	2073.8	7.543	1428.6	1.43	0.94
2010/9/13 5:00	Start	added	34.2	30.17	2157.0	2011.5	7.687	984.1	1.9	
2010/9/13 6:56	End	added	34.2	30.29	2170.6	2016.9	7.704	947.8	1.99	1.76
2011/5/19 22:15	Start	natural	34.5	25.18	2253.9	1957.2	8.050	383.9	3.35	
2011/5/20 1:15	↓	natural	34.6	25.16	2242.2	1966.5	8.015	421.5	3.13	−0.97
2011/5/20 3:00	End	natural	34.6	25.11	2263.3	1982.5	8.022	417.9	3.19	3.01
2011/5/19 22:50	Start	added	34.5	25.23	2253.2	1993.8	7.983	463.3	2.97	
2011/5/20 1:35	End	added	34.5	25.23	2265.2	2079.2	7.834	698.6	2.25	1.09
2011/5/19 23:05	Start	added	34.6	25.14	2253.9	2002.2	7.970	481.0	2.89	
2011/5/20 1:45	↓	added	34.6	25.14	2249.5	2030.0	7.907	569.2	2.57	−0.42
2011/5/20 3:15	↓	added	34.5	25.09	2270.0	2077.0	7.850	669.8	2.32	3.42
2011/5/20 5:50	End	added	34.6	24.9	2248.7	2096.8	7.762	837.5	1.92	−2.05
2011/5/20 1:55	Start	added	34.6	25.14	2259.4	2123.1	7.719	940.5	1.78	
2011/5/20 3:07	↓	added	34.6	25.14	2263.5	2167.1	7.613	1234.1	1.44	0.86
2011/5/20 5:40	End	added	34.5	25.09	2257.0	2199.6	7.503	1623.9	1.13	−0.64
2011/5/21 0:00	Start	natural	34.5	24.82	2251.5	1968.6	8.032	403.9	3.2	
2011/5/21 1:40	↓	natural	34.5	24.85	2259.7	1969.4	8.044	392.7	3.28	1.22
2011/5/21 5:25	End	natural	34.4	24.73	2245.9	1996.0	7.976	472.0	2.87	−0.92

Supplementary Table 2. (continued)

Time		CO_2 added or natural	Salinity	Temperature[℃]	A_T [μ mol kg^{-1}]	C_T [μ mol kg^{-1}]	pH_T	$f(CO_2)$ [μ atm]	Ω_a	Dissolution Rate [mmol m^{-2} hr^{-1}]
2011/5/21 0:10	Start	added	34.5	24.92	2246.3	2038.8	7.887	600.7	2.45	
2011/5/21 1:47	↓	added	34.5	24.95	2264.7	2059.2	7.880	617.1	2.44	2.85
2011/5/21 5:35	End	added	34.5	24.82	2262.1	2081.9	7.828	708.1	2.19	−0.17
2011/5/21 0:20	Start	added	34.5	24.82	2252.4	2154.5	7.624	1196.1	1.44	
2011/5/21 1:57	↓	added	34.5	24.85	2265.3	2171.7	7.610	1244.0	1.41	1.99
2011/5/21 5:45	End	added	34.5	24.73	2302.7	2220.8	7.577	1375.5	1.33	2.46
2011/8/17 20:26	Start	natural	34.4	31.38	2125.7	1710.5	8.170	247.7	4.64	
2011/8/17 23:29	↓	natural	34.4	31	2124.0	1735.9	8.136	275.4	4.35	−0.15
2011/8/18 2:54	↓	natural	34.4	30.37	2200.5	1848.5	8.075	343.5	4.01	5.60
2011/8/18 5:39	End	natural	34.4	30.19	2188.2	1863.9	8.036	383.0	3.71	−1.12
2011/8/26 19:50	Start	natural	34.5	30.65	2214.8	1832.3	8.114	307.1	4.35	
2011/8/26 22:30	↓	natural	34.5	30.09	2208.0	1856.7	8.075	344.5	4	−0.64
2011/8/27 0:40	↓	natural	34.4	29.99	2224.0	1898.8	8.033	392.6	3.74	1.85
2011/8/27 2:42	End	natural	34.5	29.92	2224.6	1922.0	7.996	436.9	3.5	0.07
2011/8/26 20:35	Start	added	34.5	30.52	2217.8	1934.0	7.956	487.0	3.31	
2011/8/26 22:40	↓	added	34.5	30.17	2204.7	1937.7	7.933	516.6	3.13	−1.57
2011/8/27 0:50	End	added	34.4	30.04	2218.8	1986.7	7.868	624.2	2.77	1.62
2011/8/27 1:20	Start	added	34.4	29.92	2235.3	2074.9	7.714	947.9	2.07	
2011/8/27 2:55	End	added	34.4	29.94	2261.0	2122.5	7.660	1105.5	1.88	4.07
2011/9/1 21:30	Start	natural	34.5	29.72	2231.2	1857.4	8.111	313.7	4.24	
2011/9/1 23:35	↓	natural	34.5	29.32	2239.7	1877.5	8.098	327.8	4.12	1.02
2011/9/2 1:30	↓	natural	34.5	29.27	2231.6	1876.8	8.090	335.3	4.03	
2011/9/2 3:30	↓	natural	34.6	29.19	2246.8	1904.4	8.067	360.3	3.91	1.90
2011/9/2 5:40	End	natural	34.5	29.04	2223.9	1902.1	8.041	385.0	3.68	−2.63
2011/9/1 21:50	Start	added	34.5	29.49	2247.5	1992.7	7.914	556.8	3.01	
2011/9/1 23:45	↓	added	34.6	29.24	2265.7	1983.0	7.963	488.9	3.3	2.37
2011/9/2 1:45	↓	added	34.5	29.17	2257.1	1974.4	7.967	481.9	3.3	−1.07
2011/9/2 3:45	↓	added	34.5	29.07	2249.3	2004.2	7.901	577.1	2.9	−0.98
2011/9/2 5:52	End	added	34.6	28.89	2263.1	2003.9	7.927	540.9	3.05	1.63
2011/9/2 20:10	Start	natural	34.5	29.37	2227.1	1903.6	8.038	388.3	3.7	
2011/9/2 23:03	↓	natural	34.5	29.44	2258.5	1922.7	8.051	378.9	3.85	2.72
2011/9/3 1:15	↓	natural	34.5	29.41	2254.6	1938.6	8.020	413.8	3.64	−0.44
2011/9/3 3:15	↓	natural	34.6	29.29	2257.8	1948.6	8.010	427.1	3.57	0.40
2011/9/2 20:22	Start	added	34.5	29.34	2249.4	2085.5	7.728	919.7	2.1	
2011/9/2 23:20	↓	added	34.5	29.39	2271.9	2026.8	7.893	595.9	2.92	1.90
2011/9/3 1:30	↓	added	34.5	29.34	2279.2	2028.0	7.904	580.1	2.99	0.85
2011/9/3 3:25	↓	added	34.6	29.22	2270.5	2037.3	7.872	630.5	2.79	−1.14
2011/9/3 6:05	End	added	34.6	28.99	2288.4	2059.4	7.865	648.5	2.76	1.68
Non-flow-control chamber experiment at day time										
2010/9/3 10:28	Start	natural	34.7	29.49	2209.3	1907.8	8.000	428.7	3.46	
2010/9/3 14:14	End	natural	34.3	30.62	2201.4	1885.4	8.015	409.8	3.65	−0.52
2010/9/3 10:43	Start	natural	34.3	29.37	2205.8	1898.8	8.017	408.9	3.53	
2010/9/3 14:29	End	natural	34.3	30.6	2199.4	1881.6	8.019	404.9	3.67	−0.42
2010/9/3 11:01	Start	natural	34.3	29.64	2201.6	1879.2	8.039	382.9	3.69	
2010/9/3 14:47	End	natural	34.4	30.7	2191.5	1856.1	8.046	372.1	3.84	−0.66
2010/9/4 13:18	Start	natural	33.9	29	2191.2	1838.1	8.105	316.4	4.01	
2010/9/4 16:18	End	natural	34.0	29.16	2196.5	1845.4	8.098	323.6	3.99	0.44
2010/9/4 13:25	Start	natural	33.9	28.84	2189.3	1843.6	8.096	325.1	3.92	
2010/9/4 16:25	End	natural	33.9	29.09	2198.7	1848.1	8.098	323.9	3.99	0.78
2010/9/4 13:32	Start	natural	33.9	28.84	2194.0	1837.8	8.112	310.8	4.04	
2010/9/4 16:32	End	natural	33.9	29.19	2202.6	1839.6	8.115	308.4	4.12	0.71
2010/9/7 11:13	Start	natural	34.2	30	2221.4	1886.7	8.052	372.6	3.85	
2010/9/7 14:08	↓	natural	34.2	31.33	2210.0	1857.2	8.063	356.7	4.06	−0.98
2010/9/7 15:53	End	natural	34.2	31.05	2210.4	2016.1	7.780	788.9	2.42	0.06
2010/9/7 11:22	Start	added	34.2	29.92	2217.9	2020.5	7.801	747.9	2.43	
2010/9/7 14:17	↓	added	34.2	31.31	2215.6	2029.4	7.758	838.8	2.34	−0.20
2010/9/7 16:04	End	added	34.2	30.52	2204.8	1868.6	8.049	371.5	3.86	−1.52
2010/9/7 11:29	Start	added	34.2	30.27	2215.8	1918.0	7.988	446.5	3.46	
2010/9/7 14:25	↓	added	34.2	31.3	2204.7	1881.3	8.018	406.3	3.75	−0.95
2010/9/7 16:13	End	added	34.2	30.57	2201.5	1847.7	8.077	342.0	4.05	−0.44
2010/9/8 12:47	Start	natural	34.3	30.39	2214.7	1833.3	8.119	304.1	4.34	
2010/9/8 15:38	End	natural	34.3	31.28	2211.2	1813.1	8.131	291.3	4.54	−0.31
2010/9/8 12:55	Start	added	34.3	30.2	2213.2	1960.3	7.908	557.7	2.99	
2010/9/8 15:44	End	added	34.3	31.15	2208.3	1985.3	7.837	675.4	2.7	−0.43

Supplementary Table 2. (continued)

Time	CO_2 added or natural	Salinity	Temperature[℃]	A_T [μ mol kg^{-1}]	C_T [μ mol kg^{-1}]	pH_T	$f(CO_2)$ [μ atm]	Ω_a	Dissolution Rate [mmol m^{-2} hr^{-1}]
2010/9/8 13:03 Start	added	34.3	30.37	2212.0	1919.1	7.977	458.5	3.41	
2010/9/8 15:50 End	added	34.3	31.26	2199.1	1889.4	7.995	432.4	3.6	−1.16
2010/9/9 13:12 Start	natural	34.3	29.87	2224.1	1839.4	8.130	296.3	4.37	
2010/9/9 15:57 End	natural	34.2	30.39	2215.1	1822.5	8.136	289.0	4.46	−0.82
2010/9/9 13:25 Start	added	34.2	29.87	2216.9	1870.6	8.073	350.0	3.96	
2010/9/9 16:03 End	added	34.2	30.14	2205.8	1819.8	8.132	291.7	4.38	−1.05
2010/9/9 13:30 Start	added	34.2	29.79	2214.7	1991.9	7.856	644.7	2.68	
2010/9/9 16:09 End	added	34.2	30.19	2205.9	1999.6	7.818	711.6	2.52	−0.83
2011/8/23 15:55 Start	natural	34.4	31.87	2195.5	1779.9	8.149	272.7	4.72	
2011/8/23 18:20 End	natural	34.5	31.56	2207.8	1998.4	7.801	743.0	2.57	1.27
2011/8/23 16:15 Start	added	34.5	31.97	2204.4	1908.6	7.958	479.9	3.46	
2011/8/23 18:35 End	added	34.4	31.46	2186.5	1773.5	8.153	268.7	4.67	−1.92
2011/8/24 15:35 Start	natural	34.6	31.89	2191.0	1782.4	8.138	280.8	4.63	
2011/8/24 17:40 ↓	natural	34.5	31.64	2200.9	1781.2	8.156	267.3	4.75	1.19
2011/8/24 19:27 End	natural	34.4	30.85	2189.6	1778.1	8.159	264.7	4.64	−1.58
2011/8/24 15:45 Start	added	34.5	32.02	2210.0	1849.3	8.062	355.9	4.15	
2011/8/24 17:45 ↓	added	34.5	31.61	2220.2	1921.9	7.965	474.7	3.49	1.28
2011/8/24 19:40 End	added	34.5	30.8	2223.3	1927.1	7.973	465.7	3.45	0.41
2011/8/24 15:55 Start	added	34.5	31.82	2194.5	1941.3	7.885	586.0	3.01	
2011/8/24 17:55 ↓	added	34.5	31.43	2229.6	2049.2	7.739	886.0	2.29	4.38
2011/8/24 19:50 End	added	34.5	30.8	2227.8	2058.3	7.723	923.4	2.17	−0.23
2011/8/25 14:02 Start	natural	34.4	32.12	2157.7	1705.8	8.204	225.1	5.07	
2011/8/25 16:07 ↓	natural	34.5	32.05	2164.0	1720.7	8.191	235.1	4.98	0.75
2011/8/25 18:41 End	natural	34.5	30.93	2186.2	1752.6	8.189	241.0	4.86	2.16
2011/8/25 14:10 Start	added	34.5	32.02	2169.4	1869.3	7.971	455.2	3.49	
2011/8/25 16:16 ↓	added	34.4	31.92	2179.7	1913.9	7.910	543.2	3.14	1.22
2011/8/25 18:50 End	added	34.4	30.85	2203.9	1897.5	7.993	435.6	3.55	2.36
2011/8/25 14:18 Start	added	34.5	32.1	2172.1	1913.7	7.894	565.2	3.06	
2011/8/25 16:25 ↓	added	34.4	31.89	2201.9	2026.6	7.725	909.0	2.23	3.52
2011/8/25 18:58 End	added	34.5	30.93	2201.1	1995.7	7.803	737.0	2.51	−0.07

Experimental design for non-flow-controlled chamber

In order to estimate net dissolution/calcification rate *in situ* at a sand area without flow condition, a closed chamber was constructed and placed on the bottom (Supplementary Figure 1). The chamber was 0.5 × 0.5 × 0.5 m, and consisted of three parts: an acrylic baseboard, clear acrylic side panels, and a clear acrylic top. The seawater inside the chamber could be exchanged by opening the top. In order to collect seawater inside the chamber, 30cm long tube (6 mm diameter) was connected with its outside end sealed by a cock. Two rubber gloves and 1L bottle(s) were installed into the chamber in order to increase pCO_2 in seawater within the sealed chamber. One litter bottles were filled with CO_2 saturated seawater beforehand. By opening these bottles, pCO_2 in seawater within the chamber was able to be increased. A plastic curtain (30 cm length) was attached to the bottom of the acrylic baseboard by a bond to prevent seawater from passing through gaps between the base and the seafloor. The curtain and base were buried in the sediment. These techniques created a closed system within the chamber.

Light intensity was indicated by [μmol m^{-2} s^{-1}] and recorded by a photon flux sensor (ALW-CMP, JFE Advantech Co., Ltd). This sensor and a temperature logger (CO-U22-001, Climatic Co., Ltd) were deployed inside the chamber. They recorded at 10-mins intervals.

The procedure of experiments was as follows: (1) 1L bottle(s) filled with CO_2 saturated seawater was placed inside the chamber, and the chamber top was closed, (2) opening the 1L bottle cap inside the chamber using two rubber gloves, (3) a sample of seawater in the chamber was collected by a connected tube and syringe at the beginning. (4) Seawater in the sealed chamber was re-sampled after about 3h. (5-1) When we wanted to continue experiment, procedure (4) was repeated. (5-2) When we wanted to change CO_2 condition in seawater, the chamber was opened and seawater in the chamber was exchanged with the surrounding water,

and (6) after waiting more than 15 min, the procedure (1) was repeated. Seawater samples were collected by 300-mL borosilicate glass bottles (Duran, Schott) with 0.2 ml of saturated mercuric chloride ($HgCl_2$) solution for preservation.

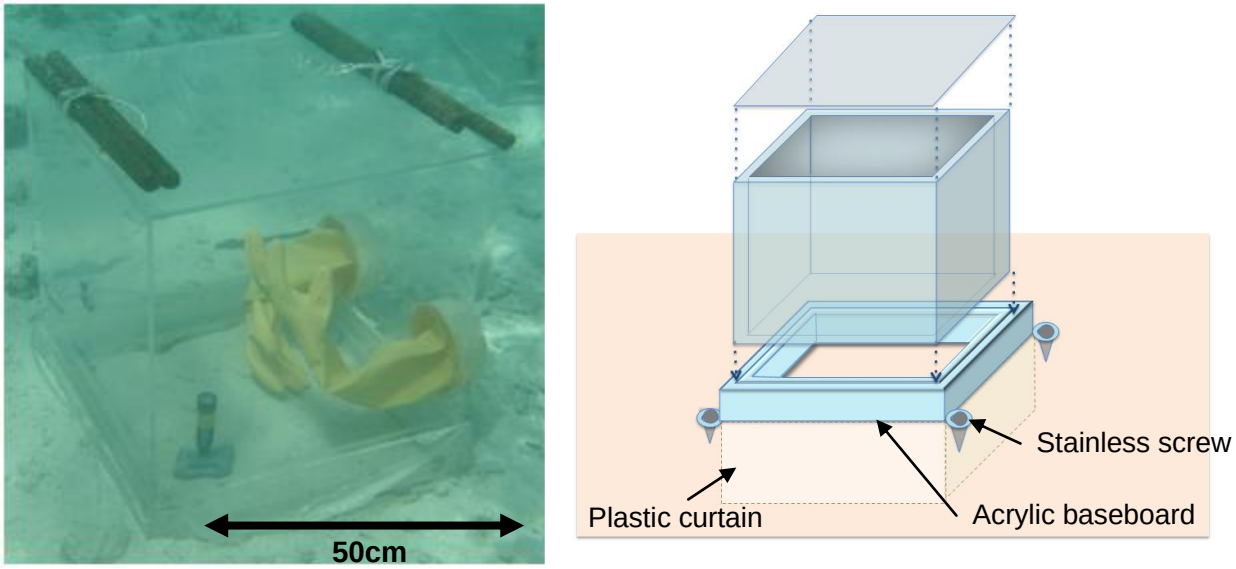

Supplementary Figure 1. Picture and schematic design of non-flow-controlled chamber (0.5 × 0.5 × 0.5 m): Acrylic baseboard with plastic curtain was fixed by stainless screw, and was jointed with chamber. Top of chamber can be removed and it can be attached to the chamber.

Evaluation of the chamber experiment system

The conditions for each experiment and the results of all experiments are listed in Supplementary Tables 2 and 3. Supplementary Figure 2 shows the average dissolution/calcification rates, calculated from A_T changes (equation 4-1), plotted against averaged Ω_a calculated by initial and end values assuming that constant dissolution rate during experiment duration. Calcification is denoted by negative values, and dissolution is denoted by positive values. From flow-controlled chamber experiment, either day or

nighttime dissolution/calcification rate did not show a significant correlation with Ω_a (R = -0.44 and R = -0.36, respictively, $p > 0.05$). When $\Omega_a > 3.1$ during day time, net calcification mainly caused by biological calcifers were observed for 12/15 cases, whereas $\Omega_a < 3.1$ during night, net dissolution were observed for 9/10 cases. On the other hand, from non-flow-controlled chamber experiment, their data had wider ranges. Because there are no flow in non-flow-controlled chamber, seawater in the chamber was not fully mixed, and thus dissolution rate could not be correctly measured. In order to evaluate sand dissolution rate under several current conditions, results of flow-controlled chamber were mainly used hereafter.

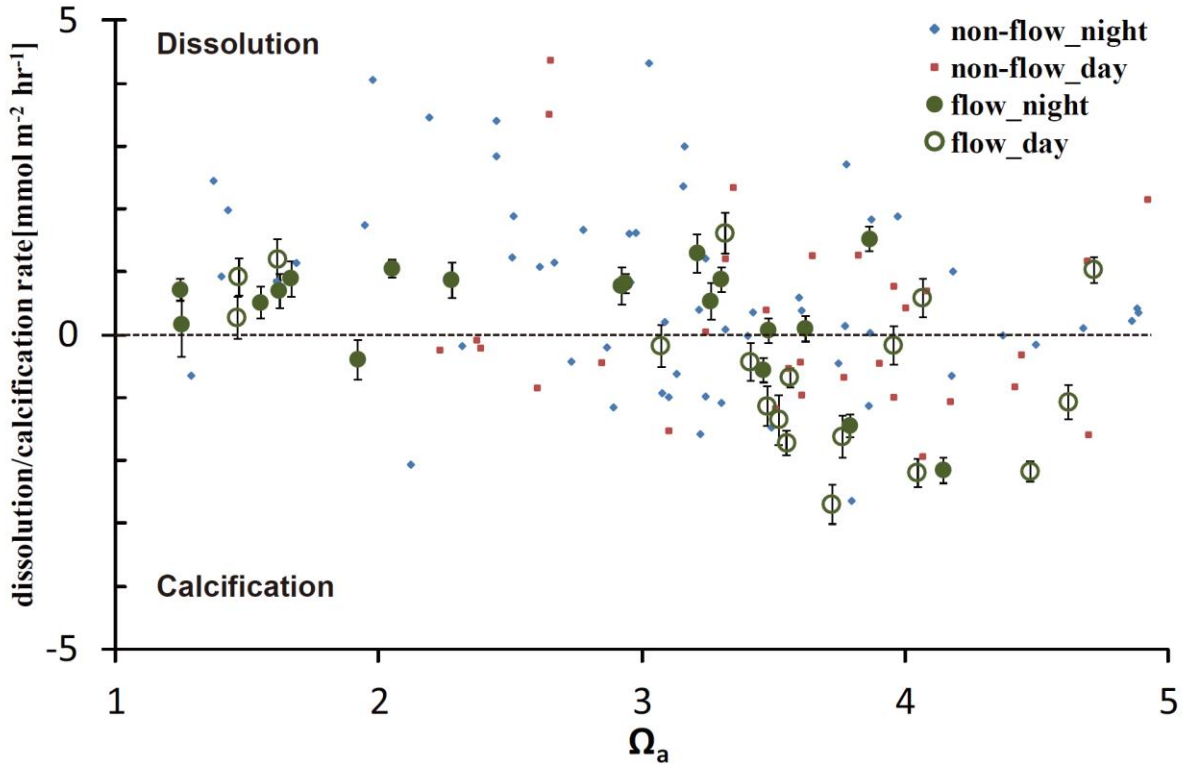

Supplementary Figure 2. The relationship between average dissolution rate and Ω_a (all chamber experiments): Only error bars for flow-controlled chamber were shown. Error bars for non-flow-controlled chamber were almost the same as flow-controlled chamber.

Supplementary Table 3. Salinity, temperature, total alkalinity (A_T), total dissolved inorganic carbon (C_T): calculated pH, fugacity of CO_2, and aragonite saturation state (Ω_a): and dissolution rate and flow rate between each chamber experiment
"Slow" corresponds to about 2 cm s^{-1}, "Middle" about 5 cm s^{-1}, and "Fast" 15 cm s^{-1}

Time	CO_2 added or natural	Salinity	Temperature[℃]	A_T [μ mol kg^{-1}]	C_T [μ mol kg^{-1}]	pH_T	f(CO_2) [μ atm]	Ω_a	Dissolution Rate [mmol m^{-2} hr^{-1}]	flow rate
Flow-control chamber experiment at night										
2011/5/20 2:40 Start	added	34.5	25.51	2256.4	2107.4	7.745	877.7	1.90		Middle
2011/5/20 5:22 End	added	34.5	25.90	2270.7	2091.1	7.809	747.5	2.20	1.06	Middle
2011/5/20 23:50 Start	added	34.5	25.22	2263.4	2262.4	7.329	2492.0	0.79		Middle
2011/5/21 2:05 End	added	34.4	25.90	2271.5	2146.9	7.679	1050.3	1.70	0.72	Middle
2011/5/21 2:35 Start	added	34.3	25.03	2228.9	1974.8	7.982	460.1	2.91		Middle
2011/5/21 5:15 End	added	34.3	25.71	2240.0	1982.9	7.977	469.4	2.96	0.83	Middle
2011/8/26 20:22 Start	natural	34.5	32.00	2227.2	1852.9	8.079	340.8	4.31		Middle
2011/8/26 22:20 ↓	natural	34.4	32.00	2206.1	1861.5	8.038	381.1	3.98	−2.15	Middle
2011/8/27 0:30 ↓	natural	34.5	32.00	2190.5	1881.3	7.983	444.3	3.60	−1.44	Middle
2011/8/27 2:30 ↓	natural	34.5	32.00	2184.9	1901.5	7.939	501.3	3.32	−0.55	Middle
2011/8/27 4:35 End	natural	34.3	32.00	2194.2	1916.5	7.930	518.3	3.28	0.89	Middle
2011/9/1 21:15 Start	natural	34.5	29.54	2241.0	1888.1	8.081	345.2	4.03		Slow
2011/9/1 23:20 ↓	natural	34.5	29.24	2256.9	1935.0	8.033	400.1	3.70	1.53	Slow
2011/9/2 1:20 ↓	natural	34.5	29.19	2257.9	1951.6	8.007	430.6	3.54	0.11	Slow
2011/9/2 3:22 End	natural	34.5	29.16	2258.7	1964.4	7.988	455.7	3.42	0.08	Slow
2012/2/22 19:45 Start	added	34.6	23.31	2216.8	1917.4	8.088	340.1	3.28		Fast
2012/2/22 21:45 End	added	34.6	26.52	2225.5	1939.9	8.015	417.3	3.14	1.30	Fast
2012/2/22 22:10 Start	natural	34.6	23.20	2266.0	1963.2	8.087	348.6	3.34		Fast
2012/2/23 0:10 End	natural	34.6	26.49	2269.6	1982.7	8.011	431.1	3.18	0.54	Fast
2012/2/23 0:50 Start	added	34.6	23.77	2268.0	2151.3	7.686	1023.9	1.56		Fast
2012/2/23 3:12 End	added	34.6	27.15	2272.1	2158.2	7.633	1185.3	1.54	0.52	Fast
2012/2/23 3:45 Start	added	34.5	23.65	2275.5	2114.5	7.798	769.5	1.96		Fast
2012/2/23 5:40 End	added	34.5	26.63	2273.0	2121.1	7.735	909.6	1.88	−0.39	Fast
2012/2/25 19:28 Start	added	34.4	23.14	2263.5	2139.0	7.718	941.2	1.63		Fast
2012/2/25 21:34 End	added	34.4	26.36	2269.8	2137.7	7.693	1015.1	1.70	0.91	Fast
2012/2/25 21:50 Start	natural	34.5	22.91	2265.4	1988.5	8.048	390.4	3.08		Fast
2012/2/25 23:55 End	natural	34.5	26.15	2270.9	2010.5	7.969	485.0	2.92	0.79	Fast
2012/2/26 0:20 Start	added	34.5	22.62	2267.4	2076.6	7.882	613.7	2.24		Fast
2012/2/26 2:28 End	added	34.5	25.71	2273.7	2076.0	7.852	668.5	2.31	0.88	Fast
2012/2/26 3:08 Start	added	34.5	22.52	2278.7	2180.6	7.654	1115.3	1.41		Fast
2012/2/26 5:20 End	added	34.5	25.29	2283.9	2161.6	7.679	1053.4	1.62	0.71	Fast
2012/2/26 5:50 Start	added	34.5	21.50	2283.4	2219.0	7.570	1374.5	1.15		Fast
2012/2/26 7:00 End	added	34.4	23.36	2284.0	2194.1	7.620	1220.8	1.35	0.17	Fast
Flow-control chamber experiment at day time										
2011/8/23 15:35 Start	natural	34.5	32.05	2183.8	1775.2	8.137	280.1	4.63		Slow
2011/8/23 17:35 ↓	natural	34.5	33.61	2194.3	1775.3	8.128	287.5	4.80	1.05	Slow
2011/8/23 19:05 End	natural	34.5	33.44	2186.3	1800.0	8.084	327.3	4.44	−1.06	Slow
2011/8/24 15:10 Start	natural	34.4	31.89	2176.6	1766.1	8.145	273.3	4.65		Middle
2011/8/24 17:30 ↓	natural	34.4	31.03	2151.3	1769.6	8.120	292.6	4.30	−2.17	Middle
2011/8/24 19:20 End	natural	34.5	30.24	2131.2	1795.1	8.063	344.1	3.79	−2.19	Middle
2011/8/25 13:54 Start	added	34.5	32.21	2152.5	1852.2	7.971	450.5	3.48		Middle
2011/8/25 15:56 ↓	added	34.5	32.30	2135.1	1820.4	7.997	414.5	3.62	−1.71	Middle
2011/8/25 18:30 End	added	34.5	32.40	2126.5	1823.2	7.977	436.8	3.50	−0.67	Middle
2012/2/13 12:10 Start	natural	34.6	23.33	2270.9	1956.0	8.105	332.5	3.47		Fast
2012/2/13 14:05 End	natural	34.6	26.93	2263.7	1947.3	8.055	378.4	3.48	−1.13	Fast
2012/2/13 14:20 Start	natural	34.6	23.73	2247.8	1883.7	8.181	263.0	3.95		Fast
2012/2/13 16:15 End	natural	34.6	27.48	2246.8	1881.8	8.127	304.2	3.96	−0.16	Fast
2012/2/13 16:27 Start	natural	34.6	24.01	2217.3	1840.7	8.202	243.7	4.05		Fast
2012/2/13 18:25 End	natural	34.6	24.57	2221.2	1842.2	8.196	247.5	4.08	0.59	Fast
2012/2/14 11:55 Start	natural	34.6	23.08	2248.2	1944.1	8.095	338.8	3.35		Slow
2012/2/14 13:50 End	natural	34.6	24.00	2245.5	1928.6	8.103	330.0	3.47	−0.42	Slow
2012/2/14 14:02 Start	natural	34.7	23.72	2250.0	1907.5	8.147	291.3	3.73		Slow
2012/2/14 15:55 End	natural	34.6	24.40	2233.1	1892.3	8.138	296.0	3.71	−2.69	Slow
2012/2/14 16:10 Start	natural	34.6	24.07	2226.0	1877.5	8.156	280.2	3.78		Slow
2012/2/14 17:58 End	natural	34.6	24.36	2216.3	1871.0	8.148	284.8	3.74	−1.62	Slow
2012/2/20 12:05 Start	added	34.7	21.47	2255.3	2000.4	8.028	410.7	2.85		Middle
2012/2/20 13:55 End	added	34.7	23.13	2254.3	1955.9	8.081	352.6	3.29	−0.17	Middle
2012/2/20 14:25 Start	added	34.8	21.81	2210.6	1914.2	8.104	324.5	3.24		Middle
2012/2/20 16:15 End	added	34.8	23.20	2220.6	1909.3	8.107	322.2	3.39	1.62	Middle
2012/2/20 16:35 Start	added	34.7	21.94	2258.7	1929.3	8.151	290.5	3.60		Middle
2012/2/20 18:05 End	added	34.7	22.90	2252.0	1938.2	8.111	323.3	3.44	−1.34	Middle
2012/2/21 11:35 Start	added	34.6	22.47	2277.8	2171.5	7.676	1053.2	1.48		Fast
2012/2/21 13:40 End	added	34.6	26.17	2284.2	2182.2	7.613	1249.6	1.45	0.93	Fast
2012/2/21 14:05 Start	added	34.5	22.61	2242.8	2155.0	7.625	1179.1	1.31		Fast
2012/2/21 15:55 End	added	34.5	26.08	2244.5	2121.2	7.675	1049.2	1.61	0.28	Fast
2012/2/21 16:20 Start	added	34.6	23.17	2251.9	2140.8	7.681	1028.9	1.51		Fast
2012/2/21 18:10 End	added	34.6	25.87	2259.3	2124.5	7.704	977.6	1.72	1.21	Fast

Supplementary Table 4. Pore water chemistry and envrionment information: C_T and Ω_a were calculated by A_T, pH_{total}, Temperature, and salinity. Salinity of all data were 34.5.

Time	Depth [mm]	Temperature[℃]	Light Intensity [μmol m^{-2} s^{-1}]	A_T [μmol kg^{-1}]	pH_{Total}	calculated C_T [μmol kg^{-1}]	calculated Ω_a	NO_2 [μmol l^{-1}]	NO_3 [μmol l^{-1}]	NH_4 [μmol l^{-1}]	PO_4 [μmol l^{-1}]	SiO_2 [μmol l^{-1}]
2012/10/4 20:15	0.0	26.7	0.0	---	---	---	---	0.017	0.344	0.625	0.058	1.123
2012/10/4 20:10	−5.0	26.7	---	---	---	---	---	0.012	0.095	0.142	0.196	0.199
2012/10/4 20:10	−15.0	26.7	---	---	---	---	---	0.029	0.206	0.167	0.254	0.478
2012/10/4 20:10	−25.0	26.7	---	---	---	---	---	0.113	1.042	0.326	0.378	0.776
2012/10/4 20:10	−35.0	26.7	---	---	---	---	---	0.310	1.907	1.234	1.274	4.556
2012/10/4 20:10	−45.0	26.7	---	---	---	---	---	0.420	2.542	2.271	0.892	2.267
2012/10/4 20:10	−55.0	26.7	---	---	---	---	---	0.633	1.970	1.606	0.804	4.530
2012/10/4 22:50	0.0	26.5	0.0	---	---	---	---	0.017	0.172	0.140	0.041	1.045
2012/10/4 23:00	−5.0	26.5	---	2409.3	7.937	2153.2	3.05	0.025	0.053	0.329	0.168	0.610
2012/10/4 23:00	−15.0	26.5	---	2400.2	7.940	2142.8	3.06	0.166	0.567	0.409	0.394	1.745
2012/10/4 23:00	−25.0	26.5	---	2338.6	7.923	2095.0	2.88	0.097	0.710	1.748	0.764	3.501
2012/10/4 23:00	−35.0	26.5	---	2342.5	7.928	2093.3	2.91	0.333	1.018	1.773	0.849	3.179
2012/10/4 23:00	−45.0	26.5	---	2287.7	7.915	2052.2	2.78	0.044	0.261	0.362	0.274	3.738
2012/10/5 0:56	0.0	26.2	0.0	2285.7	8.092	1951.8	3.78	0.021	0.335	0.285	0.035	1.172
2012/10/5 0:55	−5.0	26.2	---	2347.9	7.970	2080.5	3.13	0.071	0.249	0.276	0.457	1.216
2012/10/5 0:55	−15.0	26.2	---	2347.9	7.953	2090.1	3.03	0.055	0.287	0.324	0.356	1.318
2012/10/5 0:55	−25.0	26.2	---	2330.9	7.951	2075.4	3.00	0.063	0.420	0.326	0.181	1.640
2012/10/5 0:55	−35.0	26.2	---	2293.9	7.957	2037.9	2.98	0.068	0.563	0.544	0.445	2.729
2012/10/5 0:55	−45.0	26.2	---	2345.1	7.942	2093.3	2.96	0.083	1.016	1.208	0.728	2.955
2012/10/5 0:55	−55.0	26.2	---	2300.7	7.937	2054.7	2.88	0.095	0.769	0.981	0.482	2.980
2012/10/5 4:00	0.0	25.6	0.0	2295.2	8.060	1985.2	3.52	0.030	0.279	0.383	0.027	1.035
2012/10/5 4:00	−5.0	25.6	---	2389.2	7.882	2170.0	2.65	0.024	0.052	0.206	0.124	1.252
2012/10/5 4:00	−15.0	25.6	---	2439.4	7.932	2191.0	2.97	0.139	0.406	0.572	0.551	1.325
2012/10/5 4:00	−25.0	25.6	---	2418.0	7.945	2163.9	3.02	0.289	0.798	0.870	0.753	2.906
2012/10/5 4:00	−35.0	25.6	---	2476.6	7.919	2232.2	2.95	0.182	0.921	0.617	0.683	3.249
2012/10/5 4:00	−45.0	25.6	---	2383.4	7.955	2126.1	3.03	0.233	0.674	0.988	1.110	3.372
2012/10/5 4:00	−55.0	25.6	---	2336.0	7.947	2086.7	2.92	0.048	0.447	0.252	0.272	2.500
2012/10/5 6:00	0.0	25.3	0.0	2302.8	8.002	2028.6	3.15	0.062	0.457	0.537	0.046	0.966
2012/10/5 6:00	−5.0	25.3	---	2453.5	7.904	2221.2	2.81	0.037	0.170	0.417	0.306	1.210
2012/10/5 6:00	−15.0	25.3	---	2431.0	7.918	2192.8	2.86	0.043	0.101	0.164	0.281	2.963
2012/10/5 6:00	−25.0	25.3	---	2408.8	7.927	2167.0	2.88	0.064	0.339	0.238	0.384	3.832
2012/10/5 6:00	−35.0	25.3	---	2405.0	7.964	2143.8	3.08	0.245	1.363	1.049	0.966	5.746
2012/10/5 6:00	−45.0	25.3	---	2366.8	7.967	2106.7	3.04	0.172	0.800	0.739	0.855	4.402
2012/10/5 6:00	−55.0	25.3	---	2343.1	7.968	2084.2	3.02	0.147	0.682	0.636	0.509	3.934
2012/10/6 10:00	0.0	27.6	216.9	2299.0	8.114	1936.6	4.12	0.009	0.189	0.243	0.023	0.978
2012/10/6 10:00	−5.0	27.6	---	2215.4	7.954	1956.7	2.99	0.033	0.055	0.216	0.184	0.909
2012/10/6 10:00	−15.0	27.6	---	2229.6	7.938	1978.4	2.92	0.150	0.381	0.646	0.570	1.983
2012/10/6 10:00	−25.0	27.6	---	2220.4	7.938	1969.6	2.91	0.166	0.557	1.077	0.757	4.727
2012/10/6 10:00	−35.0	27.6	---	2122.1	8.002	1845.3	3.12	0.249	0.767	1.206	0.957	4.018
2012/10/6 10:00	−45.0	27.6	---	2180.6	7.965	1918.6	3.00	0.122	0.681	0.483	0.623	3.806
2012/10/6 10:00	−55.0	27.6	---	2126.5	7.947	1878.6	2.83	0.174	0.775	0.956	0.686	3.703
2012/10/6 12:30	0.0	27.6	57.4	2260.3	8.222	1828.8	4.81	0.000	0.206	0.157	0.023	0.892
2012/10/6 12:30	−5.0	27.6	---	2270.8	7.948	2010.7	3.04	0.040	0.099	0.151	0.228	3.600
2012/10/6 12:30	−15.0	27.6	---	2322.5	7.912	2077.6	2.91	0.152	0.823	0.788	1.137	5.104
2012/10/6 12:30	−25.0	27.6	---	2326.0	7.926	2073.8	2.99	0.102	0.638	0.445	0.798	6.285
2012/10/6 12:30	−35.0	27.6	---	2309.0	7.939	2050.9	3.04	0.118	0.599	0.467	0.773	8.910
2012/10/6 12:30	−45.0	27.6	---	2334.5	7.940	2073.6	3.08	0.117	0.467	0.655	0.652	8.269
2012/10/6 12:30	−55.0	27.6	---	2216.1	7.955	1956.8	3.00	0.043	0.108	0.328	0.391	7.362
2012/10/6 14:50	0.0	28.5	63.8	2247.9	8.271	1772.9	5.28	0.000	0.169	0.188	0.042	0.956
2012/10/6 14:50	−5.0	28.5	---	2278.7	7.968	1999.9	3.25	0.069	0.134	1.981	0.281	2.737
2012/10/6 14:50	−15.0	28.5	---	2294.7	7.932	2034.4	3.07	0.074	0.106	2.311	0.274	4.579
2012/10/6 14:50	−25.0	28.5	---	2321.8	7.903	2075.4	2.94	0.114	0.401	0.495	0.585	5.560
2012/10/6 14:50	−35.0	28.5	---	2171.3	7.934	1919.5	2.91	0.033	0.131	0.396	0.361	5.130
2012/10/6 14:50	−45.0	28.5	---	2279.3	7.890	2042.8	2.82	0.045	0.260	1.421	0.391	6.839
2012/10/6 14:50	−55.0	28.5	---	2228.2	7.915	1982.2	2.89	0.076	0.204	0.463	0.425	6.263
2012/10/6 16:30	0.0	28.5	33.5	2211.9	8.319	1707.0	5.56	0.000	0.221	0.229	0.054	0.899
2012/10/6 16:30	−5.0	28.5	---	2343.5	7.948	2070.5	3.23	0.027	0.063	0.254	0.234	2.387
2012/10/6 16:30	−15.0	28.5	---	2257.8	7.959	1985.6	3.17	0.126	0.759	0.399	0.427	4.379
2012/10/6 16:30	−25.0	28.5	---	2253.6	7.945	1989.5	3.09	0.050	0.228	0.259	0.442	7.092
2012/10/6 16:30	−35.0	28.5	---	2225.8	7.979	1945.3	3.24	0.102	0.471	0.272	0.442	5.454
2012/10/6 16:30	−45.0	28.5	---	2336.4	7.937	2069.8	3.16	0.147	0.497	0.488	0.549	7.382
2012/10/6 16:30	−55.0	28.5	---	2289.0	7.904	2044.0	2.91	0.168	0.640	0.906	0.702	8.605